NASACR-168228

NASA

CREEP FATIGUE LIFE PREDICTION FOR ENGINE HOT SECTION MATERIALS (ISOTROPIC)

FIRST ANNUAL REPORT

by
Vito Moreno

United Technologies Corporation
Pratt & Whitney Aircraft Group
Pratt & Whitney Engineering

August 1983

Prepared For
NATIONAL AERONAUTICS AND SPACE ADMINISTRATION
LEWIS RESEARCH CENTER
21000 BROOKPARK ROAD
CLEVELAND, OHIO 44135

Under Contract NAS3-23288

1.REPORT NO.	2. GOVERNMENT AGENCY	3.RECIPIENT'S CATALOG NO.
NASA CR-168220		

4.TITLE AND SUBTITLE	5. REPORT DATE
Creep Fatigue Life Prediction for Engine Hot Section Materials (Isotropic)	August 1983
	6. PERFORMING ORG. CODE
7.AUTHOR(S)	8. PERFORMING ORG. REPT. NO.
Vito Moreno	PWA-5894-17
9.PERFORMING ORG. NAME AND ADDRESS	10. WORK UNIT NO.
UNITED TECHNOLOGIES CORPORATION	
Pratt & Whitney Engineering	11. CONTRACT OR GRANT NO.
	NAS3-23288
12. SPONSORING AGENCY NAME AND ADDRESS	13. TYPE REPT./PERIOD COVERED
National Aeronautics and Space Administration	Annual Report (First)
Lewis Research Center	
21000 Brookpark Road, Cleveland, Ohio 44135	14. SPONSORING AGENCY CODE

15. SUPPLEMENTARY NOTES
Project Manager: G.R. Halford, NASA Lewis Research Center, Cleveland, Ohio

16. ABSTRACT

This report summarizes the activities performed during the first year of the NASA Hot Section Technology (HOST) program, "Creep Fatigue Life Prediction for Engine Hot Section Materials (Isotropic)", being conducted by Pratt & Whitney Aircraft. The program is a two phase effort aimed at improving the high temperature crack initiation life prediction technology for gas turbine hot section components. Significant results produced thus far includes: 1) Cast B1900 and wrought IN 718 selected as the base and alternative materials respectively; 2) Examination of fatigue test specimens indicated that measurable [0.76mm (.030 in.) surface cracks appear early in the specimen lives, i.e., 15% of total life at 871°C(1600°F) and 50% of life at 538°C (1000°C). This has been used as the definition of crack initiation for the initial evaluation work; 3) Observed crack initiation sites are all surface initiated and are associated with either grain boundary carbides or local porosity. The initiation life is not significantly affected by the character of the site. Transgrannular cracking is observed at the initiation site for all conditions tested; and 4) An initial evaluation of two life prediction models, representative of macroscopic (Coffin-Manson) and more microscopic (Damage Rate) approaches, was conducted using limited data generated at 871°C (1600°F) and 538°C (1000°F). In general, the microscopic approach provided a more accurate regression of the data used to determine crack initiation model constants, but overpredicted the effect of strain rate on crack initiation life for the conditions tested.

17. KEY WORDS (SUGGESTED BY AUTHOR(S))	18. DISTRIBUTION STATEMENT
creep fatigue , crack initiation life prediction, Isotropic material	

19. SECURITY CLASS THIS (REPT)	20. SECURITY CLASS THIS (PAGE)	21. NO. PGS	22. PRICE *

[redacted] VA 22161

PREFACE

The Annual Report contained in this document covers the activities performed during the first year of the NASA HOST Program, "Creep Fatigue Life Prediction for Engine Hot Section Materials (Isotropic)", under Contract NAS3-23288 to improve the high temperature crack initiation prediction technology for gas turbine hot section components. This program is being conducted under the direction of Dr. G.R. Halford who serves as the NASA Program Manager. The Program Manager and Principal Investigator at United Technologies Corporation (UTC) is Mr. Vito Moreno of the Structures and Dynamics Group at United Technologies Corporation. Dr. J.L. Lin provided the deformation and failure mode characterizations.

Table of Contents

Section		Page
1.0	INTRODUCTION	1
2.0	SUMMARY	3
3.0	TECHNICAL PROGRESS	6
3.1	Task I - Material/Coating/Component Selection and Acquisition	6
3.1.1	Hot Section Survey and Material Selection	6
3.1.2	Base Material Description	8
3.1.3	Tensile and Creep Characterization	10
3.2	Task II - Screen Candidate Life Prediction Approaches	26
3.2.1	Fatigue Specimen Design, Fabrication, and Test Facility	26
3.2.2	Baseline Fatigue Testing	39
3.2.3	Life Prediction Model Selection	55
3.2.4	Ranking Criteria	60
3.3	Task III - Crack Initiation Model Evaluations	71
3.3.1	- Coffin-Manson Model	72
3.3.2	- Damage Rate Model	77
4.0	FUTURE WORK	84
	REFERENCES	84
	LIST OF DISTRIBUTION	86

SECTION 1.0

INTRODUCTION

The overall operating cost of the modern gas turbine engine is greatly influenced by the durability of combustor and turbine structural components operating at high temperatures. Inadequate durability results in reduced engine efficiency and increased maintenance costs due to premature repair and replacement. To increase the durability of these components, more accurate structural analysis and life prediction methods must be developed for components operating at higher temperatures. However, improvements in the state-of-the art technology for elevated temperature durability prediction have been hampered by 1) the severe operating conditions of the engine, 2) the inability of analytical and life prediction tools used in the design of lower temperature components to predict complex material behavior and interaction of damage mechanisms of components at elevated temperatures, and 3) the high cost of engine development testing which prohibits the accumulation of adequate failure data and local operating conditions required for the systematic development and calibration of durability prediction models.

Traditionally, component durability associated with fatigue cracking has been attributed to separate crack initiation and crack propagation processes. Current cyclic crack initiation prediction methodology is based on correlative fatigue models generally developed to address a specific component or loading configuration. These prediction models are directly calibrated to macroscopically observable and predictable quantities (strain range, mean stress, etc.) and do not address the specific mechanisms associated with the initiation process. This approach has been successful at lower temperatures but its applicability at higher temperatures, where interaction of deformation mechanisms and damage accumulation is strongly temperature dependent, has not been established. This is particularly true for the higher strength isotropic alloys used in gas turbine hot section structures.

The NASA Hot Section Technology (HOST) program is aimed at developing improved life prediction technology for structures operating at elevated temperatures. As part of HOST, the present program will investigate fundamental approaches to high temperature crack initiation life prediction, identify modeling strategies and develop specific models for component relevant loading conditions. The program is a 5-year, 2-part effort (2-year base program plus a 3 year optional program) that will consider two isotropic hot section materials and protective coating systems. Under the base program, various life prediction approaches for high temperature applications will be investigated and basic models for simple cycle, isothermal loading conditions will be selected and developed. Models that address thermomechanical cycling, multi-axial conditions, cumulative loading, environmental effects and cyclic mean stress will be developed under the optional program. These models will be verified on an alternate material.

SECTION 2.0

SUMMARY

This report summarizes the activities performed during the first year of the NASA HOST Program, "Creep Fatigue Life Prediction for Engine Hot Section Materials (Isotropic)", being conducted by Pratt & Whitney Aircraft. The program is a 5-year, two part effort aimed at improving the high temperature crack initiation prediction technology for gas turbine hot section components. The two-year base program comprises the following tasks:

Task I - Material/Coating/Component Selection and Acquisition
Task II - Screen Candidate Life Prediction Approaches
Task III - Evaluate Best Candidate Life Prediction Approach
Task IV - Reporting

Significant results of the program produced thus far are listed below. A discussion of the technical progress of the program is provided in the following section.

The major results of Task I are summarized below:

1. Cast B1900 + Hf and wrought IN 718 were selected as the base and alternate materials, respectively.

2. A single heat of B1900 + Hf was obtained and test specimens fabricated.

3. The material was characterized with respect to grain size, γ' size, carbide distribution, and dislocation density.

4. Monotonic tensile and creep testing has shown engineering properties within anticipated scatter for this material.

5. Examination of the tensile tests has shown a transition from inhomogeneous "planar" slip within the grains at lower temperatures to more homogeneous matrix deformation.

6. Examination of the creep tests has shown a transgranular failure mode at 760°C (1400°F) and an intergranular failure mode at 871°C (1600°F) and 982°C (1800°F).

The major accomplishments/results of Task II include:

1. A study was conducted that investigated the effects of test specimen geometry and fabrication process on fatigue life. As a result, the axial strain controlled specimens were designed with a smooth (no extensometer ridges) gage section and fabricated using centerless grinding followed by light electropolishing.

2. A fatigue test matrix was established to provide baseline data to define crack initiation life as a function of major variables and for life prediction model evaluation. A total of 43 fully reversed strain controlled fatigue tests have been completed. Major variables investigated were temperature [871°C(1600°F) vs 538°C(1000°F)], strain range and strain rate.

3. Examination of specimens during testing indicated that measurable .76mm(.030 in.) surface cracks appear early in the specimen cycle lives; i.e., 15% of total life at 871°C(1600°F) and 50% of life at 538°C(1000°F). This has been used as the definition of crack initiation for the initial model evaluation work.

4. Observed crack initiation sites are all surface origins associated with either grain boundary carbides or local porosity. The initiation life is not significantly affected by the character of the site.

5. Transgrannular cracking is observed at the initiation site for all conditions tested.

6. Grain dislocation structure is significantly less than that observed in monotonic tensile or creep tests.

7. A ranking procedure for evaluation of the prediction models has been established. The procedure assigns a numerical score based on the amount of data required, the predictive capability and the adaptability to engine relevant loading conditions for each model considered.

Task III obtained the following results:

1. Life prediction models representative of macroscopic (Coffin-Manson) and microscopic (Damage-Rate) approaches were selected for preliminary evaluation using the model ranking procedure developed in Task II.

2. Using limited data obtained at 871°C (1600°F - (2 strain rates) and 538°C (1000°F) - (1 strain rate), the macroscopic approach obtained a higher overall score on the basis of data requirements and predictive capability but scored lower than the microscopic model on the application to more complex loading cycles.

SECTION 3.0

TECHNICAL PROGRESS

3.1 TASK I - MATERIAL/COATING/COMPONENT SELECTION AND ACQUISITION

3.1.1 Hot Section Survey and Material Selection

A survey was conducted of the isotropic materials and surface protection coating systems currently in use in the hot section of commercial gas turbine engines. The results of the survey, shown in Table I, indicate that the predominant hot section materials are high strength nickel base alloys in either cast or wrought form. Furthermore, the surface protection coating systems currently can be classified as either diffusion aluminide or overlay. A recommendation identifying the materials and coating systems for the base and option programs was submitted to the NASA Program Manager who approved the following selections:

Base Material: Cast B1900 + Hf (PWA 1455)
Alternate Material: Wrought IN 718 (AMS 5663)
Coatings: Diffusion Aluminide (NiAl)/Overlay (MCrAlY)

These selections provide an opportunity to investigate generic creep-fatigue crack initiation mechanisms and life prediction approaches for a wide range of relevant hot section materials and applications. The use of cast and wrought alloys allows the development and examination of life prediction models for two materials having the same matrix (Ni) but significantly different composition and microstructure (e.g., high vs low volume fraction γ'). The selection of a diffusion and an overlay coating also provides a variation in composition and microstructure and will be useful in developing mechanistically based life prediction models. These material/coating systems provide the broadest range of generic information consistent with the goals of the HOST program.

Table I

Hot Section Materials and Surface Protection Coating Systems

Material Designation	Form/Base	Usage/Comments
B1900 + Hf (PWA 1455)	Cast - Ni	o High Pressure Turbine (HPT) Blade and Vane Application o Potential Segmented Combustor Use
IN 792 (PWA 1467)	Cast + HIP - Ni	o Sideplate and Vane Application
IN 713C (PWA 655)	Cast - Ni	o Extensive Low Pressure Turbine (LPT) Vane Application o HPT Sideplate Application
MAR-M-509 (PWA 647)	Cast - Co	o HPT 1st Vane Application o Strategic Material
IN 718 (AMS 5662)	Wrought - Ni	o Extensive Projected Use in Hot Section Static and Rotating Structures
Hastelloy X (PWA 1038)	Wrought - Ni	o Combustor Liner Sheet Alloy o Single Phase Alloy - Conclusions may not be Relevant to Other Hot Section Superalloys
Haynes 188 (PWA 1042)	Wrought - Co	o Combustor Liner Sheet Alloy o Strategic Material
Coating Type	**Composition**	**Comments**
Diffusion Aluminide	NiAl	o Extensive Blade and Vane Application o State of the Art for Oxidation Coatings
Overlay	MCrAlY	o Different Composition and Microstructure o Compatible with Application of Thermal Barrier

3.1.2 Base Material Description

The B1900 + Hf material selected for the program was part of a single heat, designated W-0098, obtained from Certified Alloy Products Inc., Long Beach, California. The chemical composition of this heat is compared to nominal specifications in Table II. A total of 2500 pounds of material was obtained for specimen fabrication.

Table II

Chemical Composition of B1900 + Hf (Heat W-0098)

Element	Nominal (%)	Heat W-0098
C	0.11	0.09
Cr	8.0	7.72
Co	10.0	9.91
Mo	6.0	5.97
Al	6.0	6.07
Ta	4.3	4.21
Ti	1.0	0.99
B	0.015	0.016
Zr	0.08	0.04
Fe	0.35*	0.17
W	0.1*	0.04
Cb	0.1*	0.08
Bi	0.5 ppm	0.1
Pb	10.0 ppm	0.1
Hf	1.5	1.19
Ni	Remainder	Remainder

*Maximum

Two casting geometries were selected for specimen fabrication. The "standard" bar shown in Figure 1A was initially selected because it could accommodate all anticipated test specimen configurations. The constant section bar (Figure 1B) was later cast to investigate the effects of porosity on material properties (see Section 3.1.4). For both bar geometries the casting parameters, melt and mold temperatures, were established to produce a uniform small grain size in each bar. This would result in a large number of grains in a specimen cross-section and insure an "isotropic" material response.

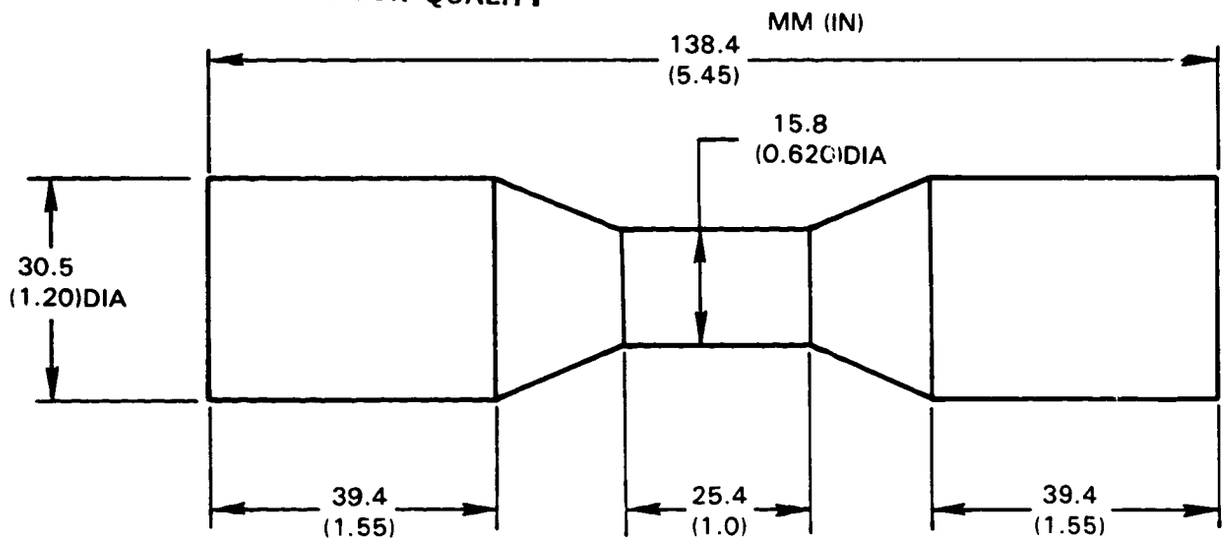

(A) "Standard" Bar Configuration

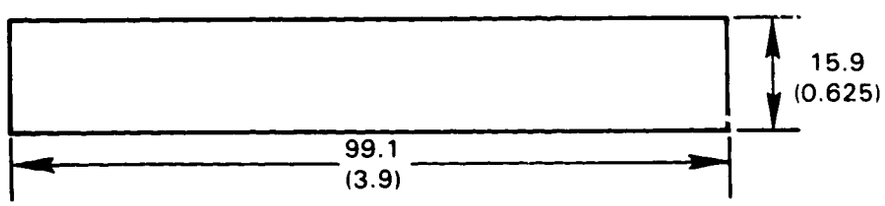

(B) Constant Section Bar

Figure 1 Casting Geometries Used for Test Specimens

All bars were fully heat treated prior to machining. The heat treatment cycle included:

Solution - 1079 ± 14°C (1975 ± 25°F) for 4 hours; air cool

Precipitation - 899 ± 14°C (1650 ± 25°F) for 10 hours; air cool

For future reference, all cast bars were given an identifying designation. The "standard" bars were cast four bars at a time. The molds were numbered sequentially from number one, with individual bars designated A, B, C or D. The cylindrical bars were numbered sequentially starting with 647.

The structure of the material was documented in both the as-cast and fully heat treated condition using optical, SEM and TEM techniques. The following observations were made:

1. Use of a micrograph (300X) showed the grain size of both the as-cast and fully heat treated material to be between ASTM No. 1 and 2. This represents an average grain diameter of 0.018 cm (0.007 in) to 0.025 cm (0.010 in) which should produce isotropic stress and strain conditions in the test specimens. A comparison of the micrographs and the ASTM standard is shown in Figure 2.

2. The replica technique was used to study the gamma prime, γ', size and distribution within the grains. In the as-cast material, the γ' size was 0.6 μm while the fully heat treated material showed an increase in size to 0.9 μm (see Figure 3).

3. MC carbides were observed in the grain boundaries of both the as-cast and fully heat treated material (see Figure 4). Microprobe analysis indicated that the carbides are enriched in Ta, Ti, Mo, and Hf.

4. For future assessment of deformation accumulated in specimens after testing, initial dislocation density measurements were made. Representative dislocation networks for the as-cast and fully heat treated materials are shown in Figure 5. Calculated densities are about $9.3 \times 10^9/cm^2$ for the as-cast material and about $5.7 \times 10^9/cm^2$ for the fully heat treated material.

3.1.3 Tensile and Creep Characterization

Monotonic tensile and creep testing of B1900 + Hf specimens was conducted to document typical engineering quantities and define deformation and failure mechanisms. Specimen geometries used for this testing are shown in Figure 6.

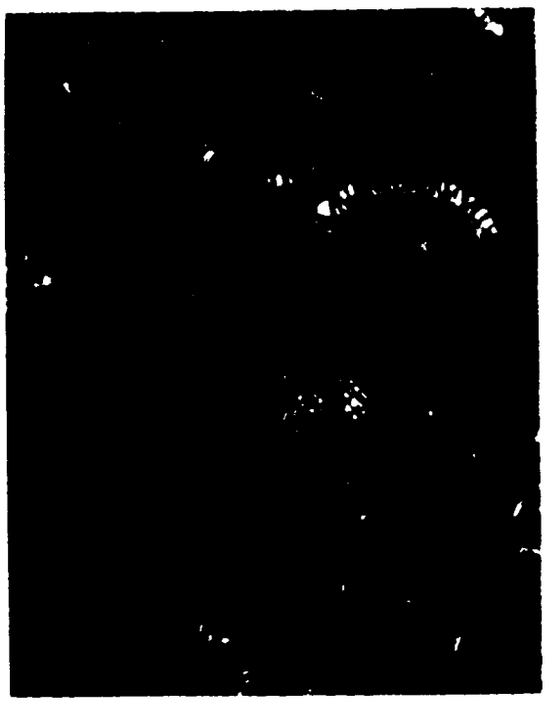

AS-CAST

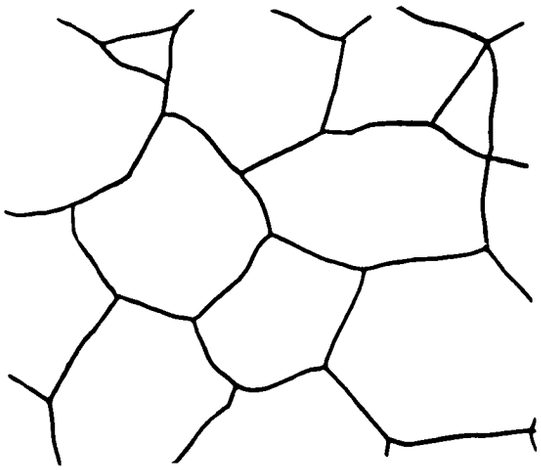

ASTM STANDARD No. 1 100 μm

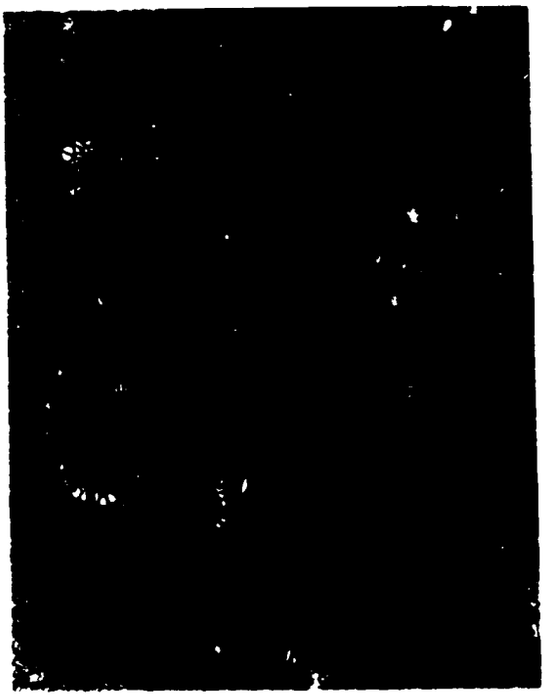

FULLY HEAT TREATED

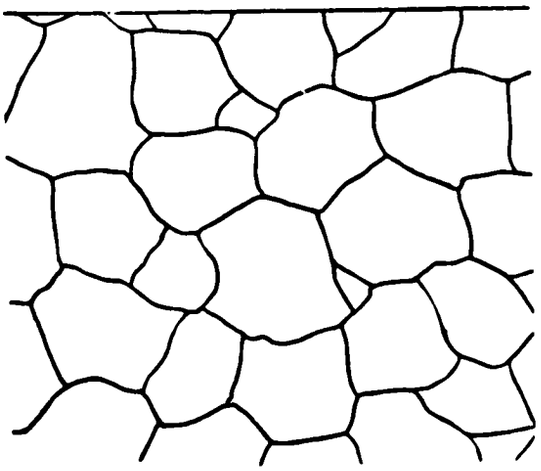

ASTM STANDARD No. 2 100 μm

Figure 2 Grain Size of As-Cast and Fully Heat Treated Material

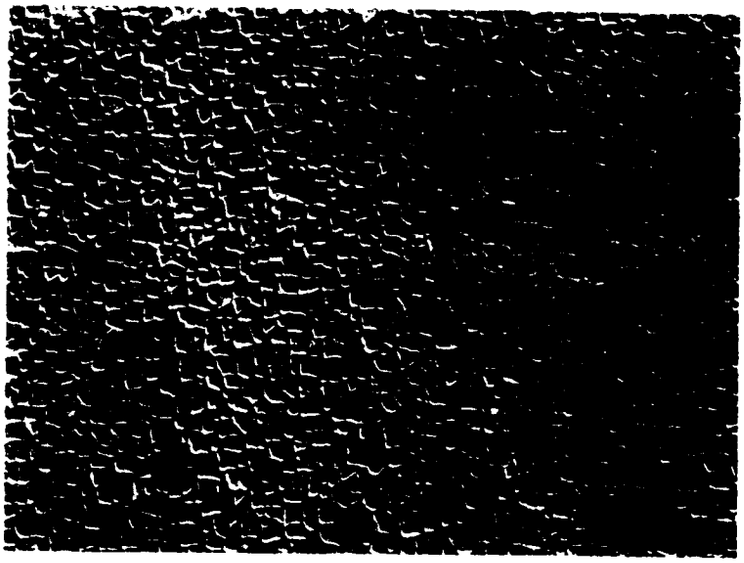

As-Cast $\gamma' = 0.6\,\mu m$ 10μm

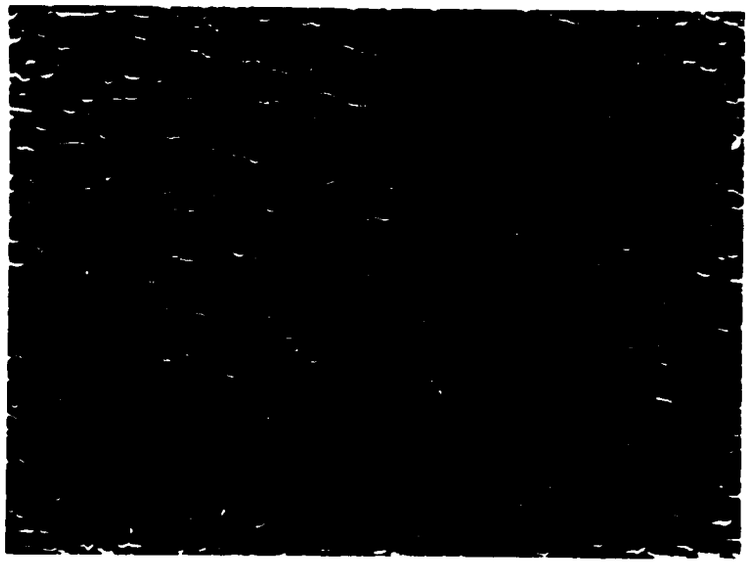

Fully Heat Treated $\gamma' = 0.9\,\mu m$ 10μm

Figure 3 Gamma Prime (γ') Shows Increase with Heat Treatment

As-Cast

Fully Heat Treated

Figure 4 Typical Distribution of Carbides Along Grain Boundaries

As-Cast $\rho = 9.3 \times 10^9/cm^2$ 1μm

Fully Heat Treated $\rho = 5.7 \times 10^9/cm^2$ 1μm

Figure 5 Dislocation Networks for As-Cast and Fully Heat Treated Materials

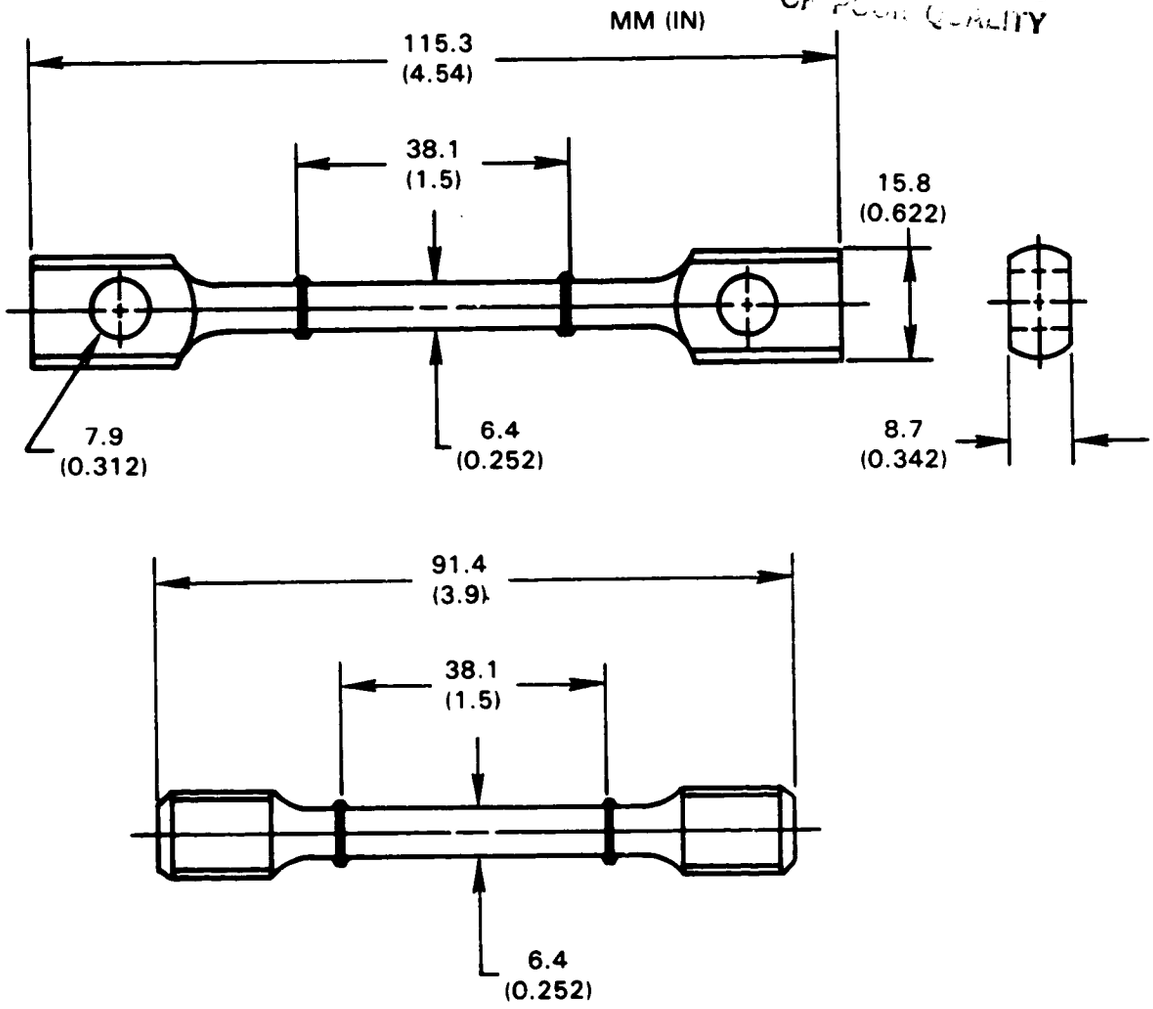

Figure 6 Test Specimens for Monotonic Tensile and Creep Testing

Tensile Tests

A total of 21 monotonic tensile tests have been conducted to date. A summary of all test conditions and observed properties is presented in Table III. A majority of the tests were run at the ASTM standard rate of 0.005 $min.^{-1}$. Several tests were also conducted at 0.0005 min^{-1} to investigate rate effects on the tensile properties. As indicated, a number of tests terminated with fracture occurring outside of the gage section of the specimen. Despite these failures, most of the properties measured early in these tests (e.g., modulus, 0.2% yield) are consistent with results obtained from tests in which failure occurred within the specimen gage section. An examination of these specimens suggested that the tendency to fail outside the gage section is

Table III

Summary of Tensile Testing

Temp. C(°F)	Spec. ID	$\dot{\varepsilon}$ min^{-1}	Ex10^{-3} MPa(KSI)	.2% Yield MPa(KSI)	Ult. MPa(KSI)	Elong %	RA %	Comments
RT	18A	0.005	187.5(27.2)	714(103.5)	-	4.1	5.9	
260(500)	18B	0.005	169.6(24.6)	702(104.8)	888(128.8)	8.3	10.7	
538(1000)	2A	0.005	149.6(21.7)	727(105.4)	-	-	-	stopped at 1.5% for exam
649(1200)	19A	0.005	143.4(20.8)	701(101.7)	-	4.7	7.2	
760(1400)	2C	0.005	150.3(21.8)	709(102.8)	-	-	-	O.G.[1]
	2D	0.005	122(17.7)	721(104.6)	796(115.5)	-	-	O.G.
	38B	0.005	144.1(20.9)	739(107.2)	-	-	-	O.G.
	650[2]	0.005	157.8(22.9)	709(102.8)	955(138.5)	8.0	9.1	
	38A	0.0005	122.7(17.8)	774(112.3)	-	-	-	O.G.
	647	0.0005	146.8(21.3)	709(102.8)	947(137.4)	7.8	7.6	
871(1600)	19B	0.005	146.9(21.3)	650(94.6)	-			stopped at 1% for exam.
	39B	0.005	147.5(21.4)	677(98.3)	-	-	-	O.G.
	651	0.005	131(19.0)	640(92.8)	792(114.8)	5.7	6.8	
	39A	0.0005	156.5(22.7)	490(71.1)	-	-	-	stopped at 1% for exam.
	648	0.0005	146.8(21.3	626(90.8)	780(113.1)	5.7	5.3	
982(1800)	20A	0.005	117.2(17.0)	355(51.5)	-	-	-	stopped at 1% for exam.
	41B	0.005	111(16.1)	349(50.6)	470(68.1)	6.5	5.0	
	652	0.005	135.8(19.7)	340(49.3)	492(71.4)	7.7	8.8	
	41A	0.0005	119.3(17.3)	281(40.7)	-	-	-	stopped at 1% for exam.
	649	0.0005	144.1(20.9)	283(41.1)	471(68.3)	6.5	7.2	
1093(2000)	20B	0.005	101.3(14.7)	168(24.3)	-	-	-	stopped at 1% for exam.

[1] fractured outside gage section
[2] specimens 648 - 652 machined from 5/8 inch diameter bars

associated with a higher degree of porosity at the thicker ends of each casting as illustrated in Figure 7. To further investigate these failures, a series of specimens was fabricated from 15.9mm(5/8") diameter cylindrical bars. While cast with the same parameters as the previous castings, tne cylindrical shape was thought to produce a more uniform distribution of porosity. To date, six tensile tests have been run with these specimens (designated 647 to 652). As shown in the table, the tensile properties are consistent with previous tests and all failures have occurred in the specimen gage section.

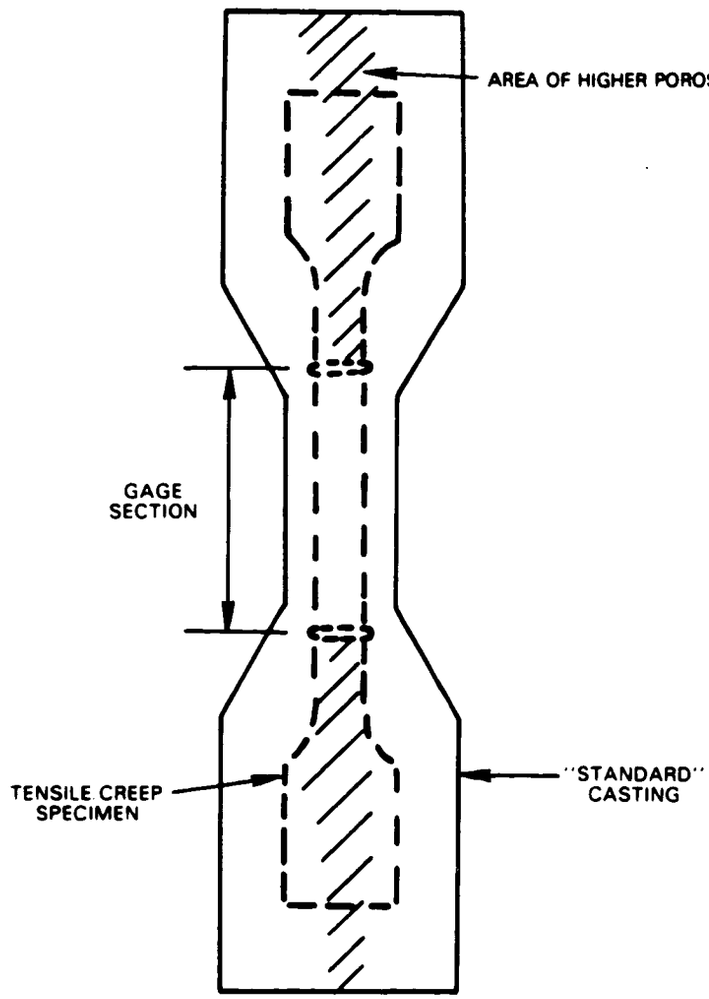

Figure 7 Observed Area of Higher Porosity in As-Cast Bar

Comparisons of the 0.2% yield strength and measured static modulus of elasticity vs the anticipated representative scatter in B1900 + Hf are presented in Figures 8 and 9. Representative stress - strain responses at various test temperatures are shown in Figure 10.

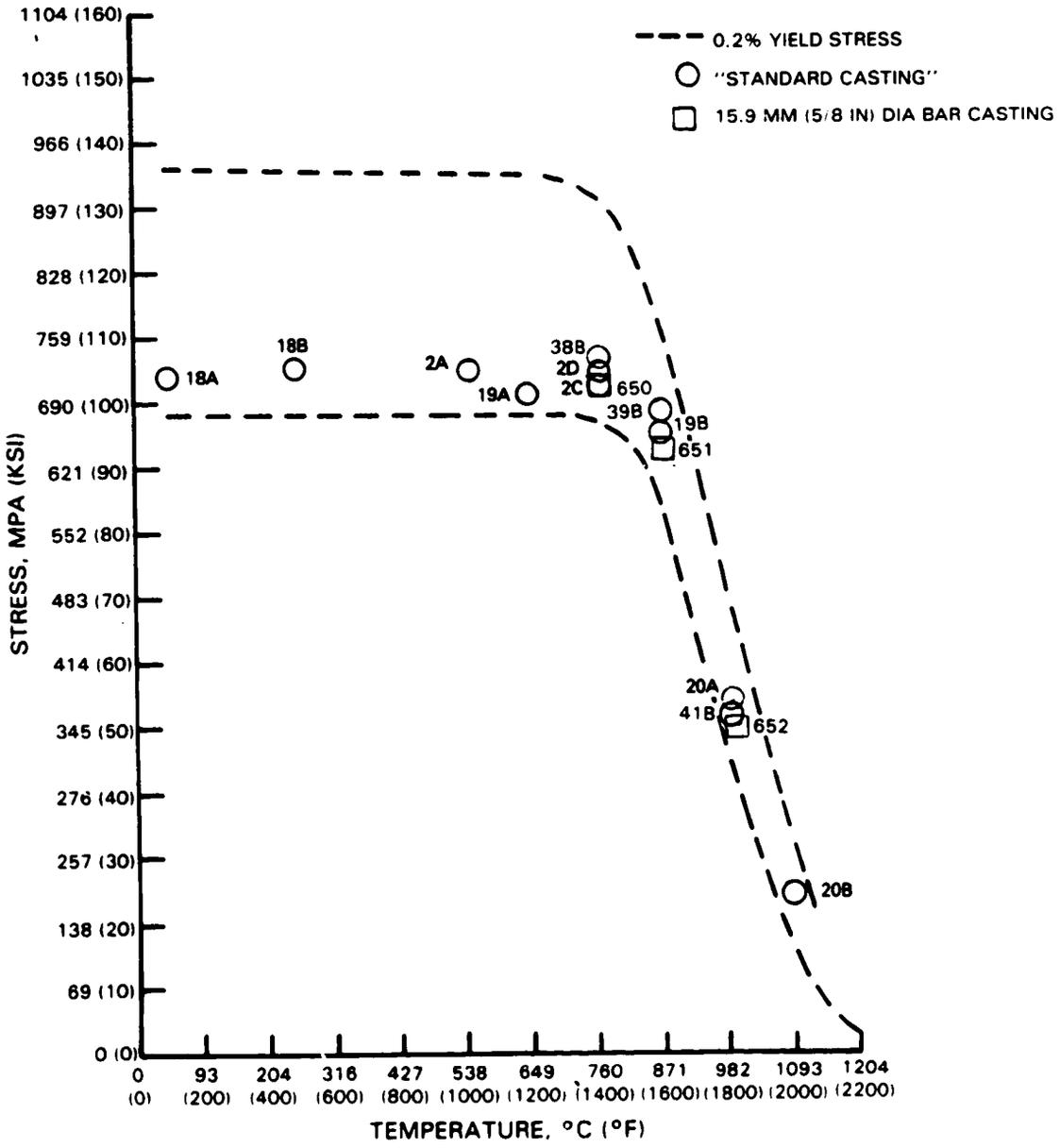

Figure 8 0.2% Yield Stress vs Representative Scatter (B1900 + Hf)

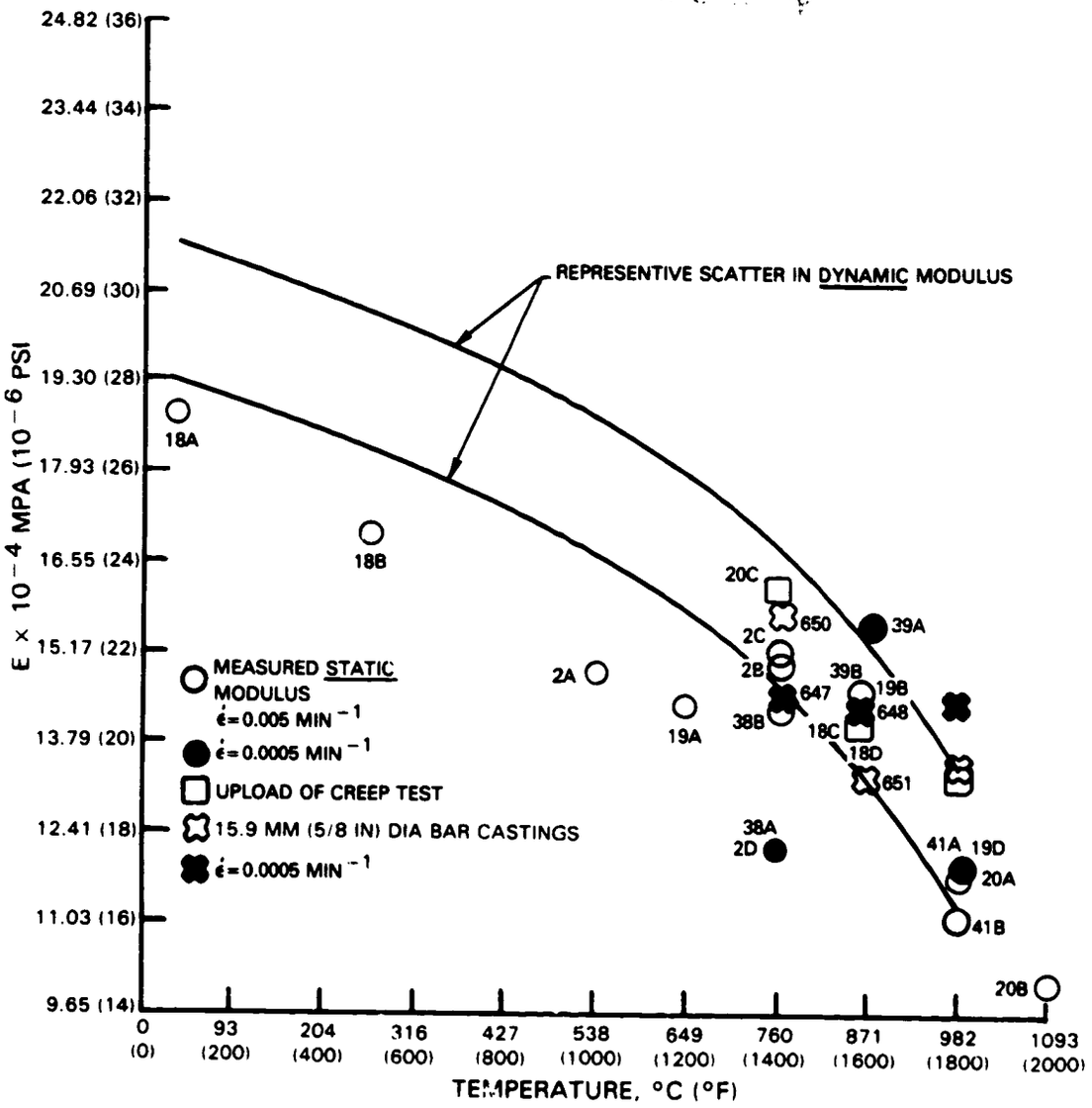

Figure 9 Measured Static vs Dynamic Modulus (B1900 + Hf)

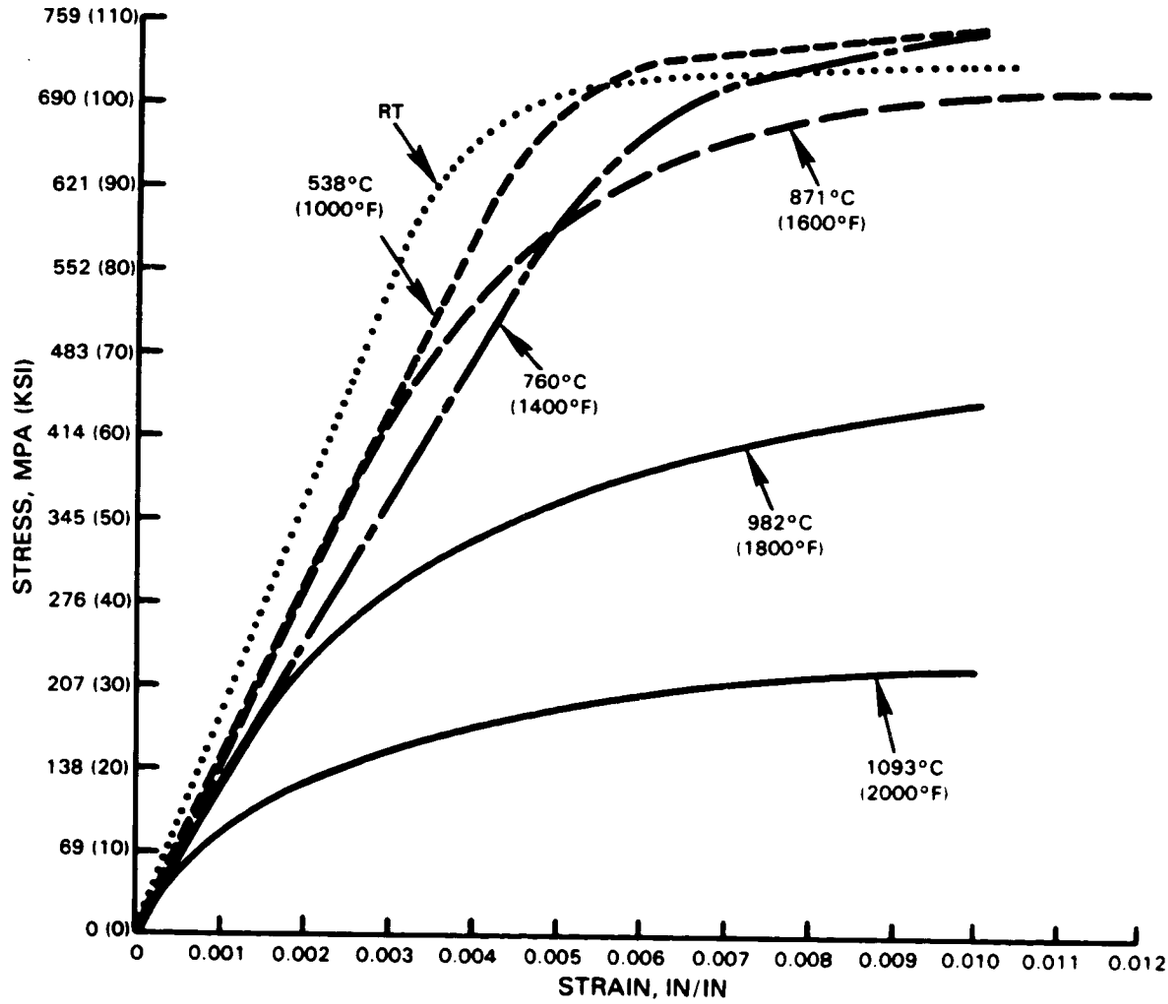

Figure 10 Monotonic Tensile Response - $\dot{\epsilon} = .005\ \text{min}^{-1}$

Six specimen tests were terminated at approximately 1 - 1.5% strain for examination to characterize the change in dislocation structure with increasing temperature. As expected, the lower temperature $\leq 871°C (\leq 1600°F)$ deformation is characterized by inhomogeneous slip as illustrated by the 760°(1400°F) deformation shown in Figure 11. At higher temperatures, a transition between the inhomogeneous "planar" slip to more homogeneous matrix deformation in the grains is observed. The deformation at 1093°C(2000°F) is shown in Figure 12. A composite for all the temperatures examined at the same strain is presented in Figure 13. Note that microtwins were observed in the latter stages of deformation ($\approx 4.5\%$) at 760°C(1400°F).

Figure 11 Planar Deformation at 1400°F

Figure 12 Homogeneous Matrix Deformation at 2000°F

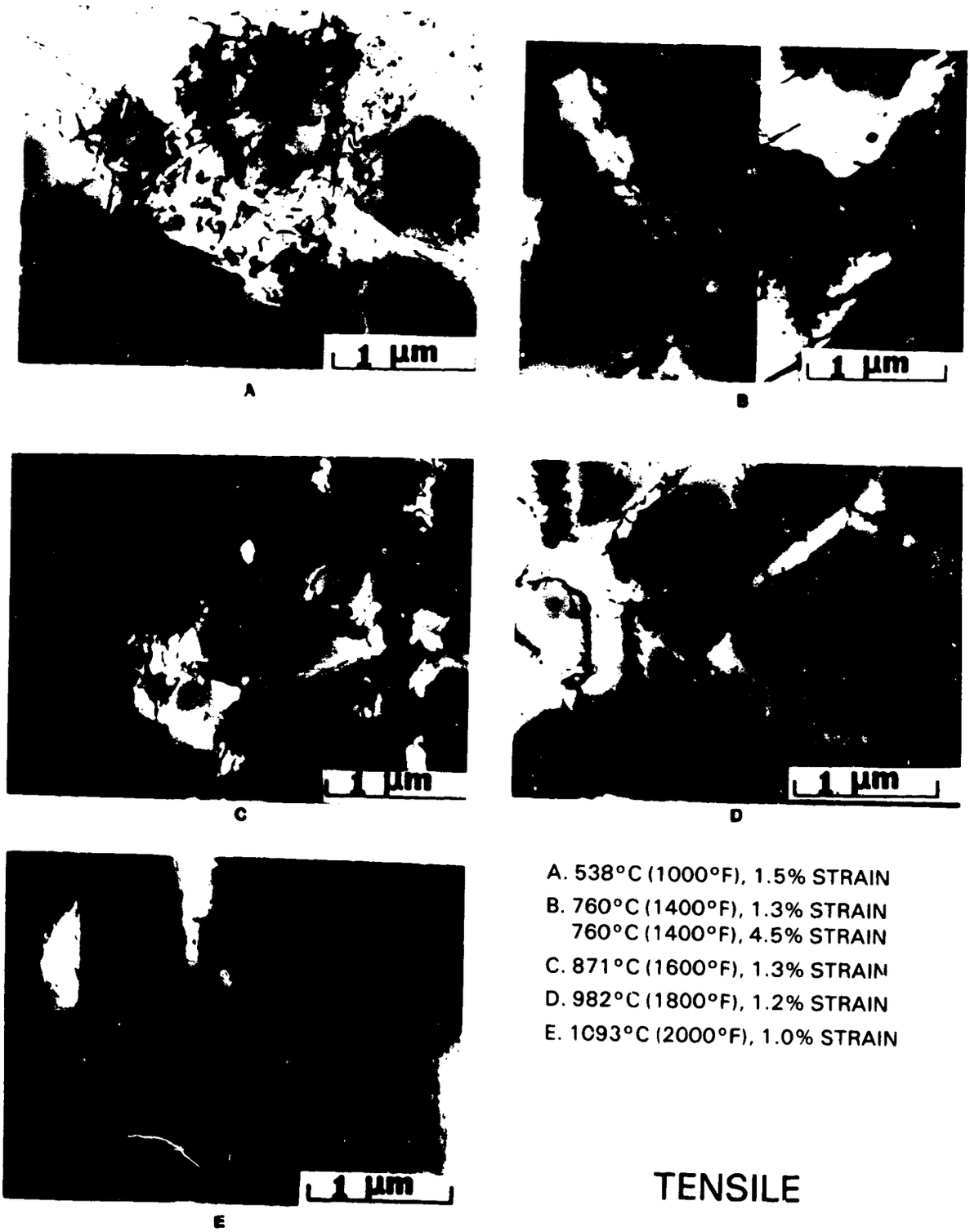

Figure 13 Composite TEM Photos of Tensile Tested B-1900 Hf Specimens at Various Temperatures

Creep Tests

A summary of the test conditions and observed properties for all eleven monotonic creep tests conducted to date is presented in Table IV. As indicated, the tests were conducted at three temperatures [760°C (1400°F), 871°C(1600°F), 982°C(1800°F)] and at stress levels representing 50, 75, 90 or 100% of the bottom of the yield stress scatter band. Using this approach, it was found that the normalized stress reduces the apparent temperature effect for specimens having the same deformation mode. Figure 14 shows the observed rupture lives and the anticipated scatter for this material. Specimens tested at 871°C(1600°F) and 980°C(1800°F) have similar rupture lives for the same normalized stress, while specimens tested at 760°C(1400°F) show a significantly longer life for the same, or higher, normalized stress level. This effect can also be observed in the secondary, or steady state creep rates for these specimens (see Figure 15).

Table IV

Summary of Creep Test Results

Specimen	Temp. °C(°F)	Stress MPa(KSI)	% Min. Yield	Fracture*	Life (Hrs.)	Secondary Creep Rate (Min^{-1})	Elong. %	RA %
19C	982(1800)	234(34)	75	I	20.6	2.5 E-05	6.0	7.8
19D	982(1800)	283(41)	90	I	4.1	0.7 E-04	3.0	2.4
39C	982(1800)	283(41)	90	**	2.9	2.0 E-04	5.5	5.5
18C	871(1600)	427(62)	75	I	18.2	2.5 E-05	3.2	4.9
40B	871(1600)	427(62)	75	**	20.3	1.5 E-05	2.26	2.7
18D	871(1600)	517(75)	90	I	2.8	1.0 E-04	3.2	5.4
40A	871(1600)	517(75)	90	**	2.5	1.25 E-04	2.3	3.5
41C	871(1600)	283(41)	50	**	441	3.0 E-07	2.6	**
20C	760(1400)	600(87)	90	T	134.8	**		3.1
20D	760(1400)	669(97)	100	T	30.2	7.9 E-06	2.9	9.4
39D	760(1400)	669(97)	100	**	49.8	7.5 E-05	3.78	5.9

*I = Intergranular
T = Transgranular
** Not Available

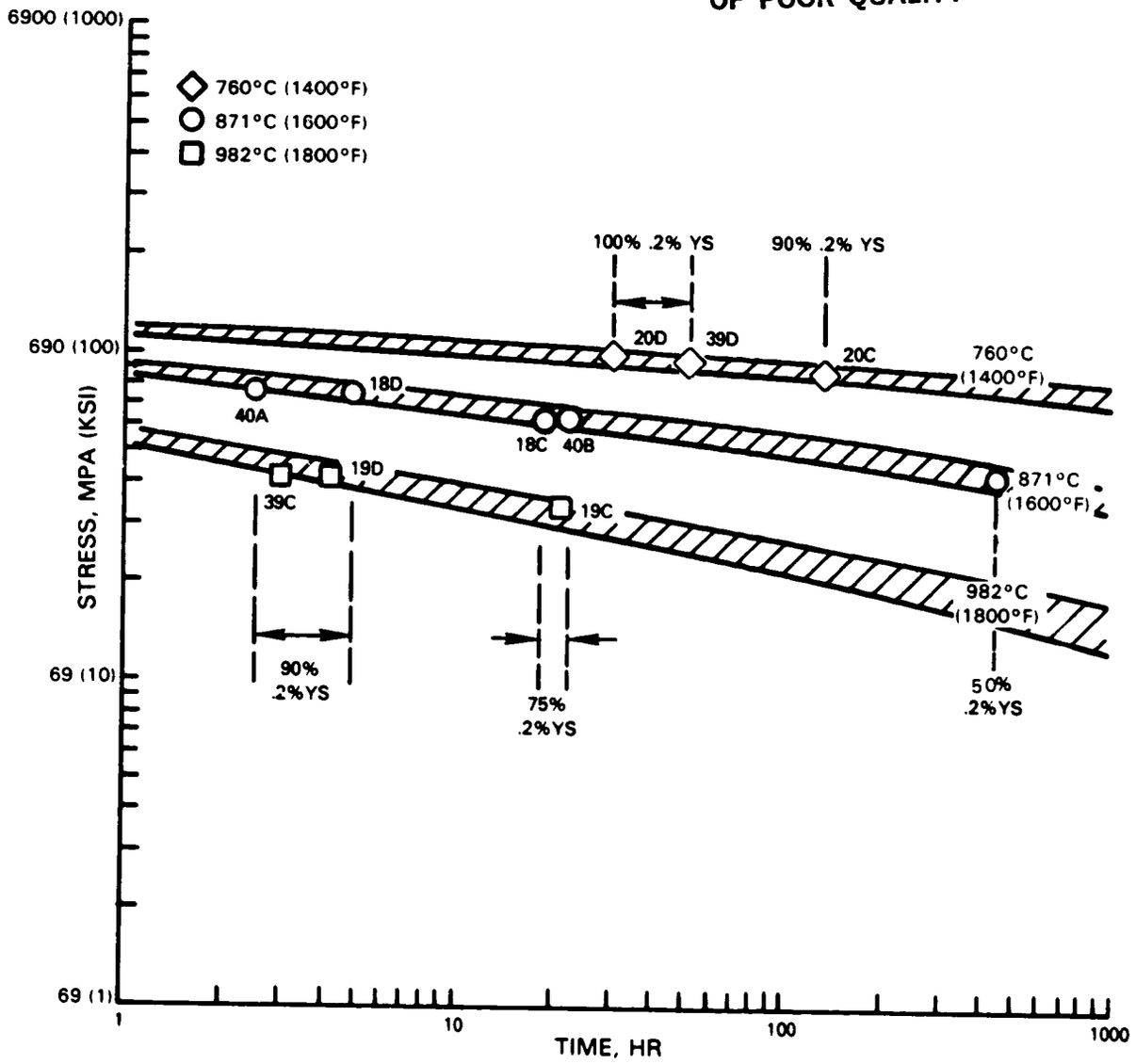

Figure 14 Specimen Rupture Life vs Representative Rupture Life Scatter Bands

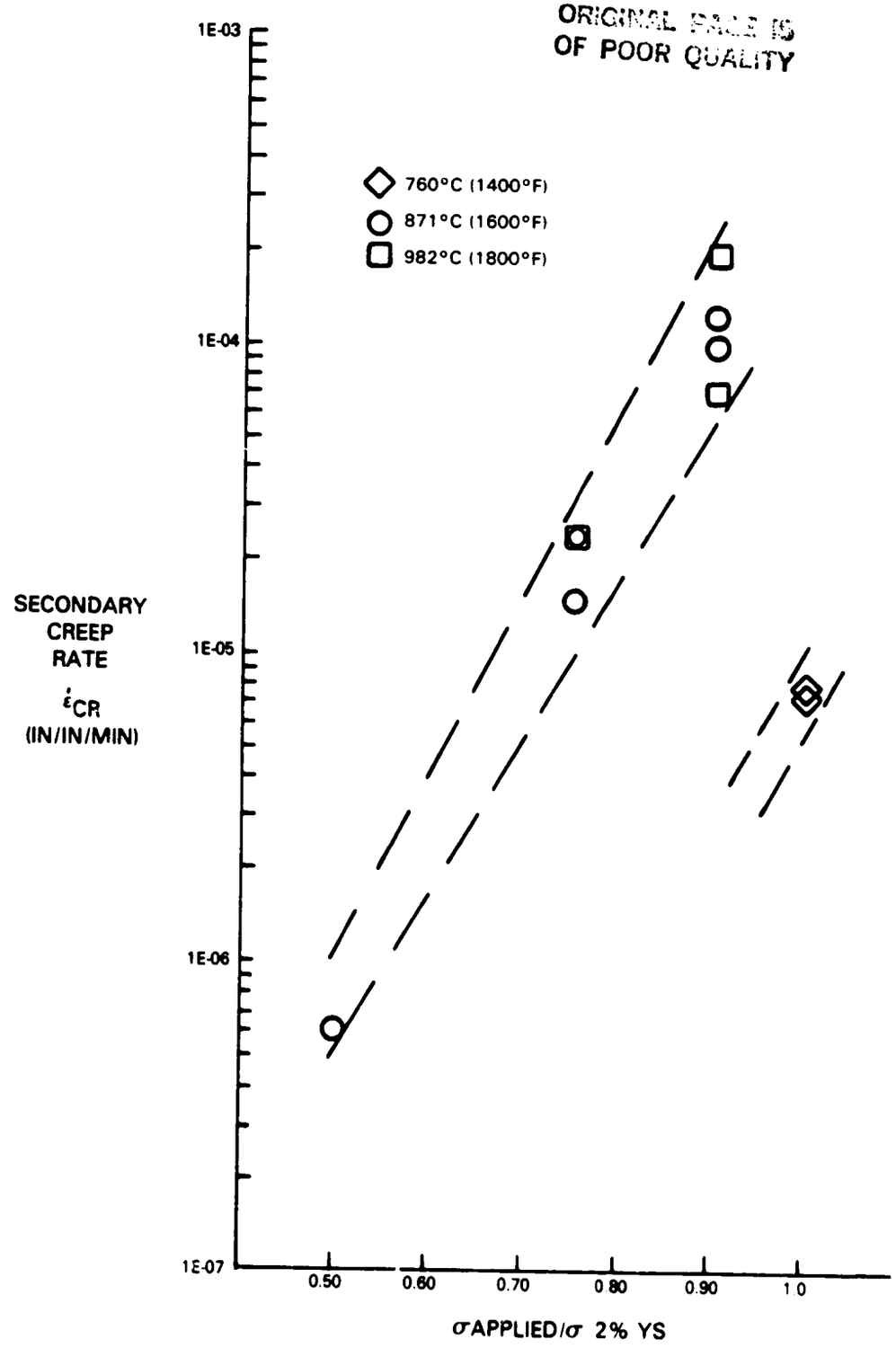

Figure 15 Secondary Creep Rate vs Normalized Stress

Examination has shown that at the higher temperatures [871°C(1600°F) and 982°C(1800°F)] the specimens failed in an intergranular cracking mode, while the specimens tested at 760°C(1400°F) showed a greater tendency for transgranular cracking (see Figures 16 through 19). Substantial differences in the grain dislocation structure were also observed. In specimens tested at 1800°F and 1600°F (Figures 20 and 21), dislocation networks surrounding the gamma prime (γ') particles are the dominant features. This is an indication of a loss of coherency of the γ' and the matrix. At 1400°F, no dislocation network is observed; instead short segments of dislocation and microtwins (similar to the tensile tests) are inhomogeneously dispersed throughout the grains. The presence of the microtwins at this temperature may account for the tendency of cracks to progress in a transgranular manner.

A comparison of the percent elongation observed in the specimens during the monotonic tensile and creep testing is presented in Figure 22. As indicated, the creep elongation is generally smaller than the tensile elongation.

3.2 TASK II - SCREEN CANDIDATE LIFE PREDICTION APPROACHES

3.2.1 Fatigue Specimen Design, Fabrication and Test Facility

The three axial, strain control specimen designs used in the initial fatigue testing are shown in Figure 23. Type A has integral, large extensometer ridges; type B has integral "mini" ridges; and type C is a smooth cylindrical gage section design. An initial group of 18 specimens was fabricated to investigate machining and geometry effects on fatigue life. Six type A specimens were electrochemically ground and six each of types B and C were centerless ground from "standard" B1900 + Hf castings (see Figure 1A). All specimens were then electrochemically polished. Fully reversed, strain controlled fatigue tests were conducted at:

$$871°C(1600°F),\ \Delta\epsilon = \pm 0.25\%,\ \dot{\epsilon} = 1.67\ E\text{-}03\ S^{-1}$$
$$538°C(1000°F),\ \Delta\epsilon = \pm 0.25\%,\ \dot{\epsilon} = 1.67\ E\text{-}03\ S^{-1}$$

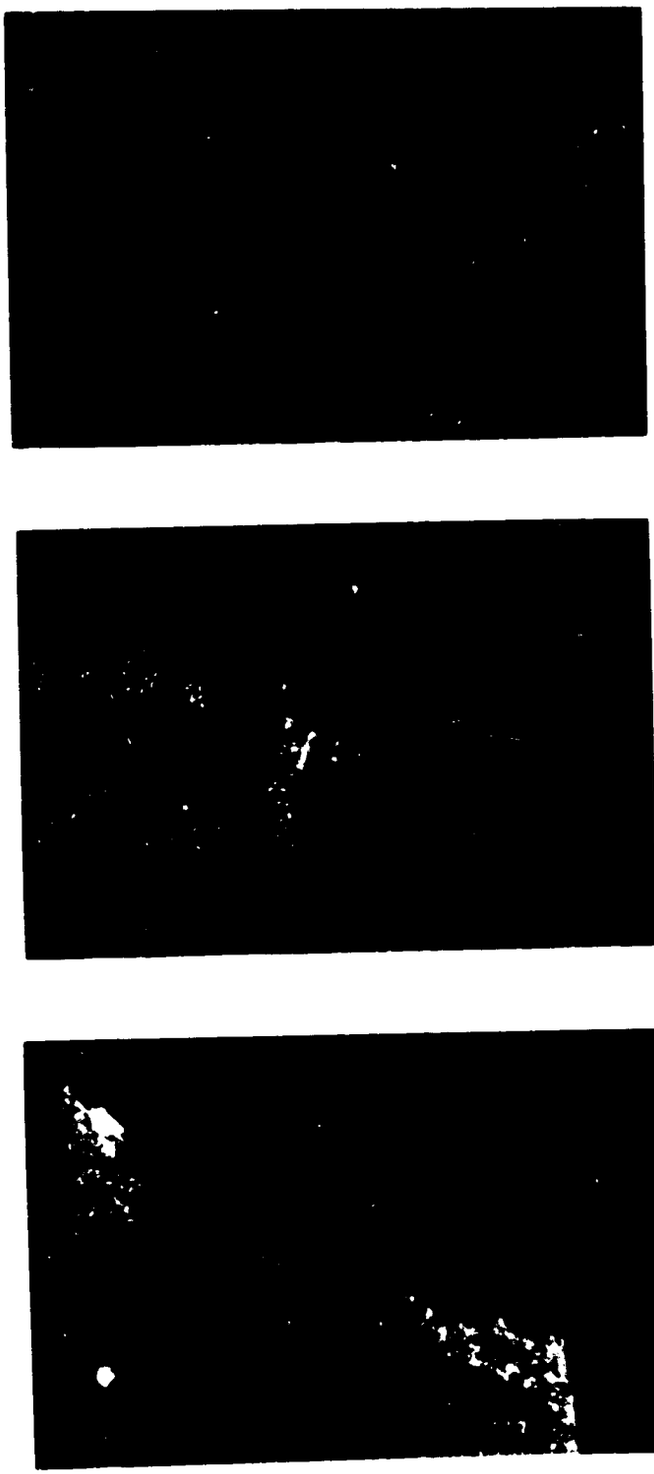

Figure 16 Creep Fracture Mode

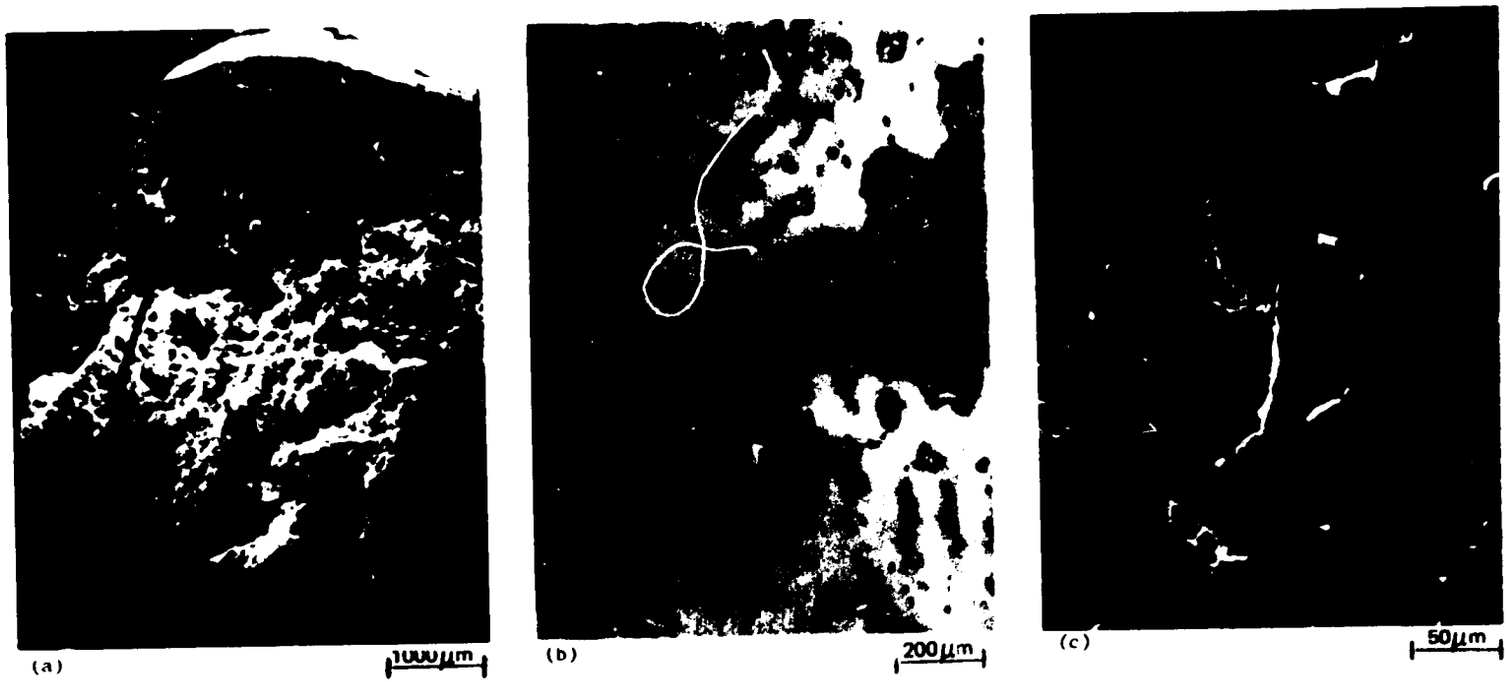

Figure 17 Specimen 19C After Being Creep Tested at 982°C/234 MPa (1800°F/34 ksi) for 20.6 Hours. (a) Heavily oxidized fracture surface (b) Longitudinal section along Line AA' showing intergrannular fracture by optical microscopy (c) Longitudinal section along line AA' showing intergrannular fracture by SEM.

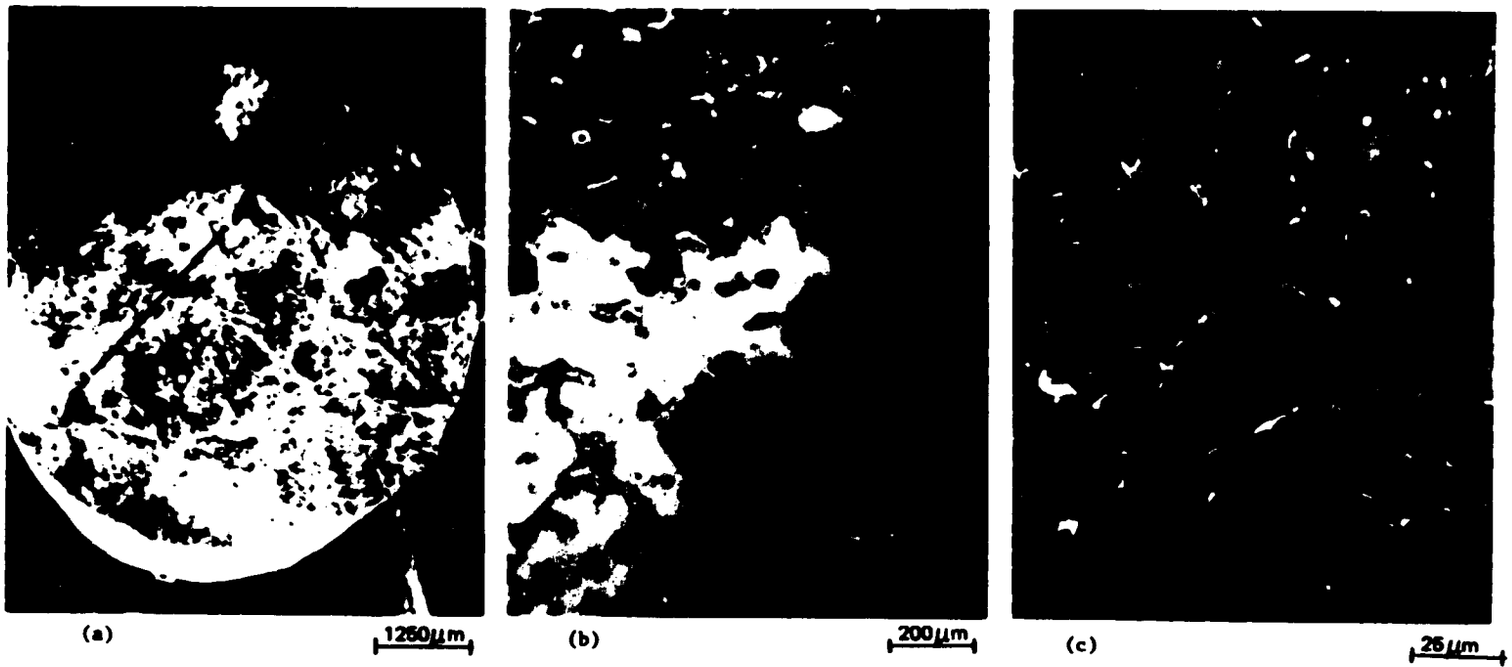

Figure 18 Specimen 18C After Being Creep Tested at 871°C/427 MPa (1600°F/62 ksi) for 18.2 Hours. (a) Heavily oxidized fracture surface (b) Longitudinal section along Line AA' showing intergrannular fracture by optical microscopy (c) Longitudinal section along line AA' showing intergrannular fracture by SEM.

Figure 19 Specimen 20C After Being Creep Tested at 760°C/600 MPa (1400°F/87 ksi) for 134.8 Hours. (a) Heavily oxidized fracture surface (b) Longitudinal section along Line AA' showing intergrannular fracture (transgrannular) by optical microscopy (c) Longitudinal section along line AA' showing no indication of intergrannular fracture by SEM.

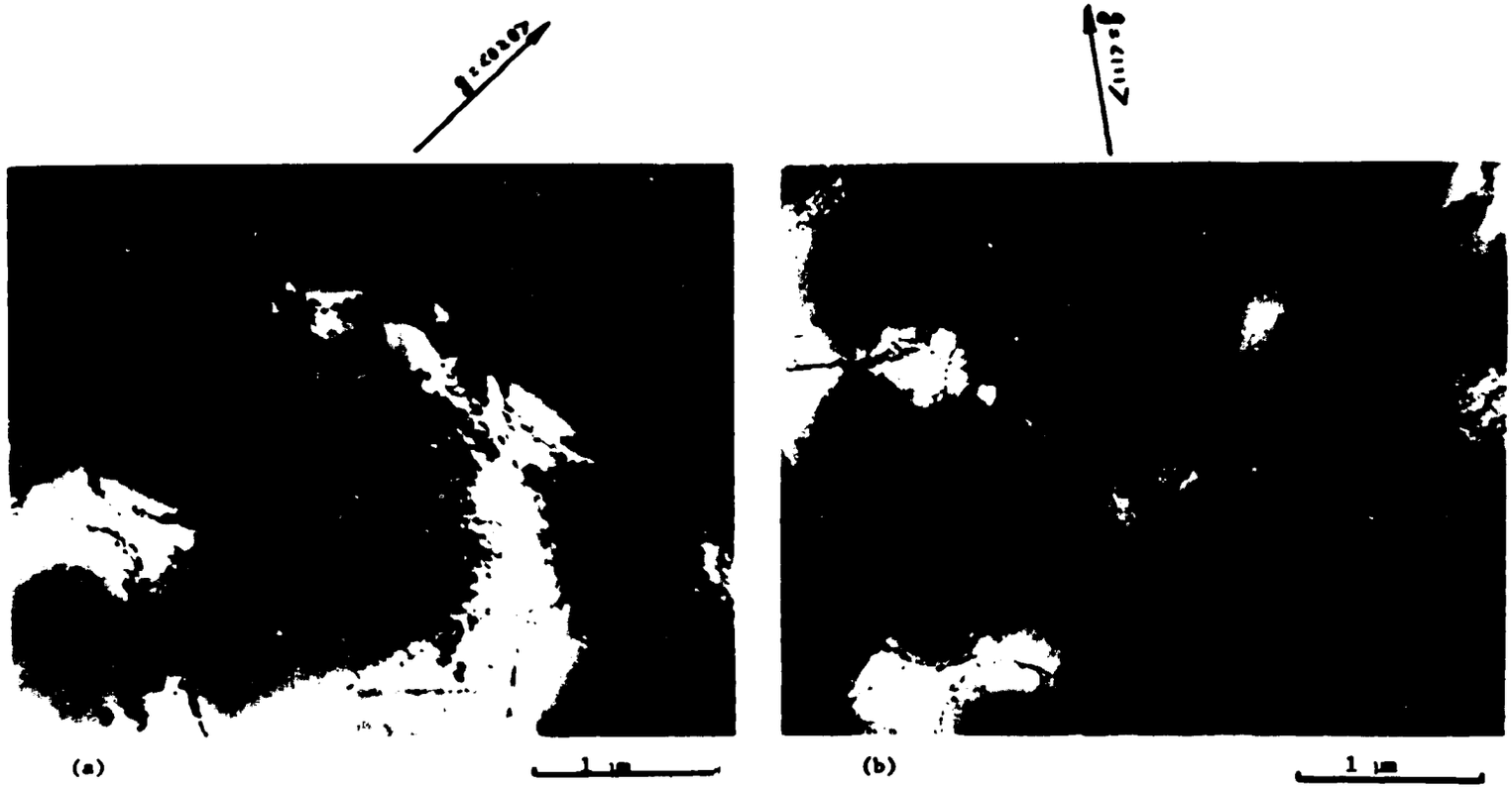

Figure 20 Dislocation Networks Surrounding Gamma Prime Indicate Loss of Coherency Between γ/γ'.(a) Specimen 19C after being creep tested at 982°C/234 MPa (1800°F/34 ksi) for 20.6 hours (b) Specimen 19D after being creep tested at 982°C/283 MPa (1800°F/41 ksi) for 4.1 hours.

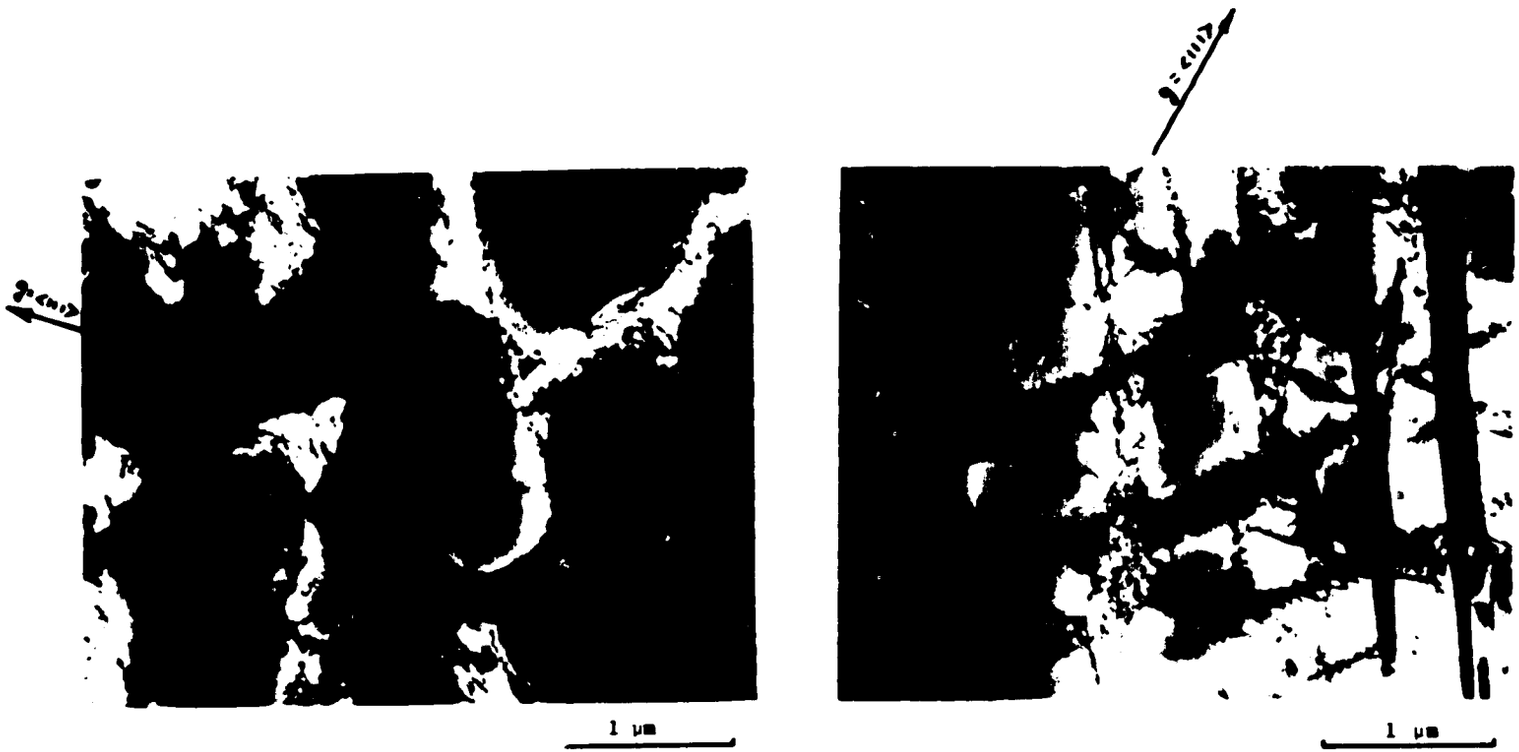

Figure 21 Dislocation Networks Surrounding Gamma Prime Indicate Loss of Coherency Between γ/γ'. (a) Specimen 18C after being creep tested at 871°C/427 MPa (1600°F/62 ksi) for 20.6 hours (b) Specimen 20C after being creep tested at 760°C/600 MPa (1400°F/87 ksi) for 134.8 hours. Dislocation segments and microtwins are the characteristic features.

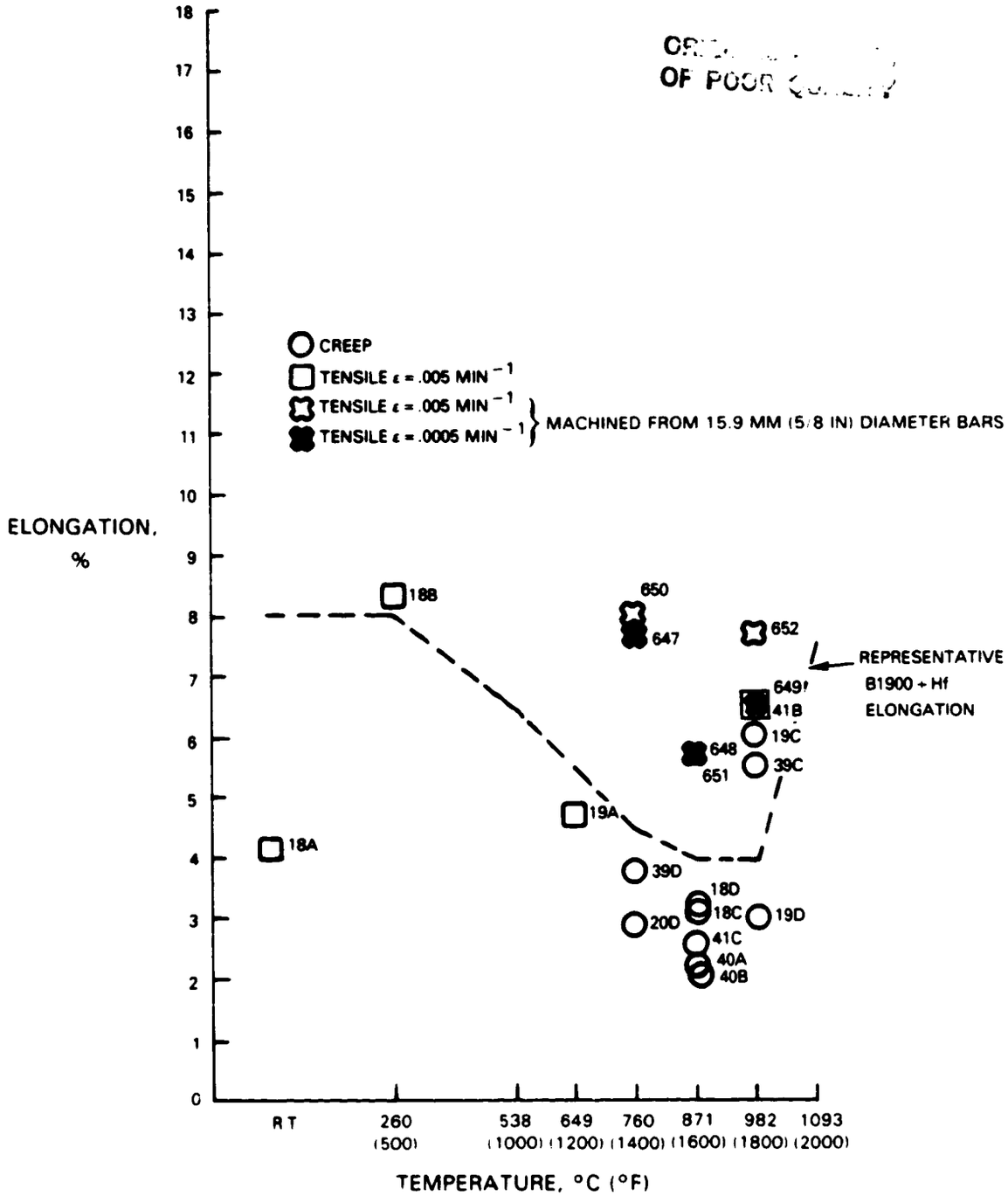

Figure 22 Elongation Observed in Tensile and Creep Tests

TYPE "A"

MM (IN)

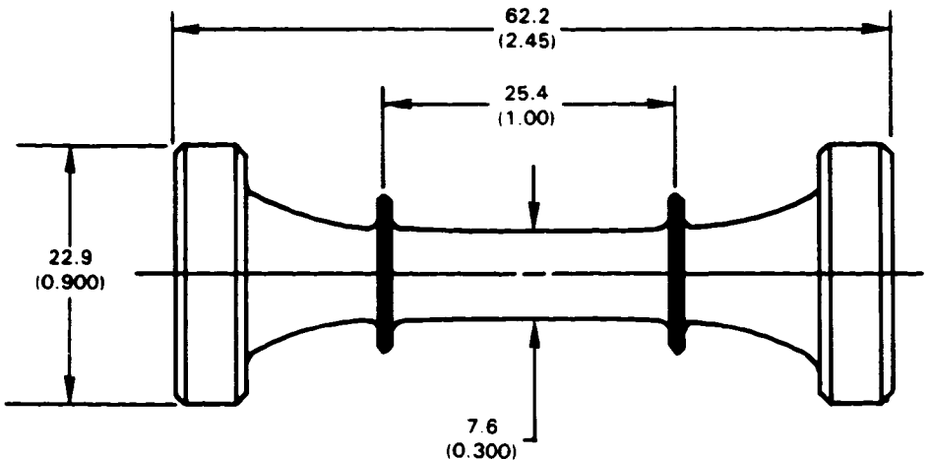

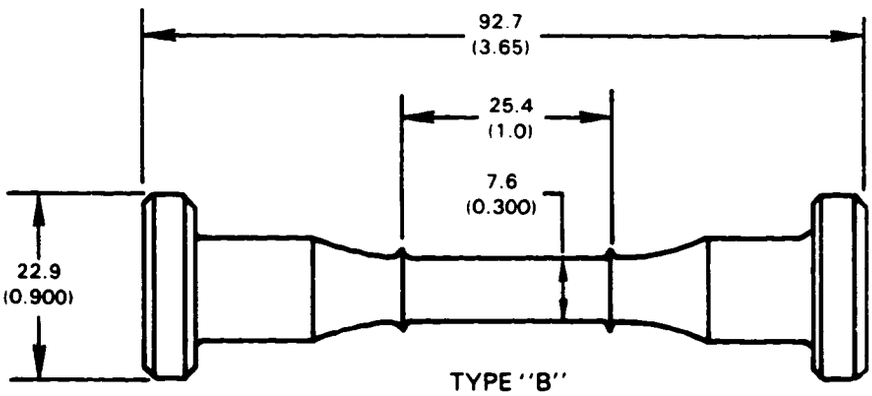

TYPE "B"

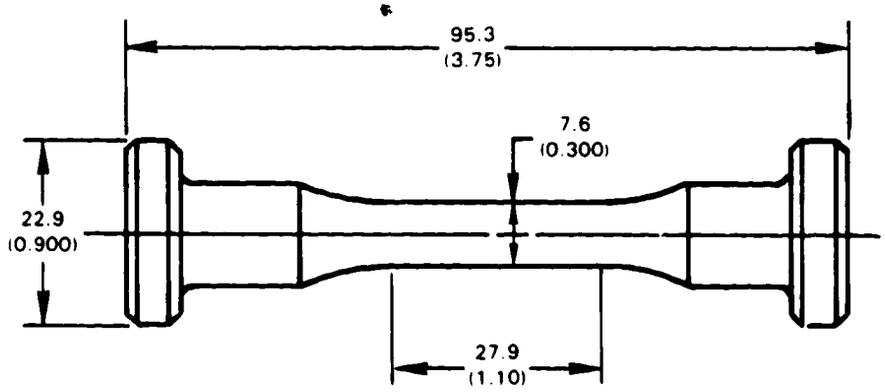

TYPE "C"

Figure 23 Fatigue Specimen Geometries for Initial Testing

Both total specimen cyclic life and failure location were recorded. Two specimens were subsequently eliminated from the study because of testing problems. A Weibull analysis of the data, presented in Figure 24, shows that the 871°C(1600°F) data for each specimen type is uniformly distributed, indicating little effect of geometry or machining procedure at this temperature. Primary failure locations occurred throughout the gage section for all specimens tested. However, at 538°C(1000°F), the type C data are grouped at the higher end of the distribution. Furthermore, the type A and B failure locations were predominantly associated with the extensometer ridge fillets, whereas the type C failures generally occurred throughout the gage section. These results suggest a fillet or "notch" effect in the fatigue life at the lower temperature. The distribution of the type A and B tests also suggests that the machining procedure (ECG vs CG) has little effect on fatigue life at these conditions.

Further investigation using X-ray diffraction to measure residual surface stresses produced by both processes resulted in similar average stress levels, but significant amounts of scatter were observed in the measurements. The X-ray diffraction (XRD) technique is successfully used on fine grain (wrought) materials; however, application to a cast material, which has a relatively larger grain size, results in fewer grains being sampled by the incident X-ray beam, and thus, much more scatter in the stress measurements. Data taken on several B1900 + Hf specimens machined using centerless grinding and electrochemical grinding is shown in Figure 25. For comparison, measurements taken on fine grain (wrought) IN 718 material show considerably less scatter, with centerless grinding producing a slightly larger compressive stress.

A second group of specimens was fabricated with the type B geometry using centerless grinding and a light [< .025mm(<0.001 in.) removal on a diameter] electropolish. The cyclic lives of these specimens, tested at the same conditions, showed similar trends to the previous data. Subsequent specimens were fabricated to the type C geometry in order to eliminate the notch effect at lower temperatures using centerless grinding and a light electropolish.

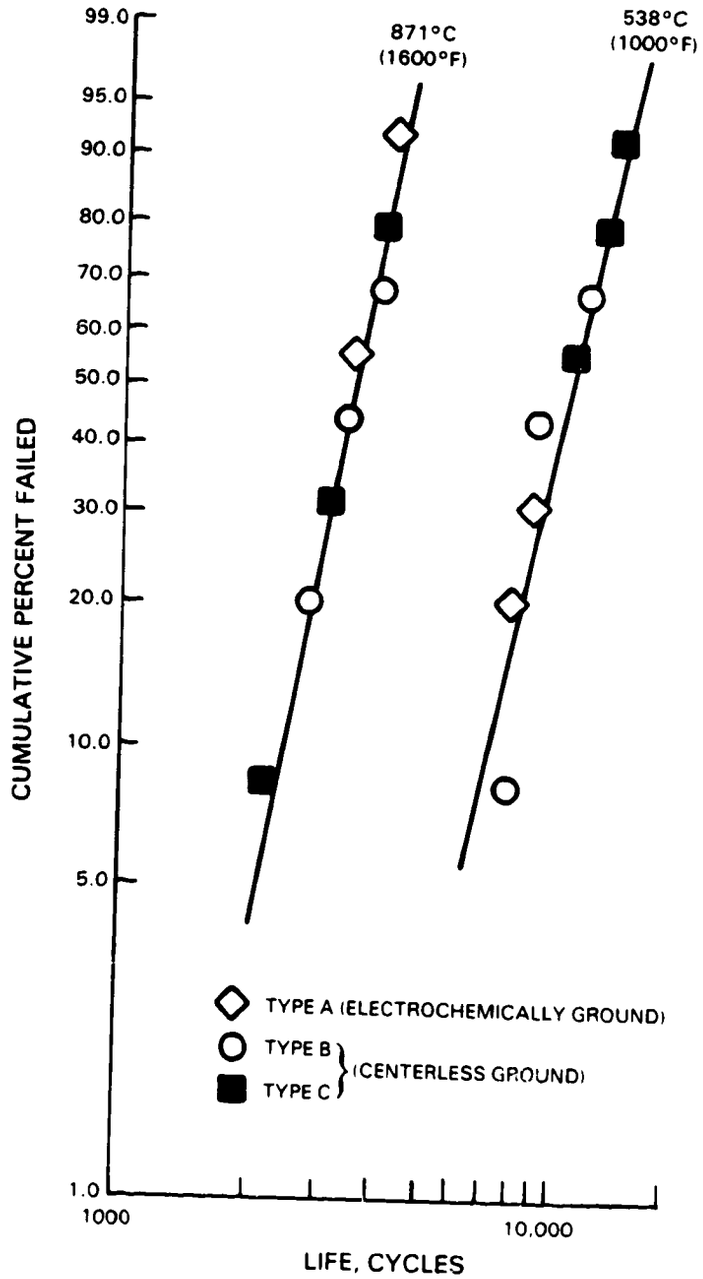

Figure 24 Weibull Analysis of Initial Fatigue Data to Investigate Geometry and Machining Effects

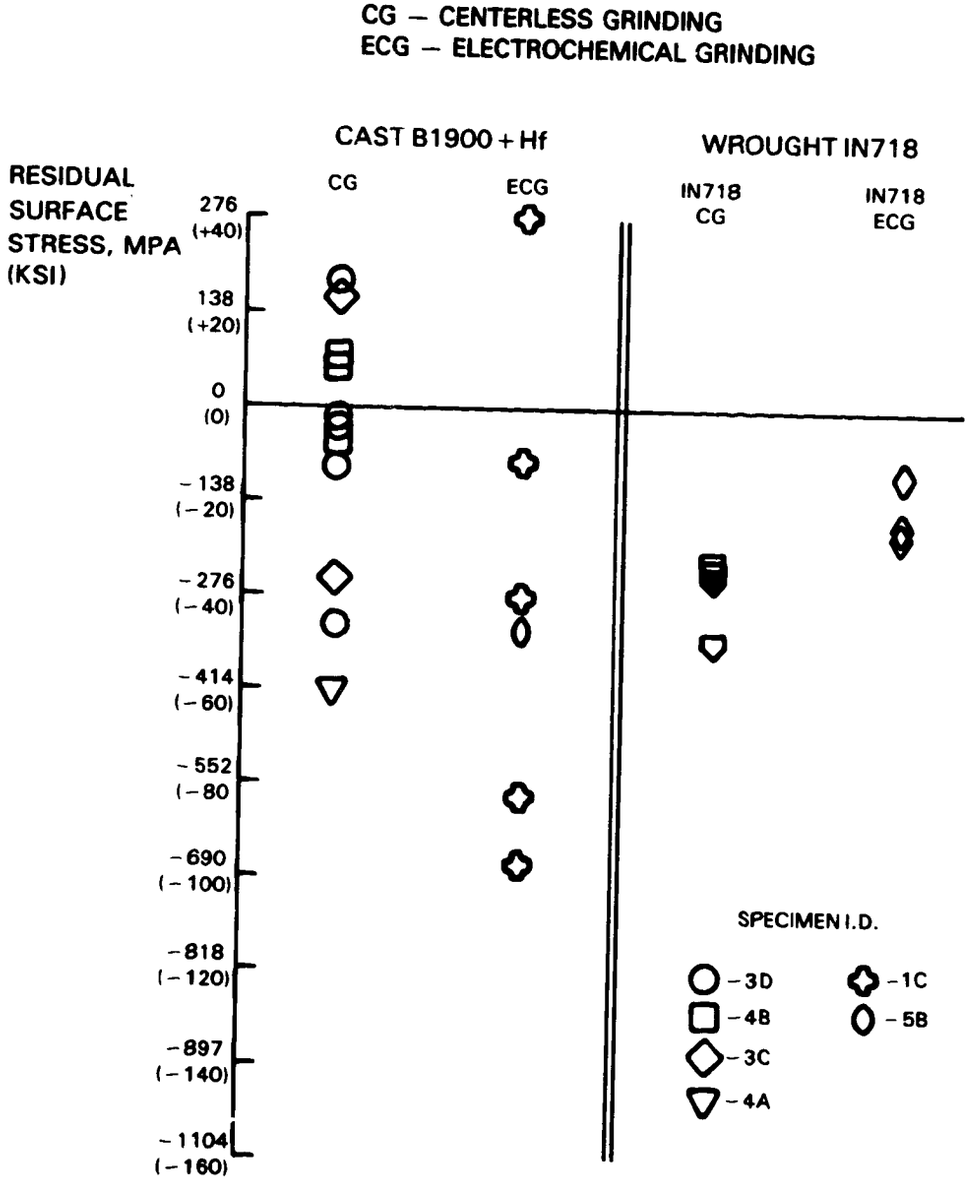

Figure 25 Residual Stresses Measured by X-Ray Diffraction

The test facility used for the isothermal fatigue tests consists of a servo-controlled, closed loop hydraulic testing machine with MTS controllers, a 7.5 kw - 10khz Tocco induction heater, and an Ircon infrared radiation pyrometer for temperature measurement. Induction heating was selected to facilitate setup and inspection of the many fatigue tests. The Ircon pyrometer is used to measure temperatures above 760°C(1400°F); below this temperature, a thermocouple monitors specimen temperature. Axial strain measurement is accomplished with an MTS extensometer. The quartz rods which define a one-inch gage section are spring loaded against the specimen and have not shown any signs of slippage during testing to date. A typical test setup is illustrated in Figure 26.

Figure 26 Typical Test Setup for Isothermal Fatigue Testing

3.2.2 Baseline Fatigue Testing

Isothermal, strain controlled fatigue tests are being conducted to define the crack initiation life of B1900 + Hf material and to provide a baseline for life prediction model evaluation. This initial testing has been limited to key variables relevant to the general creep fatigue life prediction problem. A general matrix of the planned tests is presented in Figure 27. Major variables include strain range ($\Delta\epsilon$), strain rate, strain ratio ($R\epsilon$), dwell periods and temperature. To date, fully reversed ($R\epsilon = -1$) tests have been conducted at 871°C(1600°F) and 538°C(1000°F) including variation in strain range and strain rate. This data is summarized in Tables V and VI. The tests conducted at the strain rate of 1.67 E-03 sec^{-1} represent the upper limit of rates to be tested and are considered to be fast enough to preclude a significant creep fatigue effect. Representative hysteresis loops from 871°C(1600°F) tests conducted at strain ranges of 0.5% and 0.8% indicate a small amount of inelastic strain relative to the total strain range (Figures 28 and 29). A review of the cyclic response histories of all tests indicates that the 871°C(1600°F) tests display a small amount of cyclic softening, while the 538°C(1000°F) tests remain constant at the smaller strain ranges, but cyclically harden at the larger strain ranges. The representative inelastic strain ratio of four specimens and the range of values for all specimens tested at the same conditions are presented in Figures 30 and 31. For each specimen test, the crack initiation life is being defined by three methods; (1) total separation of the specimen, (2) cycles to 5% and 10% tensile load drop from the steady state values, and (3) first indication of cracking. In Tables V and VI, first indication of specimen cracking is defined as 15% of the total separation life at 871°C(1600°F) and 50% of the separation life at 538°C(1000°F). These percentages were established based on inspection of a number of specimens during testing. At each inspection, a replica of the gage section was taken and examined to determine the number and size of surface cracks. In most tests, multiple cracks were observed. Where possible, the crack that ultimately led to specimen failure was tracked throughout the life. Both long and short life tests were examined. A summary of the data for the longest observed crack is presented in Figure 32. As shown in the figure, measurable cracks 0.13 - 0.26mm((0.005 - 0.010 in) were observed early in the specimen life with the rate of growth significantly faster at 871°C(1600°F).

Table V

871°C (1600°F) Baseline Fatigue Test Summary

(R_ϵ = -1)

Spec ID	Spec[1] Type	Strain Range $\Delta\epsilon_T$	Strain Rate $\dot{\epsilon}$ sec^{-1}	σMean Stress σMean[0][6] MPA(psi)	σMean[1/2] MPa(psi)	Plastic Strain Range $\Delta\epsilon_{pl}^0$	$\Delta\epsilon_{pl}^{1/2}$	Stress Range $\Delta\sigma^0$ MPa(psi)	$\Delta\sigma^{1/2}$ MPa(psi)	Plastic Strain Rate $\dot{\epsilon}_{pl}^0$ sec^{-1}	$\dot{\epsilon}_{pl}^{1/2}$ sec^{-1}	Cyclic Life First[2] Indication Cycles	5%[3] Cycles	10%[4] Cycles	Sep.[5] Cycles
6B	M76	0.005	1.67E-03	- 4.84 (- 702)	12.10 (+ 1755)	0.00015	0.00020	745 (108146)	731 (106039)	5.00E-05	6.67E-05	407	2600	2700	2716
6C	M75	0.005	1.67E-03	4.38 (+ 636)	7.31 (+ 1060)	0.00015	0.00025	738 (107355)	724 (105375)	5.00E-05	8.33E-05	579	3200	3600	3859
3B	M75	0.005	1.67E-03	- 4.88 (- 707)	+ 4.87 (+ 707)	0.00015	0.00025	758 (109618)	752 (108910)	5.00E-05	8.33E-05	319	2000	2100	2125
6D	M75	0.005	1.67E-03	0 (0.0)	- 2.45 (- 356)	0.00010	0.00020	786 (113960)	758 (110499)	3.33E-05	6.67E-05	445	2800	2900	2965
6A	M76	0.005	1.67E-03	- 2.45 (- 356)	- 2.45 (- 356)	0.00015	0.00025	758 (110398)	724 (105270)	5.00E-05	8.33E-05	569	2500	3500	3793
4B	M76	0.005	1.67E-03	- 4.92 (- 714)	-	0.00015	0.00035	827 (120086)	772 (112223)	5.00E-05	1.17E-04	484	2900	3050	3226
1B	M71	0.005	1.67E-03	- 2.43 (- 353)	-	0.00015	0.00020	758 (109618)	731 (105516)	5.00E-05	6.67E-05	613	2700	3300	4089
5B	M71	0.005	1.67E-03	- 15.34 (- 2225)	-	0.00015	0.00030	786 (114243)	772 (111573)	5.00E-05	1.00E-04	496	2550	3000	3308
33B	M76	0.005	1.67E-03	- 12.36 (-1793)	-	0.00010	0.00025	779 (112625)	772 (111765)	3.33E-05	8.33E-05	360	2150	2240	2400
35B	M76	0.005	1.67E-03	- 9.91 (- 712)	-	0.00010	0.00020	772 (112535)	751 (109402)	3.33E-05	6.67E-05	600	3300	3780	4000
49A	M75	0.005	1.67E-03	9.89 (+1435)	+118.70 (+17216)	0.00010	0.00012	758 (110473)	758 (110473)	3.33E-05	4.00E-05	528	3380	3420	3519
53C	M75	0.005	1.67E-03	- 5.87 (- 852)	+ 16.65 (16.65)	0.00018	0.00021	834 (120739)	827 (119744)	6.0E-05	7.0E-05	446	2343	2488	2975
35C	M76	0.008	1.67E-03	-14.83 (-2152)	-	0.00090	0.00100	1034 (150645)	1013 (146915)	1.87E-04	2.08E-04	75	410	454	500
34B	M76	0.008	1.67E-03	8.89 (-1435)	-	0.00100	0.00130	1116 (162123)	1000 (144907)	2.08E-04	2.71E-04	66	278	383	440
37A	M76	0.008	1.67E-03	-10.88 (-1578)	- 10.93 (-1585)	0.00105	0.00129	1048 (152367)	1006 (146500)	2.19E-04	2.69E-04	56	300	330	375
35A	M76	0.008	1.67E-03	- 7.36 (-1068)	- 3.93 (- 570)	0.00097	0.00103	1055 (152564)	1027 (149287)	2.02E-04	2.15E-04	71	459	468	475
36C	M76	0.004	1.67E-03	- .98 (- 142)	- 5.89 (- 855)	0.00008	0.00010	620 (90313)	627 (91311)	3.33E-05	4.17E-05	1495	8802	9252	9964
33D	M76	0.004	1.67E-03	.96 (+ 139)	- 8.12 (-1179)	0.00010	0.00009	648 (94036)	648 (93897)	4.17E-05	3.75E-05	1665	x	x	11102
52A	M75	0.004	1.67E-03	9.83 (+1425)	9.83 (+1425)	0.00005	0.00006	676 (98291)	676 (98291)	2.08E-05	2.50E-05	1711	6690	8100	11409
34C	M76	0.0035	1.67E-03	- 3.96 (- 574)	- 4.94 (- 717)	0.00005	0.00007	510 (73458)	524 (76040)	2.33E-05	3.27E-05	10200	67322	67580	68000
34A	M76	0.005	1.67E-04	- 1.96 (- 285)	- 13.51 (- 1959)	0.00020	0.00040	738 (107123)	703 (102208)	6.67E-06	1.33E-05	413	2347	2656	2745
36A	M76	0.005	1.67E-04	7.94 (+ 1151)	- 11.41 (+ 1655)	0.00028	0.00035	724 (105324)	696 (101439)	9.33E-06	1.17E-05	371	1707	2110	2470
37D	M76	0.005	1.67E-04	5.40 (+ 783)	- 4.91 (- 712)	0.00031	0.00033	676 (98433)	675 (98006)	1.03E-05	1.10E-05	456	2219	2968	3041
50D	M75	0.008	1.67E-04	6.87 (+ 997)	0	0.00132	0.00147	986 (143447)	965 (139601)	2.75E-05	3.06E-05	31	184	189	208
48C	M75	0.008	1.67E-04	14.73 (+2137)	2.94 (+ 427)	0.00134	0.00150	1013 (147436)	986 (142877)	2.79E-05	3.125E-05	34	199	208	229
17B	M75	0.008	1.67E-04	17.67 (+2564)	2750 (+ 3989)	0.00143	0.00140	1041 (150712)	1020 (147863)	2.98E-05	2.92E-05	56	255	325	376

[1] M71 = Type A, M76 = Type B, M75 = Type C
See Figure 23

[2] 15% of Total Life, See Figure 5

[3] 5% Tensile Load Drop

[4] 10% Tensile Load Drop

[5] Separation Life

[6] 0 = Initial Value, 1/2 = 1/2 Separation Life

Table VI

538°C (1000°F) Baseline Fatigue Test Summary
(R_ϵ = -1)

Spec ID	Spec[1] Type	Strain Range $\Delta\epsilon_T$	Strain Rate $\dot{\epsilon}$ sec^{-1}	Mean Stress σ Mean^0[6] MPa(psi)	Mean Stress σ Mean$^{1/2}$ MPa(psi)	Plastic Strain Range $\Delta\epsilon p^0$	Plastic Strain Range $\Delta\epsilon p^{1/2}$	Stress Range $\Delta\sigma^0$ MPa(psi)	Stress Range $\Delta\sigma^{1/2}$ MPa(psi)	Plastic Strain Rate $\dot{\epsilon}p^0$ sec^{-1}	Plastic Strain Rate $\dot{\epsilon}p^{1/2}$ sec^{-1}	Cyclic Life First[2] Indication Cycles	Cyclic Life 5%[3] Cycles	Cyclic Life 10%[4] Cycles	Cyclic Life Sep.[5] Cycles
3D	M75	0.005	1.67E-03	- 3.43 (-497)	12.24 (+1776)	0.00005	0.00005	867 (125994)	855 (124290)	1.67E-05	1.67E-05	7980	12625	13050	13000
4D	M75	0.005	1.67E-03	- 2.44 (-354)	27.98 (+4059)	0.00005	0.00005	807 (116690)	807 (117043)	1.67E-05	1.67E-05	7536	x	x	12560
4A	M75	0.005	1.67E-03	-6.41 (-929)	1.22 (+177)	0.00002	0.00002	868 (125645)	868 (126382)	6.67E-06	6.67E-06	6390	10300	10520	10650
3A	M76	0.005	1.67E-03	-3.45 (-500)	18.32 (+2658)	0.00003	0.00003	896 (130466)	910 (131927)	1.00E-05	1.00E-05	4665	x	x	7775
3C	M76	0.005	1.67E-03	-7.86 (-1140)	-9.82 (-1425)	0.00002	0.00002	979 (141595)	965 (140313)	6.67E-06	6.67E-06	5326	8133	8560	8877
4C	M76	0.005	1.67E-03	-12.36 (-1792)	8.41 (+1219)	0.00003	0.00003	931 (135484)	945 (137491)	1.00E-05	1.00E-05	6840	10630	11020	11400
1C	M71	0.005	1.67E-03	-2.42 (- 351)	.86 (125)	0.00002	0.00002	931 (135610)	945 (137015)	6.67E-06	6.67E-06	4759	x	x	7931
5C	M71	0.005	1.67E-03	-1.07 (- 115)	1.165 (+169)	0.00002	0.00002	965 (140621)	965 (139986)	6.67E-06	6.67E-06	5264	7040	7840	8774
33A	M76	0.005	1.67E-03	-15.34 (-2226)	3.07 (+445)	0.00002	0.00002	945 (137685)	938 (135905)	6.67E-06	6.67E-06	4584	5890	6660	7640
33C	M76	0.005	1.67E-03	-9.82 (-1424)	-13.74 (-1994)	0.00002	0.00002	889 (129630)	882 (128775)	6.67E-06	6.67E-06	5430	8934	8986	9050
37B	M76	0.008	1.67E-03	4.96 (-719)	-14.38 (-2086)	0.00046	0.00020	1289 (187050)	1331 (192662)	9.58E-05	4.17E-05	930	1481	1518	1550
35D	M76	0.008	1.67E-03	-3.49 (-507)	- 0	0.00058	0.00020	1365 (198116)	1420 (205797)	1.21E-04	4.17E-05	552	907	-	920
36B	M76	0.008	1.67E-03	-7.91 (-712)	- 7.36 (-1068)	0.00058	0.00024	1385 (200855)	1441 (208689)	1.21E-04	5.00E-05	558	868	875	930
37C	M76	0.010	1.67E-03	-14.79 (-2146)	-27.12 (-3934)	0.00112	0.00065	1447 (210300)	1585 (229614)	1.87E-04	1.08E-04	136	223	x	227
34D	M76	0.010	1.67E-03	-4.91 (-712)	-15.22 (-2208)	0.00082	0.00040	1420 (206553)	1537 (223789)	1.37E-04	6.67E-05	238	385	390	397
36D	M76	0.010	1.67E-03	-4.81 (-698)	- 14.44 (-2095)	0.00094	0.00048	1447 (210893)	1606 (233240)	1.57E-04	8.00E-05	183	300	x	305

[1] M71 = Type A, M76 = Type B, M75 = Type C
See Figure 23

[2] 15% of Total Life, See Figure 5

[3] 5% Tensile Load Drop

[4] 10% Tensile Load Drop

[5] Separation Life

[6] 0 = Initial Value, 1/2 = 1/2 Separation Life

Arbitrarily defining a 0.76mm(0.030 in.) crack length as initiation results in the life fractions discussed above. Inspection of several fatigue fracture surfaces has shown that the assumption of a semicircular crack to estimate crack depth is reasonable for surface crack lengths to ≈2.5mm(≈0.100 in.). Thus, the 0.76mm(0.030) in surface length represents a 0.38mm(0.015 in) depth crack as compared to a material grain size of 0.25 - 0.18mm(0.010 - 0.007 in) (see Section 3.2.1).

TEST CONDITION	STRAIN RANGE			STRAIN RATIO			STRAIN RATE			DWELL PERIODS						TEMPERATURES			
										ε_{MAX}		ε_{MIN}		ε_{INT}					
	$\Delta\varepsilon_1$	$\Delta\varepsilon_2$	$\Delta\varepsilon_3$	$-\infty$	-1	0	$\dot{\varepsilon}_1$	$\dot{\varepsilon}_2$	$\dot{\varepsilon}_3$	t_1	t_2	t_1	t_2	t_1	t_2	T_1	T_3	T_4	T_5
C 1	X				X			X										X	
C 2		X			X			X										X	
C 3			X		X			X										X	
C 4	X				X		X											X	
C 5			X		X		X											X	
6	X				X				X									X	
7			X		X				X									X	
8	X				X			X											X
9			X		X			X											X
10			X		X		X												X
11	X				X			X									X		
12			X		X			X									X		
C 13	X				X			X								X			
C 14			X		X			X								X			
15		X			X			X		X								X	
16		X			X			X				X							
17		X			X			X					X						
18			X		X			X				X						X	
19			X		X			X					X					X	
20		X				X		X										X	
21		X		X				X										X	

C = TESTING COMPLETED

Figure 27 Test Matrix for Baseline Fatigue Tests

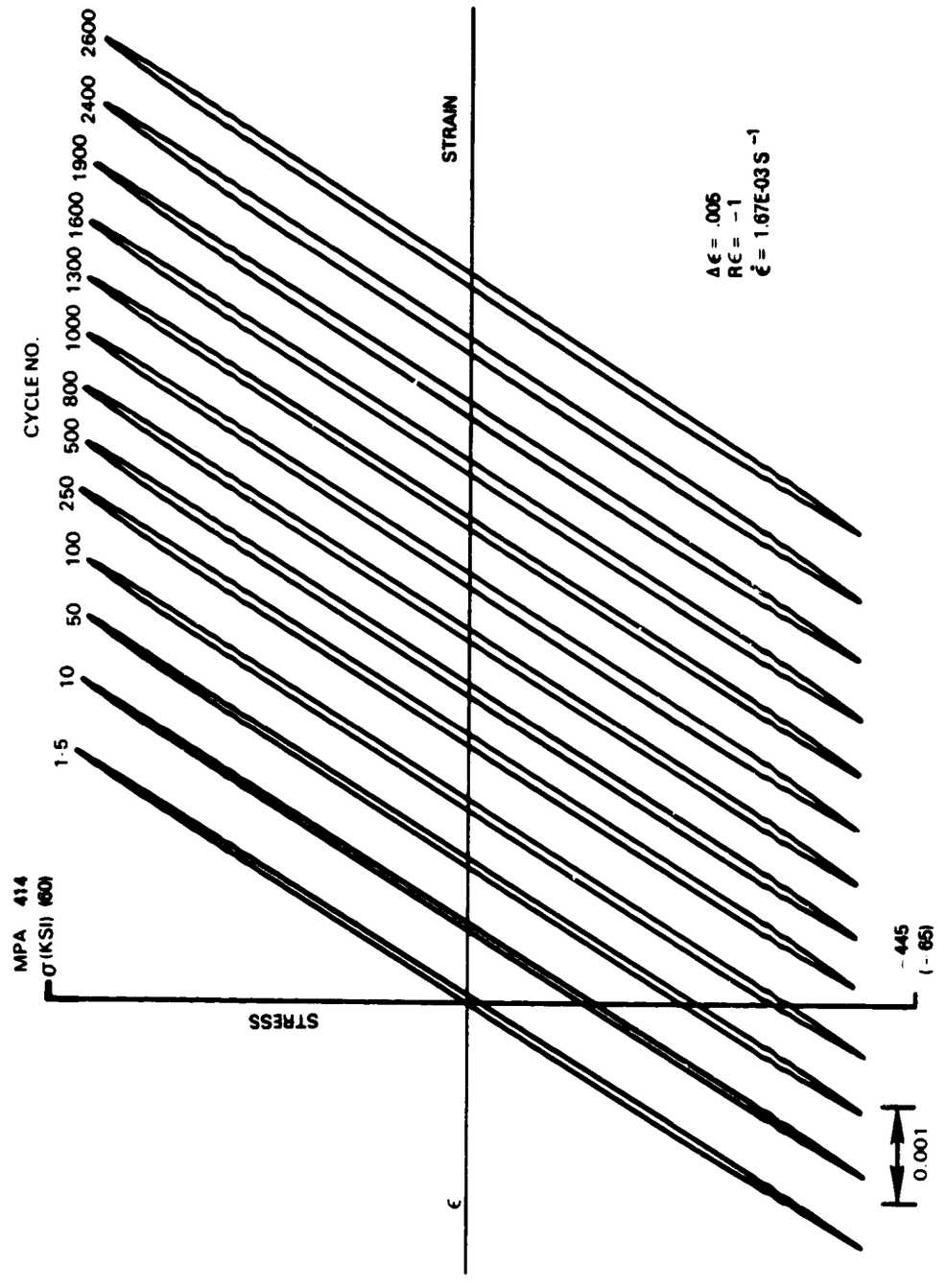

Figure 28 Cyclic Response of 871°C(1600°F) Fatigue Test with $\Delta\epsilon = \pm .25\%$

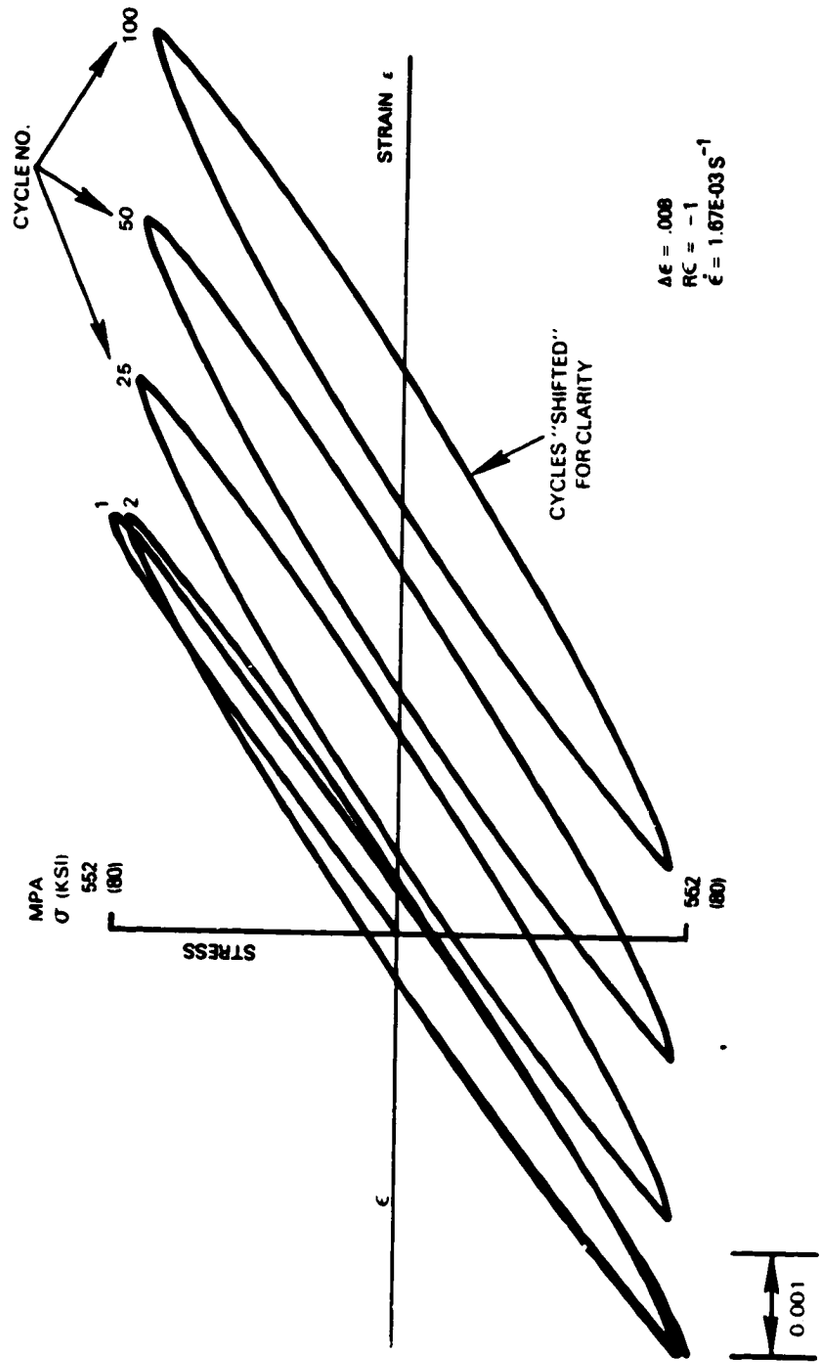

Figure 29 Cyclic Response of 871°C(1600°F) Fatigue Test at $\Delta\epsilon = \pm .4\%$

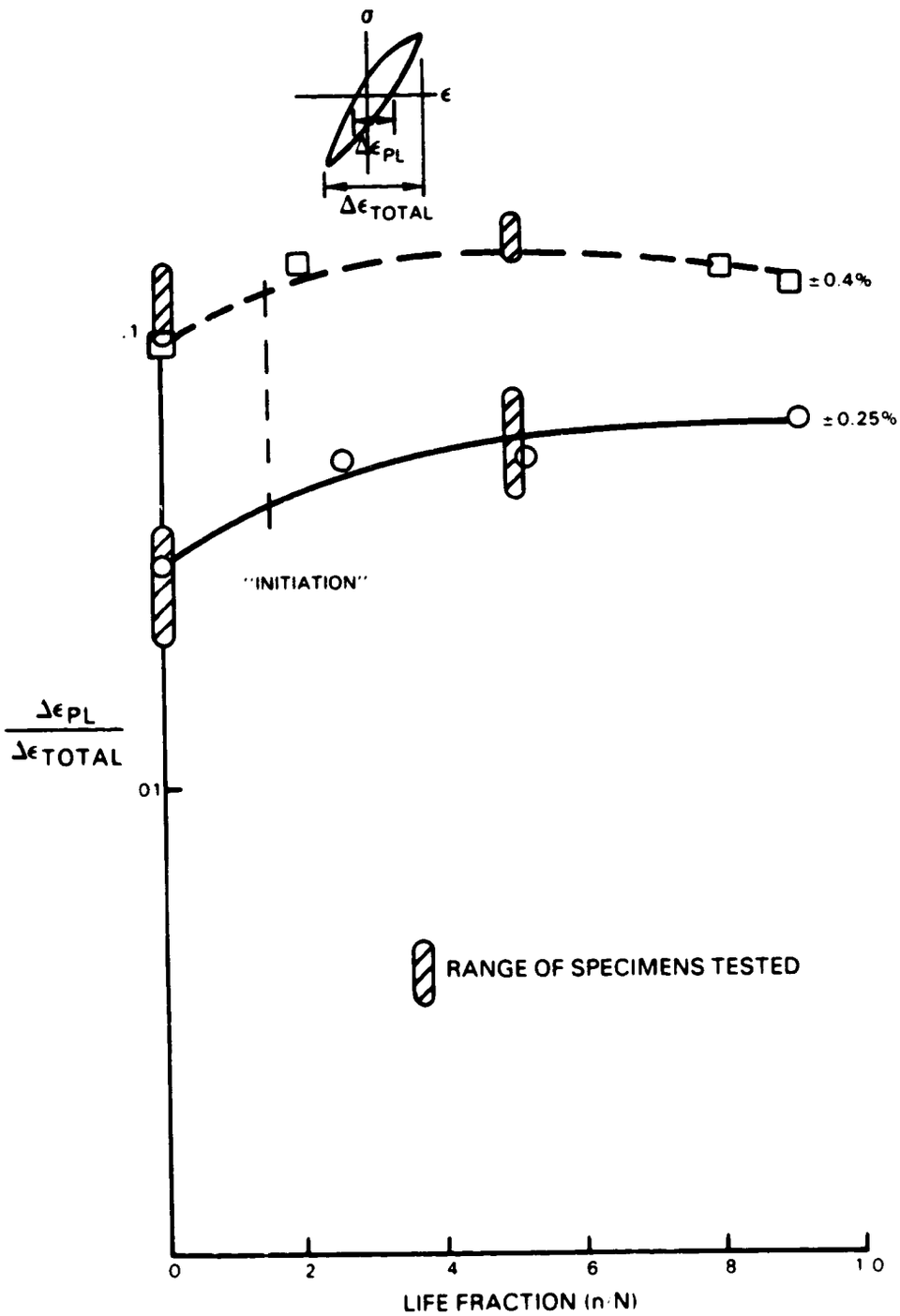

Figure 30 Inelastic Strain Ratio for 871°C(1600°F) Fatigue Tests ($\dot{\epsilon}$ = 1.67 E-03 S^{-1})

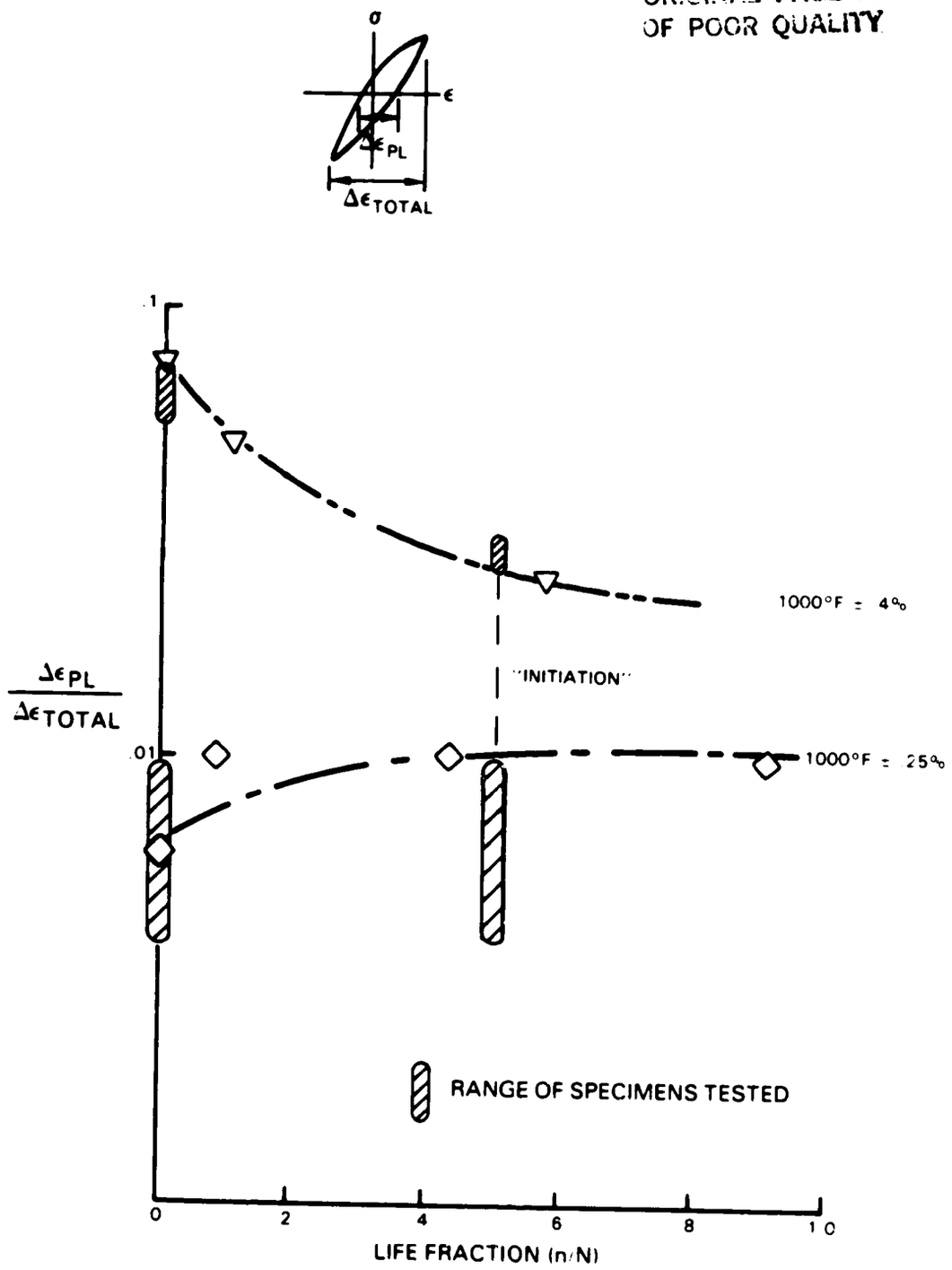

Figure 31 Inelastic Strain Ratio for 538°C(1000°F) Fatigue Tests ($\dot{\epsilon}$ = 1.67 E-03 S^{-1})

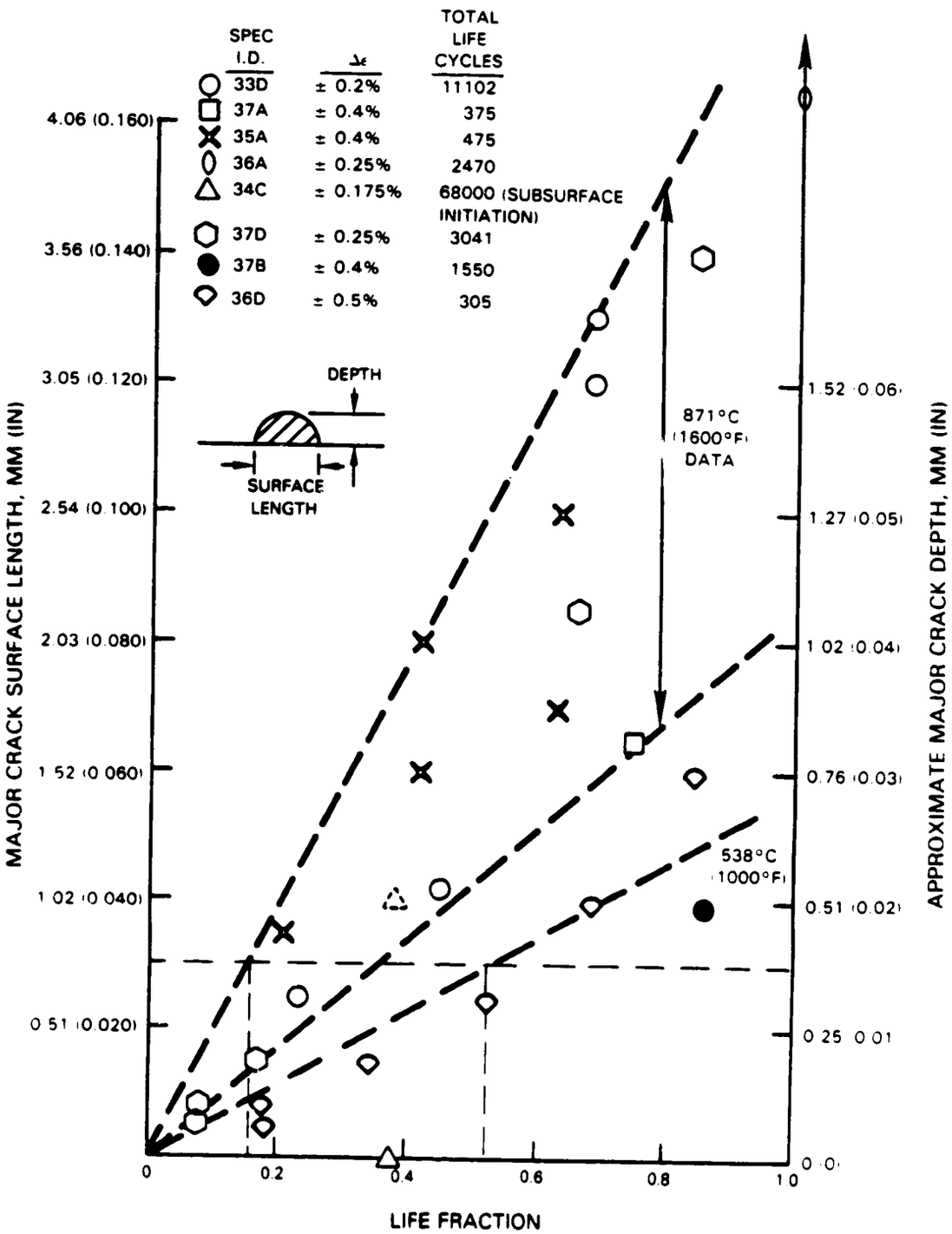

Figure 32 Summary of Replica Measurements

The original eighteen fatigue specimens used to investigate geometry and machining effects on fatigue life were also examined to determine the location of the primary failure initiation sites and the mode of cracking. All specimens were found to have surface initiated fatigue cracks associated with either carbides and/or porosity. Two representative specimens and failure sites, as identified by SEM and microprobe analysis, are presented in Figures 33 and 34. Failure sites determined to have a high tantalum (Ta)content or other constituents found in the grain boundary carbides were identified as carbide related failures. Failure sites having a chemical composition similar to tne matrix, and where a pore could be observed, were identified as porosity related failures. Analysis of the specimen life data (Figure 35) suggests that the nature of the initiation site (carbide vs porosity) is not statistically significant in determining the fatigue life. Based on this result, carbide or porosity initiation was not considered a primary variable in the analysis of subsequent fatigue tests.

In order to clearly identify the process of crack growth from the initiation site to the 0.38mm(0.015 in.) crack depth defined as initiation, several specimens were ground down longitudinally until the initiation site was exposed in the plane of polishing. Figure 36 shows the longitudinal view of a carbide initiation site in specimen 3D tested at 538°C(1000°F). The propagation path appears to be transgranular for approximately 4.8mm(0.190 in) (~20 grains) before switching to an intergranular mode. Examination of specimen 6B (see Figure 37) identified the initiation site as a 0.005mm(~0.0002 in) surface pore. The crack grows approximately 0.76mm(0.030 in) (3 grains) transgranularly before switching to an intergranular mode. Examination of additional specimens has shown varying degrees of transgranular vs intergranular cracking; however, in all cases the growth mode from the initiation site is transgranular. Figure 38 shows the representative crack growth path in specimens tested at 538°C(1000°F) and 871°C(1600°F). The approximate crack depth for 10% and 50% of the specimen test life is superimposed. Clearly, a large portion of the cyclic life is spent in transgranular crack growth.

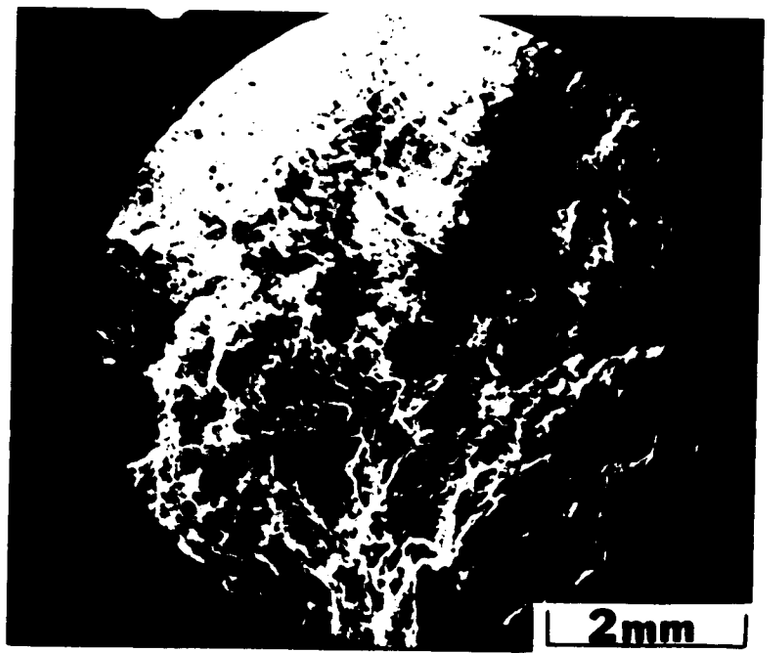

(a)

(b)

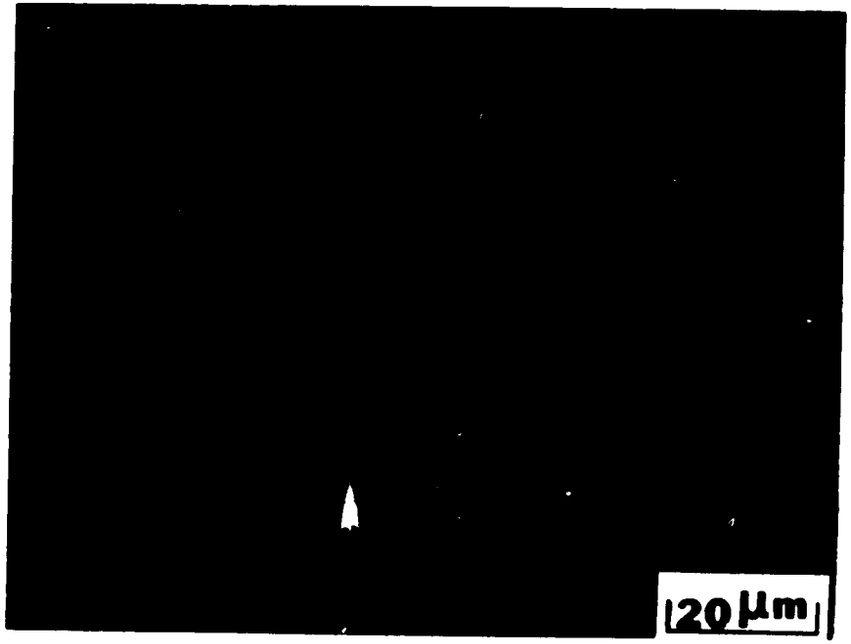

(c)

Figure 33 Fracture Surface of Specimen 6D After Being Tested at 871°C(1600°F) $\Delta\epsilon_t = \pm 0.25\%$, 10 cpm for 2,965 Cycles.
(a) Typical fractographs showing two crack initiation sites A and B.
(b) Carbide on surface at primary crack initiation site (A) is shown by arrow.
(c) X-ray map showing the distribution of Ta in area corresponding to (B).

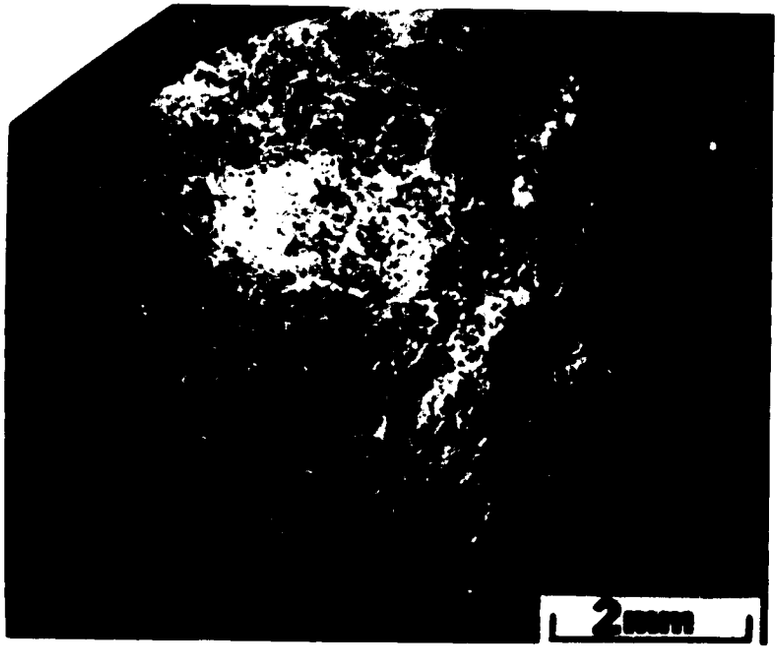

(a)

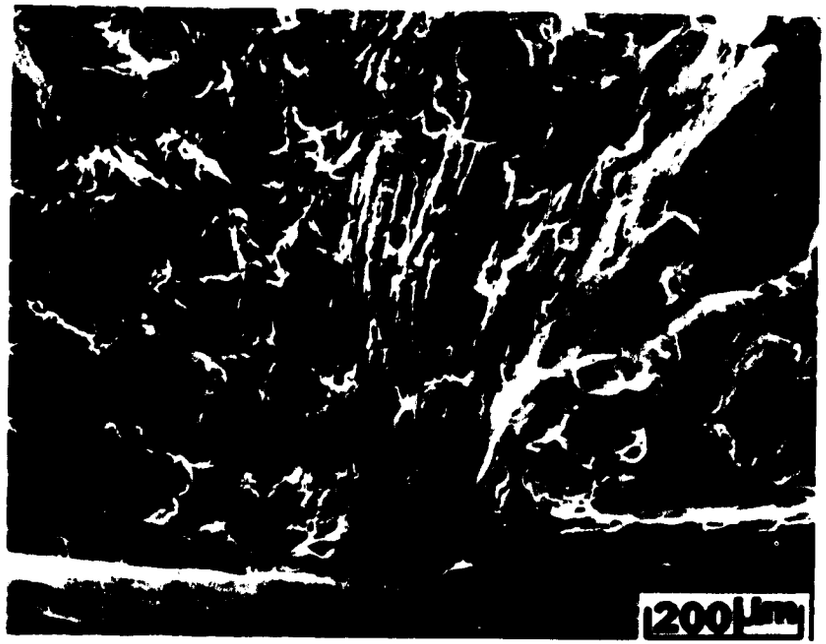

(b)

(c)

Figure 34 Fracture Surface of Specimen 4D After Being Tested at 538°C(1000°F) $\Delta\epsilon_t = \pm 0.25\%$, 10 cpm for 12,560 Cycles.

(a) Typical fractographs showing crack initiated on surface.

(b) Porosity on surface at crack initiation site

(c) Faint fatigue striations along with secondary cracks.

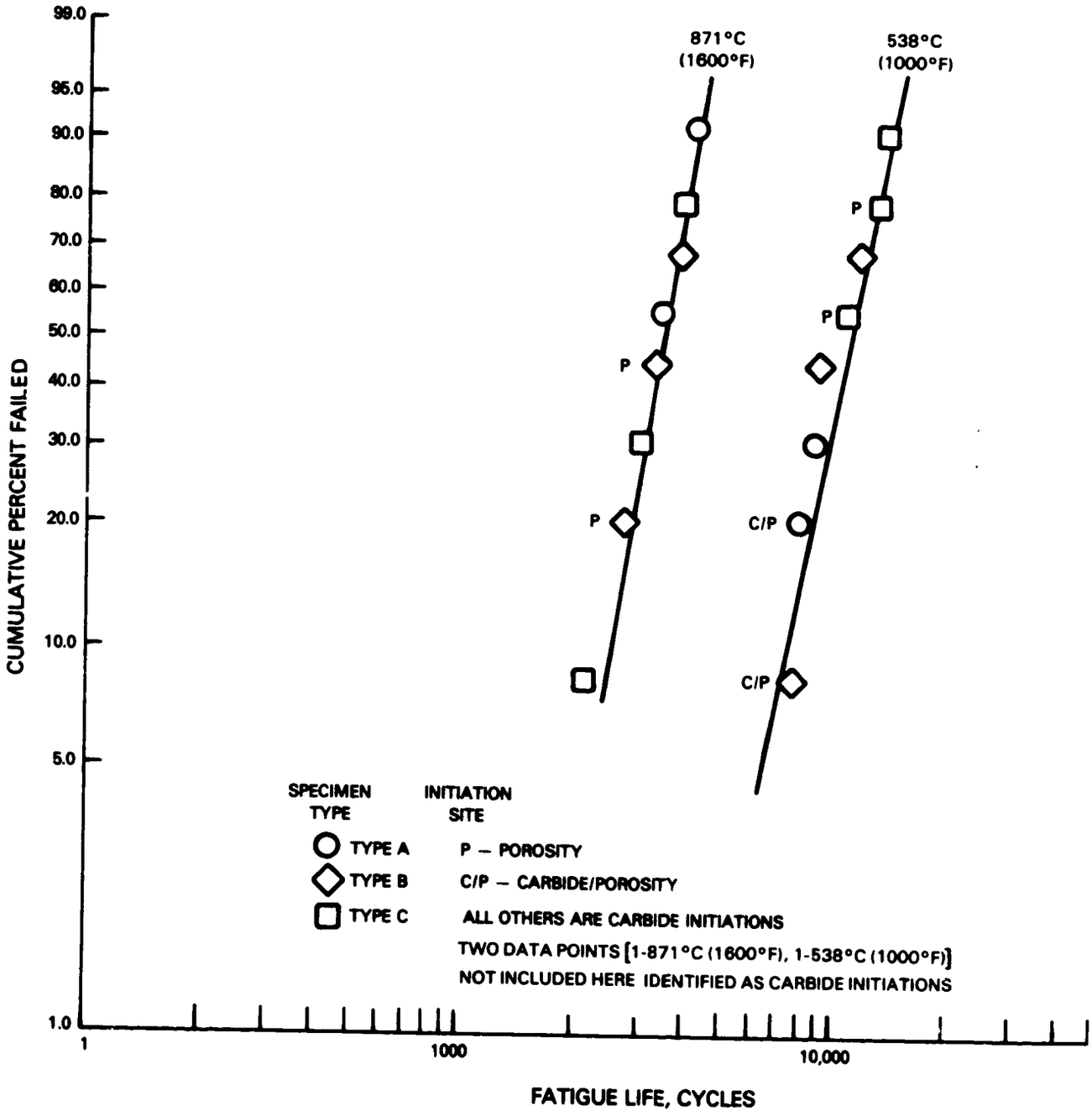

Figure 35 Distribution of Initiation Sites for Initial Fatigue Tests

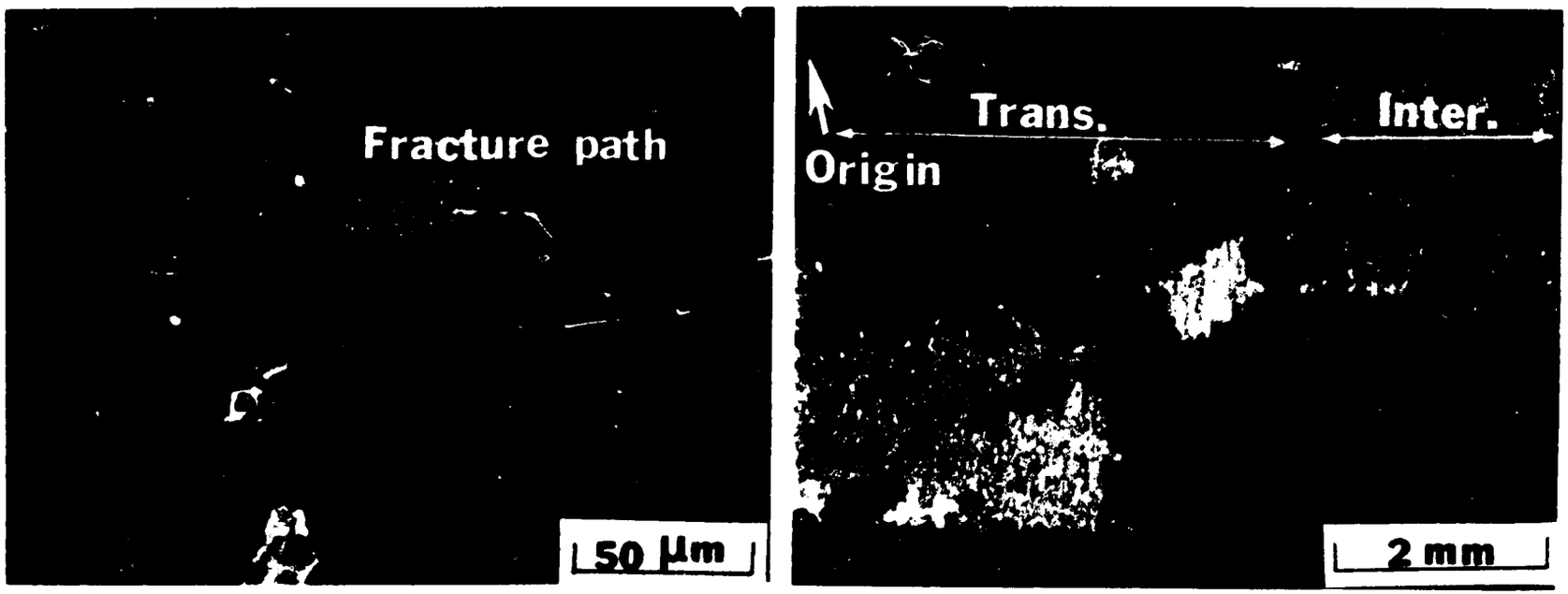

(a) (b)

Figure 36 Longitudinal View of Specimen 3D After Being LCF Tested at 538°C(1000°F), $\Delta\epsilon t$ = + 0.25%, 10cpm for 13,300 Cycles (a) Carbide at crack initiation site is shown by arrow. (b) Crack propagates transgranularly and becomes intergranular at location shown by arrow.

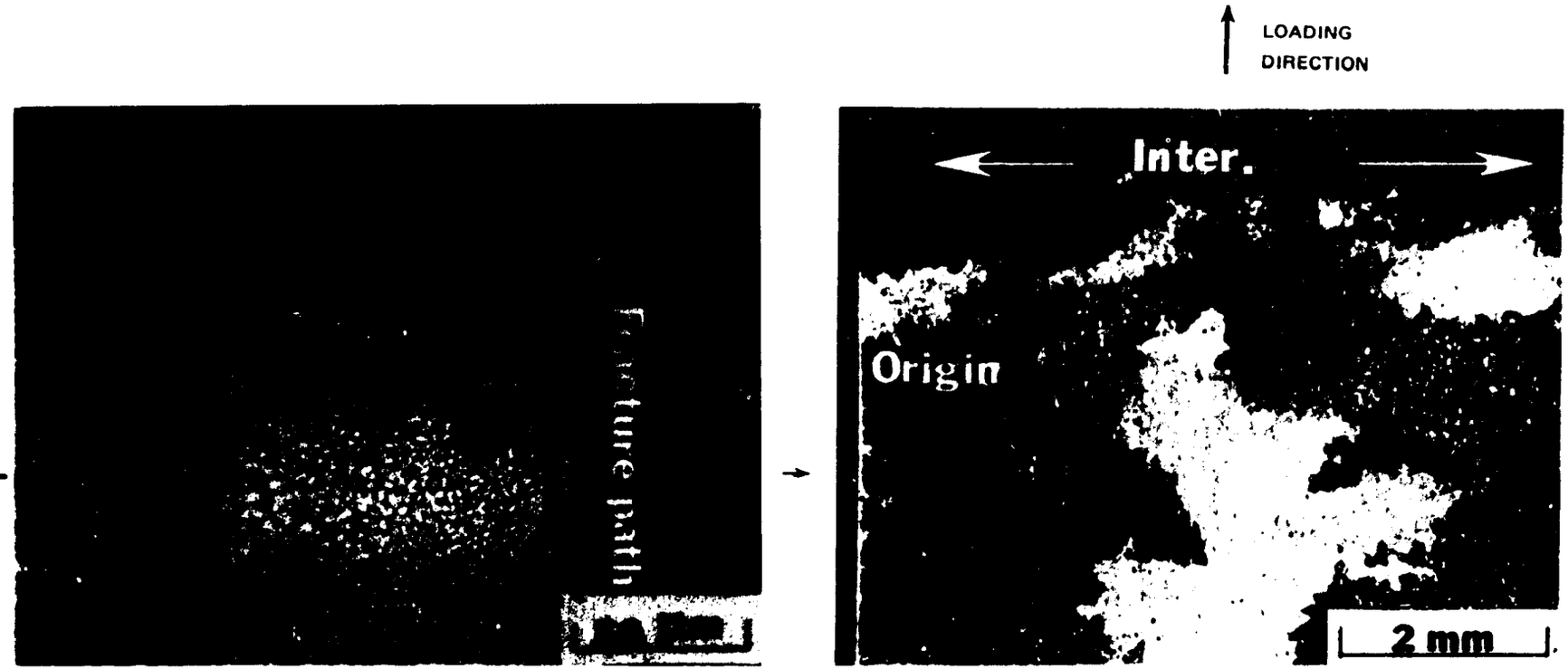

(a) (b)

Figure 37 Longitudinal View of Specimen 6B After Being LCF Tested at 871°C(1600°F), $\Delta\epsilon_t$ = + 0.25%, 10 cpm for 2,716 Cycles (a) Porosity at crack initiation site is shown by arrow. (b) Crack propagates transgranularly and becomes intergranular at location shown by arrow.

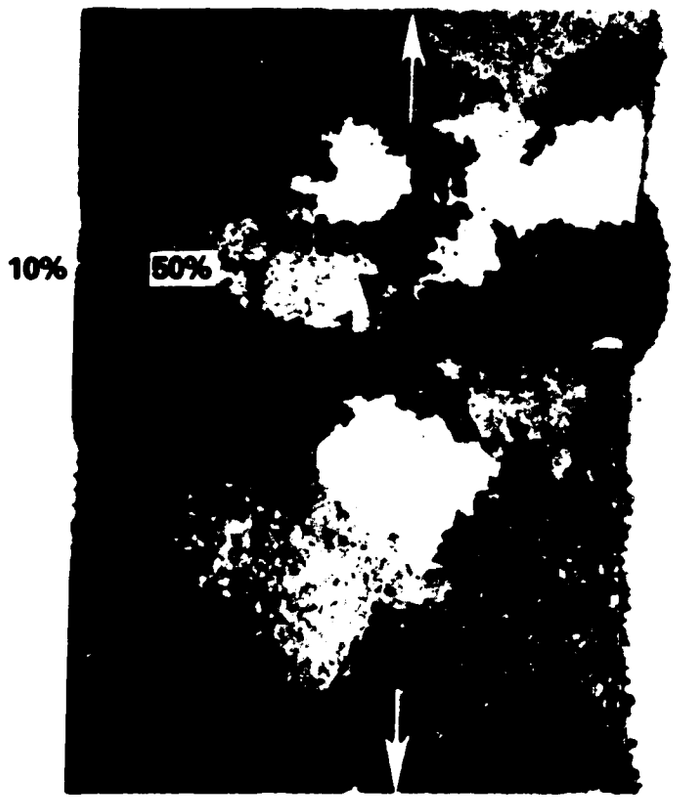

538°C (1000°F)
10,650 CYCLES (17.75 HRS)

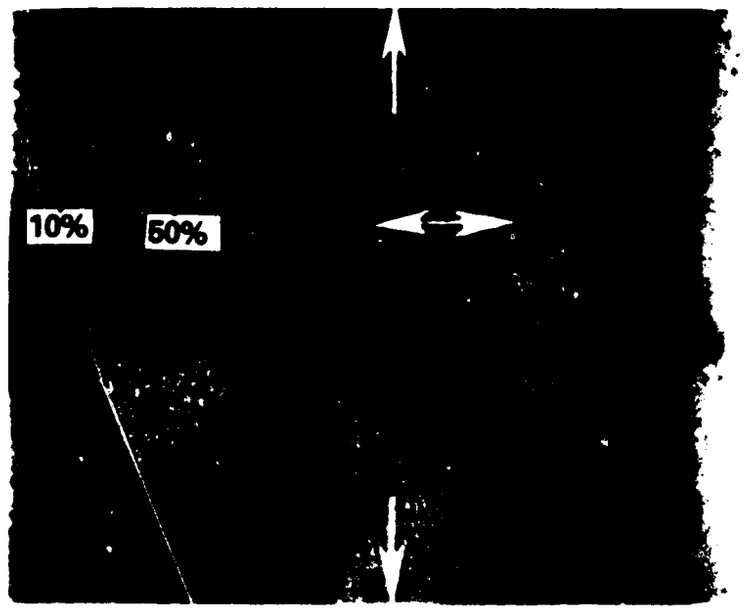

871°C (1600°F)
3,859 CYCLES (6.432 HRS)

Figure 38 Primary Crack Depth at 10% and 50% of Specimen Cyclic Life

Transmission Electron Microscopy (TEM) was used to characterize the dislocation structure developed by the cyclic testing. In all examinations, a significantly smaller dislocation density was observed in the fatigue tests than the monotonic tensile or creep tests. The typical dislocation structure of a specimen tested at 538°C(1000°F) (4D) is shown in Figure 39. It appears that the large γ' particles impede the motion of dislocations which results in the dislocations tightly encasing the individual particles of γ'. Two active octahedral slip systems were identified: $(111)\ \langle 1\bar{1}0\rangle$, location A, and $(111)\ \langle 10\bar{1}\rangle$, location B. The typical dislocation structure of a specimen tested at 871°C(1600°F) (6D) is shown in Figure 40. In this case the dislocations do not form the tight encasement of γ' particles; rather, they gather in the γ matrix regions along the direction of the Burgers vector. Since cross slip is easier at 871°C(1600°F) than at 538°C(1000°F), apparently as the dislocations encounter resistance from the γ' particles they overcome the resistance by cross slipping onto a different slip system. There appears to be a general directional alignment of the dislocation activity in Specimen 6D (see Figure 40). Three active octahedral slip systems were identified in this specimen: $(11\bar{1})\ \langle 1\bar{1}0\rangle$, $(11\bar{1})\ \langle 011\rangle$ and $(111)\ \langle 10\bar{1}\rangle$, typical of dislocations at locations A, B and C.

The thin foil specimens of 4D and 6D were taken ~7.1mm(~1/4 in) below the fracture. In order to establish that the dislocation structures observed were representative of the fracture conditions, a thin foil was made on a second specimen tested at 538°C(1000°F), Specimen 3D, immediately below the fracture (Figure 41) which generally confirmed the observations made on Specimen 4D.

3.2.3 Life Prediction Model Selection

One of the fundamental objectives of this research effort is the identification of a fatigue life methodology or approach suitable for the wide range of conditions experienced by hot section structural components. For this effort, it is necessary to distinguish between an "approach" and a "model". A life prediction approach is considered as a conceptual basis for the prediction of cyclic life. Within current life prediction technology,

Figure 39 Dislocation Structures After Being LCF Tested at 538°C(1000°F), 10cpm $\Delta\epsilon_t$ = ± 0.25% for 12,500 Cycles, Specimen 4D (~1/4 in. away from fracture surface).

Zone axis (211) { A: (111) $\langle 1\bar{1}0 \rangle$
B: (111) $\langle 10\bar{1} \rangle$

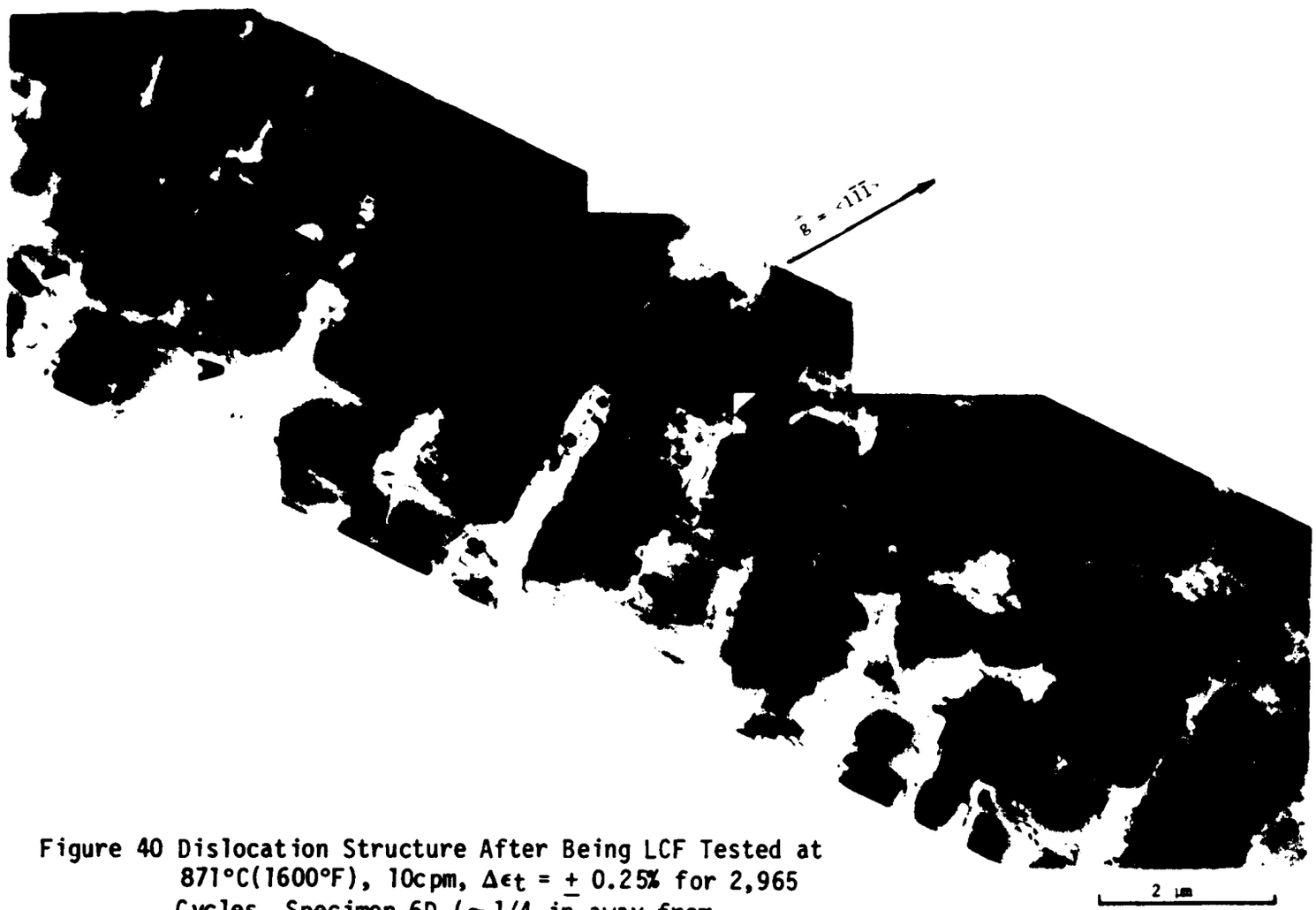

Figure 40 Dislocation Structure After Being LCF Tested at 871°C(1600°F), 10cpm, $\Delta\epsilon_t = \pm 0.25\%$ for 2,965 Cycles, Specimen 6D (~ 1/4 in away from fracture surface).
A: $(1\bar{1}1)$ $<110>$
B: (111) $<01\bar{1}>$ } Zone axis (211)
C: (111) $<10\bar{1}>$

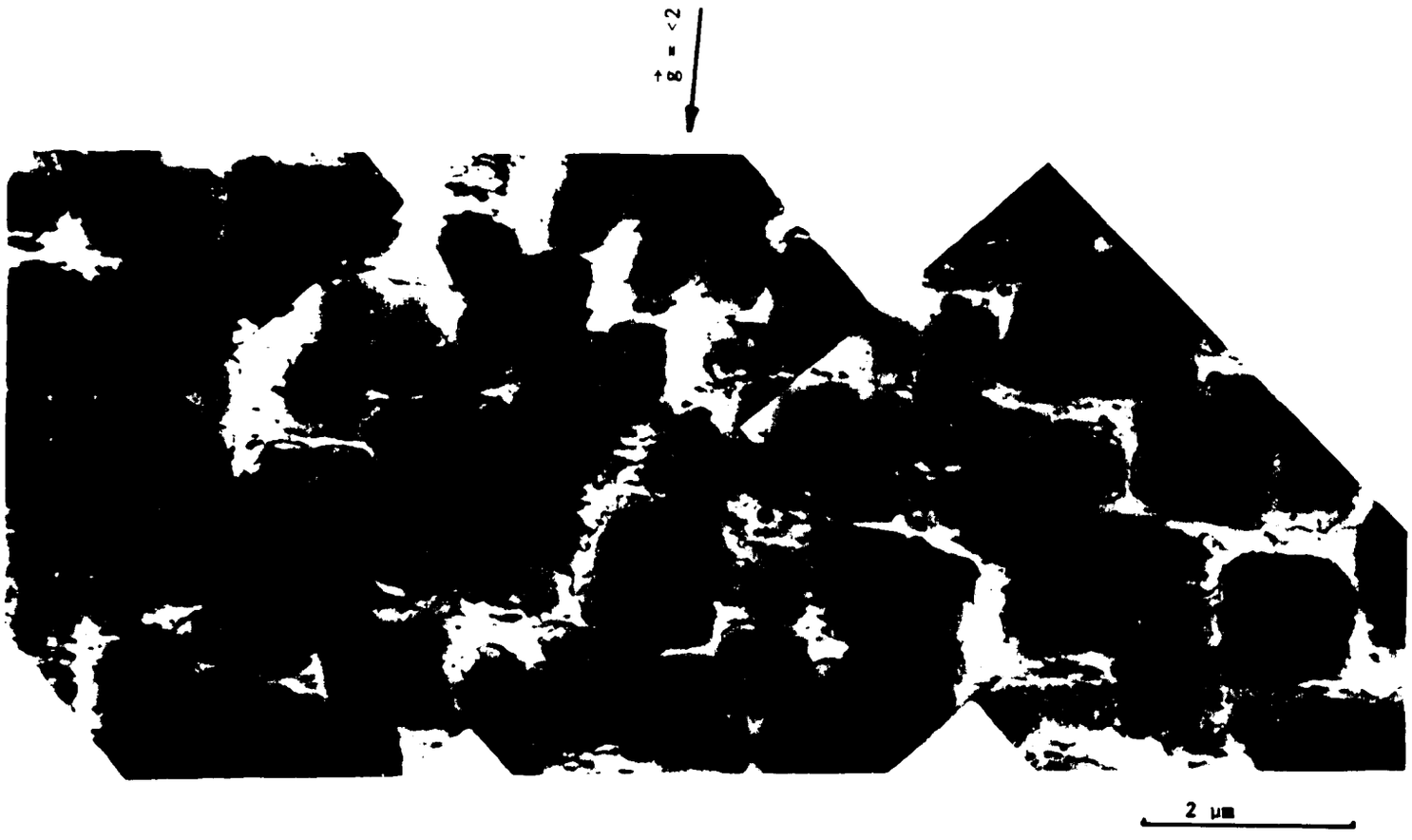

Figure 41 Dislocation Structures After Being LCF Tested at 538°C(1000°F), 10cpm, $\Delta\epsilon_t = \pm 0.25\%$ for 13,330 Cycles, Specimen 3D [1.52mm(0.06 in.) below fracture surface].

approaches span the range of purely phenomenological to mechanistic. A life prediction model is the application of an approach in a mathematical form (a function or functional) for the prediction of life. On a relative basis, existing models can be characterized as shown in Figure 42, where the extreme left represents a purely phenomenological approach with increasing degree of mechanistic basis associated with the position to the right. As suggested in the figure, a model such as the Frequency Modified Life (Refs. 1,2), which relates the fatigue to inelastic strain range and frequency, is empirically derived using the observable macroscopic variables. All of the local macroscopic effects which determine life (crack initiation) are embodied in these parameters which are considered constant through the cyclic history. The Strain Range Partitioning (Refs. 3,4,5) model also relates cyclic life macroscopic (observable) parameters, but has, as its foundation, the notion of local damage associated with reversible rate dependent effects. For this reason, it is considered to be more mechanistic than Frequency Modified Life. Chaboche's Damage Rate (Refs. 6,7,8) model represents a different approach from the previous two models. Local damage is associated with creep rupture and rapid cycle fatigue characteristics, but the rate of accumulation of the damage is nonlinear (described by a pair of nonlinear differential equations). Finally, the model of Majumdar (Refs. 9,10,11) attempts to predict the local damage as related to microscopically observable details (cavity growth, grain boundary cracking, ...). Here, the life relationships are represented as functions of the local damage process. This model is considered more mechanistically based than the three models discussed previously.

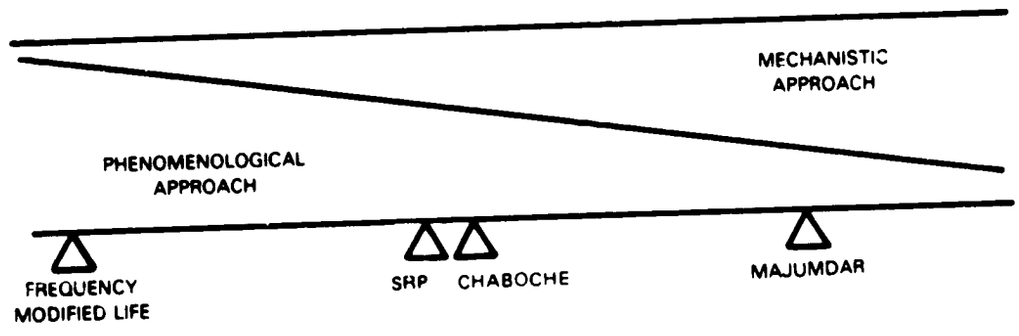

Figure 42 Characterization of Life Prediction Models

During the initial screening, models representing the entire range of approaches will be considered for selection of the best approach for prediction of elevated temperature crack initiation of the hot section structures.

3.2.4 Ranking Procedure

A ranking procedure for the models has been developed based on four criteria:

A. The amount and types of test data (called baseline data) required to determine the constants in a model.

B. The ability of a model to regress the baseline data and accurately predict verification test data.

C. The fundamental basis for the model.

D. The amount of judgement required to apply a model to an actual component loading cycle.

The first three criteria (A,B,C) will be combined to determine a total score based on the following procedure. Each criterion will be worth 10 points; however, A and B will each be weighted as 40% of the total score and C weighted as 20% of the total score. Thus, a possible score of 0-10 points will be assessed to "measure" the data requirements, predictive capability and basis of each model.

$$\text{Score}_{ABC} = 0.4A + 0.4B + 0.2C \qquad (1)$$

Criterion D, the amount of judgement required to apply the model to a component loading cycle, will be considered separately and will be worth a maximum of 10 points (least amount of approximation or judgement required). This criterion is considered of equal importance to the other three criteria because:

1) The initial test and correlation work in the base program is limited to uniaxial, isothermal conditions.

2) Actual component loading cycles will contain thermomechanical, multiaxial, cumulative, etc., loading effects which require some level of judgment for application of the models.

3) Identifying a model that can produce excellent predictions of isothermal simple cycle testing, but requires an extensive amount of judgment and approximation for application to a component loading cycle is considered to be less attractive.

The final recommendation for the models will consider the combined score for criteria A, B and C and the score for required judgement, criterion D. The models that score the highest in these two areas will be selected for further development. This is schematically shown in Figure 43. A detailed discussion of each criterion follows:

A. Amount and Types of Test Data Required. In assigning a numerical value for this criterion to a life prediction model, two data requirements will be considered. First, a sufficient number of tests and test conditions are required to guarantee that each regression coefficient is determined to a consistent degree of confidence (or uncertainty). This is demonstrated in Figure 44 for the regression of two models to a portion of the 649°C(1200°F) Rene' 95 data presented in Reference 12. As shown, nine data points are included in the data set; six tests run at 20 cpm [$\Delta\epsilon_T$ = 0.016(3), 0.009(3)] and three tests run at 1 cpm [$\Delta\epsilon_T$ = 0.016 (2), 0.009(1)].

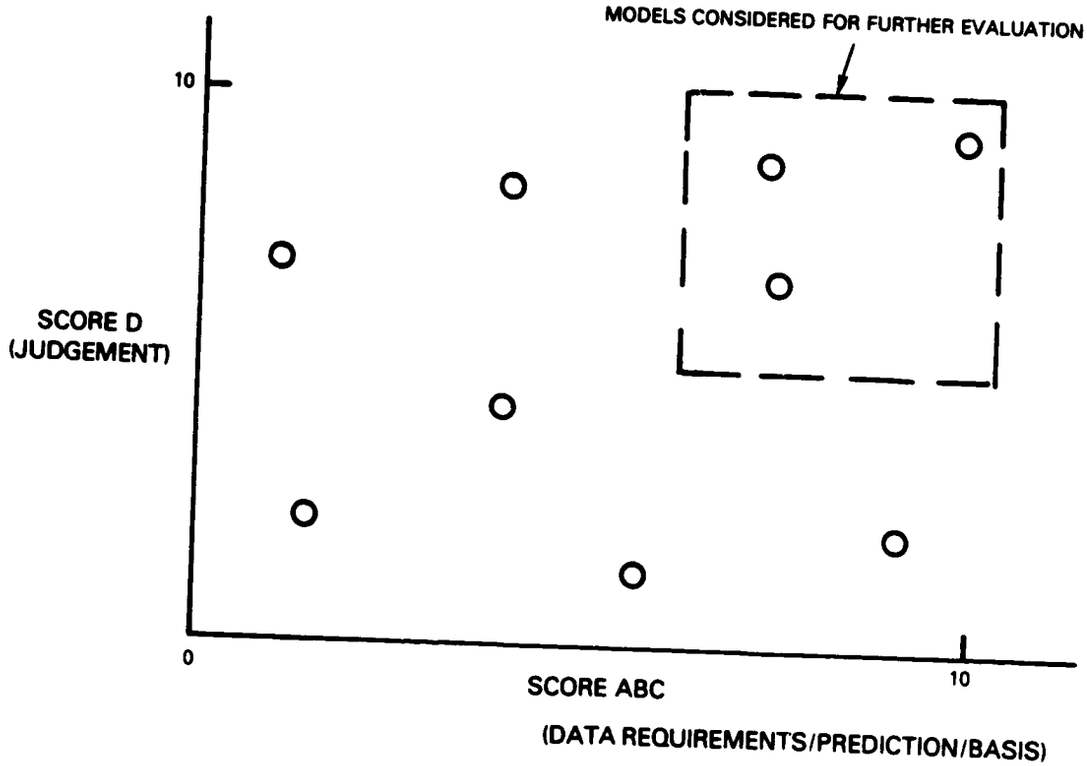

Figure 43 Ranking of Life Prediction Models

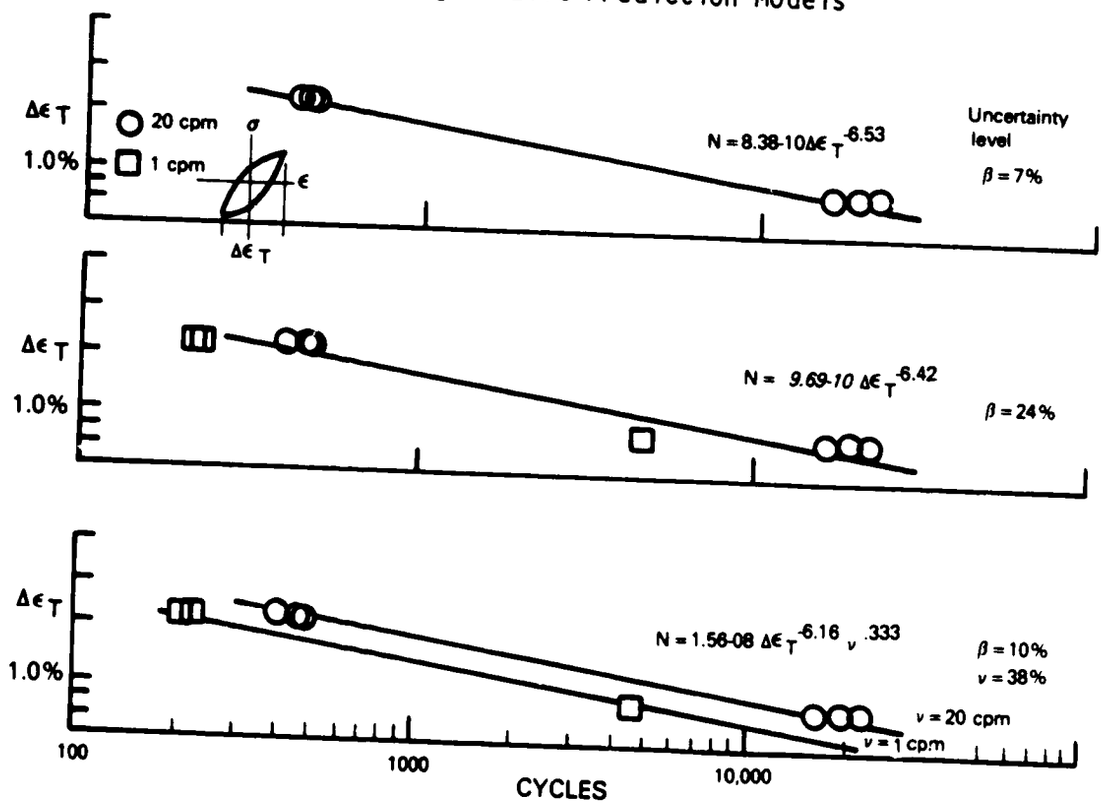

Figure 44 Variation in Uncertainty Levels with Two Life Prediction Models

Considering only the six 20 cpm points, a regression of a model as:

$$N = C\Delta\epsilon_T^{\beta}$$

results in a value of β determined with a 7% uncertainty level. The uncertainty level is defined as the ratio of the Student T value for the size of the data set to the Student T value determined from the regression (Tdata set/Tregression). Introducing the three 1 cpm data points and regressing the same form of the life equation (ignoring the frequency effect) results in an uncertainty level in the coefficient β of 24%. The poorer "fit" of the regression to the data is also shown in Figure 44. Finally introducing a frequency term and regressing the model as (see Figure 44):

$$N = C\Delta\epsilon_T^{\beta}\nu^{\eta}$$

results in a slight increase in the β uncertainty level (7% to 10%) but the uncertainty level of the coefficient η is calculated to be 38%. This is considered unacceptably large and would require either additional 1 cpm test points and/or testing conducted at a third frequency to more clearly define this effect on life. As additional points are introduced into the baseline data set, the uncertainty levels for each coefficient should approach each other and, in the limit, equal the Standard Estimate of Error (SEE). An acceptable uncertainty level for the coefficients will be determined by observing the change, with additional data points, in the R^2 and SEE parameters described in the next section. If the uncertainty level for a coefficient is not reduced when data covering the range of practical interest is included in the data set, the parameter will not be considered as having a primary effect on life and either the parameter or the entire model may be dropped from the evaluation.

The second data requirement relates to the number of tests that must be run to have 95% confidence that the observed median life is representative of the actual median life at that condition. By assuming a log-normal distribution of the fatigue lives, the relationship between the observed median life and the sample size for a certain confidence level is shown in Figure 45 where the ratio of observed median life to true median life (ηB50/NB50) is a function of the normalized standard deviation of the data set. A review of initial B1900 + Hf fatigue data indicates an average standard deviation of ≈ 0.2. This would equate to a 95% confidence band of 0.7 to 1.5, i.e., $0.7 \leq \eta B50/NB50 \leq 1.5$ for a sample size of 4. Increasing the sample size to 6 narrows the confidence band by 20%, i.e., $0.72 \leq \eta B50/NB50 \leq 1.35$. In the interest of economy, a sample size of 3 or 4 would most likely be used to define the life at each test condition.

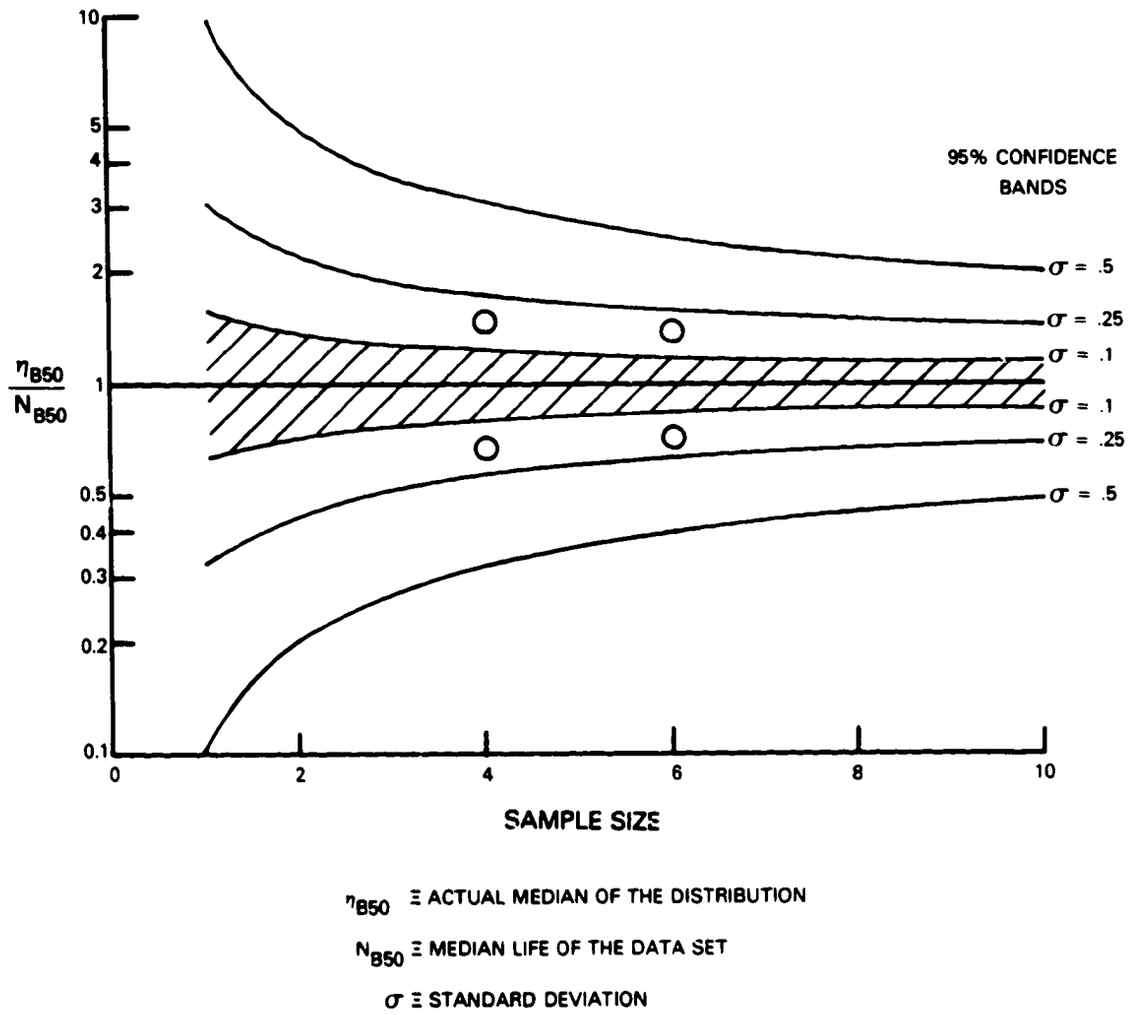

η_{B50} ≡ ACTUAL MEDIAN OF THE DISTRIBUTION

N_{B50} ≡ MEDIAN LIFE OF THE DATA SET

σ ≡ STANDARD DEVIATION

Figure 45 Effect of Sample Size on Ratio of True Median to Observed Median Lives

Determination of a total numerical score for this criterion (A) will include the calculation of two penalties. The first penalty (P_1) will reflect the number of independent variables included in the model. This penalty will be calculated as:

$$P_1 = Y-1 \tag{2}$$

where: Y = total number of independent variables (strain range, strain rate, dwell time, ...)

The second penalty (P_2) will be associated with the total number of data points required for the model. This will be calculated as:

$$P = \frac{Z-12}{12} \tag{3}$$

where: Z = total number of test points required.

Twelve data points are assumed to be required to define the effect of one independent parameter - e.g., total strain range ($\Delta\epsilon_T$) - three levels with four points each. This value may change as additional data becomes available. The total score for the f criterion will be calculated as:

$$A = 10 - (P_1 + P_2) \tag{4}$$

Thus, a model with one independent parameter and requiring 12 data points will score a perfect 10. A model with two independent parameters and requiring 24 data points will score an 8.

B. Regression of Baseline Data and Prediction of Verification Data. A numerical score for this criterion applied to each model will reflect both the ability to regress baseline data used to determine model constants and the predictive capability of verification data. Two measures of these abilities will be considered; the percent variation explained (R^2) and the Standard Estimate of Error (SEE). Both parameters are defined in Figure 46. Values of R^2 and SEE for both a baseline and verification set of data will be calculated for each model. The score for this criteria will then be calculated as:

$$\text{Score}_B = 10 - \left(\frac{R_B^2 - R_V^2}{R_B^2}\right)\left(\frac{SEE_V - SEE_B}{SEE_B}\right) \qquad (B \geq 0)$$

where $R_B^2 = R^2$ for baseline data base

$R_V^2 = R^2$ for verification data base

SEE_B = SEE for baseline data base

SEE_V = SEE for verification data base

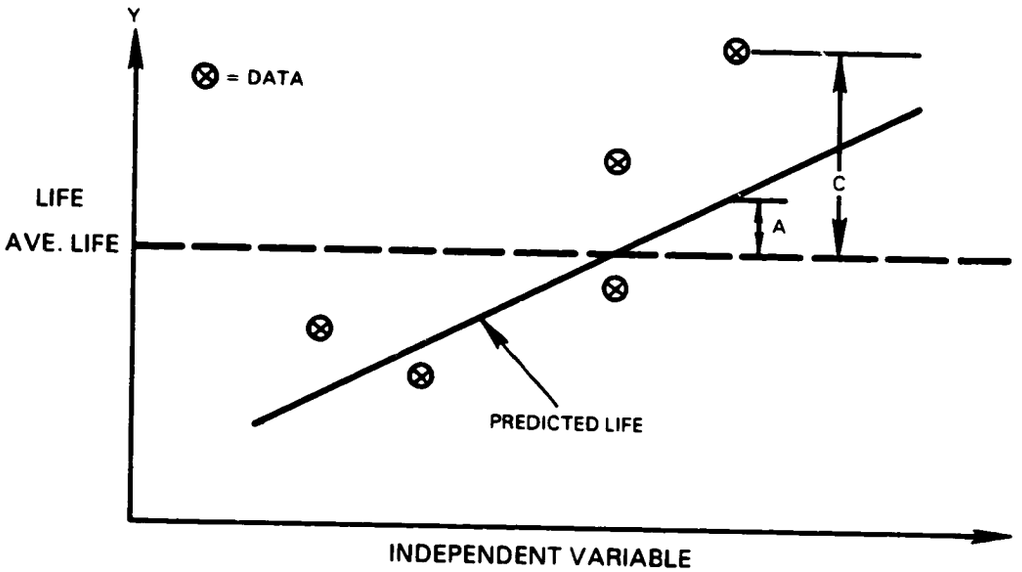

Figure 46 Statistical Analysis for Model Evaluation

% Variation Explained $R^2 = \dfrac{\Sigma\left(Y_{pred} - Y_{ave}\right)^2}{\Sigma\left(Y_{act} - Y_{ave}\right)^2} = \dfrac{\Sigma A^2}{\Sigma C^2} \qquad (1 \geq R^2 \geq 0)$

Standard Estimate of Error $SEE = \left[\dfrac{\Sigma\left(Y_{act} - Y_{pred}\right)^2}{N-(K+1)}\right]^{1/2} \qquad \left(0 \leq SEE \leq \dfrac{\Sigma Y_{act}}{(N - K+1)^{1/2}}\right.$

where: Y_{pred} ≡ predicted life

Y_{act} ≡ actual life

Y_{ave} ≡ average predicted life

N ≡ number of data points

K = number of independent variables

As an example, consider the two life models discussed in the previous section:

$$N = C\Delta\epsilon_T^{\beta}, \text{ and}$$
$$N = C\Delta\epsilon_T^{\beta}\nu^{\eta}$$

Regression of the models to the baseline data sets results in:

$N = C\Delta\epsilon_T^{\beta}$	$N = C\Delta\epsilon_T^{\beta}\nu^{\eta}$
(6 points)	(9 points)
C = 8.38 E-10	C = 1.56 E-09
β = - 6.53	β = -6.16
R_B^2 = 99.7%	η = .333
SEE_B = 5.3%	R_B^2 = 99.2%
	SEE_B = 8.6%

Introducing a separate verification data set of seven test points representing five different strain rate loading patterns shown in Figure 47 and using the same two models results in the following:

$N = C\Delta\epsilon_T^{\beta}$	$N = C\Delta\epsilon_T^{\beta}\nu^{\eta}$
R_V^2 = 11.1%	R_V^2 = 31.8%
SEE_V = 50.5%	SEE_V = 44.3%

Prediction of verification data by these models is shown in Figure 48. The score for this criterion for each model is then calculated as:

$N = C\Delta\epsilon_T^{\beta}$

$$\text{Score}_B = 10 - \left(\frac{99.7 - 11.1}{99.7}\right)\left(\frac{50.5 - 5.3}{5.3}\right) = 2.45$$

$N = C\Delta\epsilon_T^{\beta}\nu^{\eta}$

$$\text{Score}_B = 10 - \left(\frac{99.2 - 31.8}{99.2}\right)\left(\frac{44.3 - 8.6}{8.6}\right) = 7.18$$

Thus, the two parameter model would be considered to have much better predictive capability.

FAST/SLOW (F/S, 20 - 0.005 cpm)

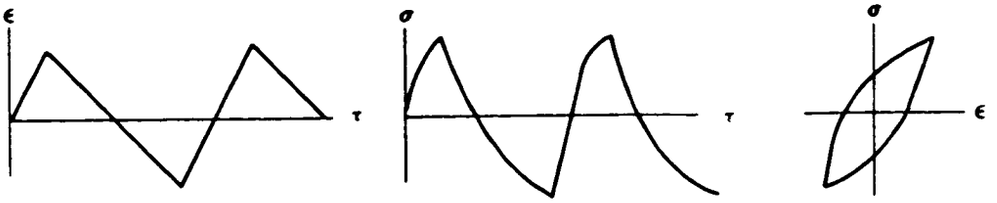

FAST/SLOW (F/S, 20 - ½ - 0.05 cmp)
WITH RATE CHANGE HALFWAY BETWEEN MAX. AND ZERO STRAIN

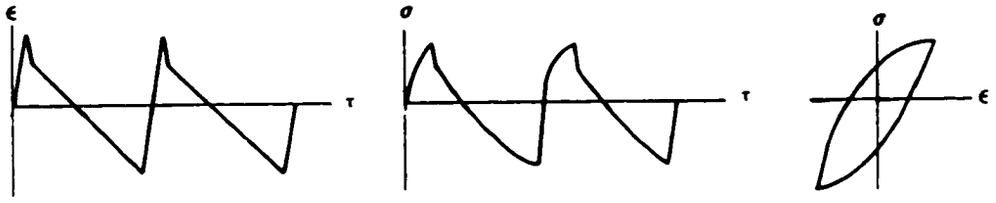

SLOW/FAST (S/F, 0.05 - 20 cpm)

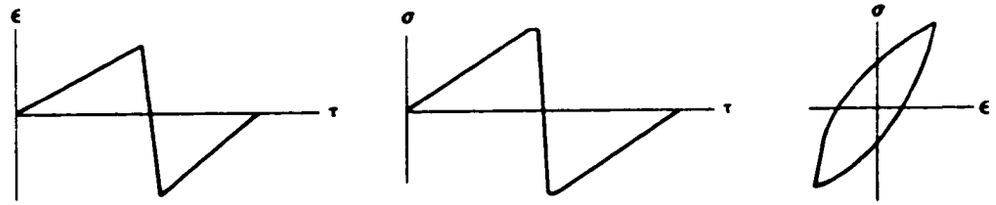

SLOW/FAST (S/F, 0.05 - ½ 20 cpm, 1 - ½ - 20 cpm)
WITH RATE CHANGE HALFWAY BETWEEN MIN. AND ZERO STRAIN

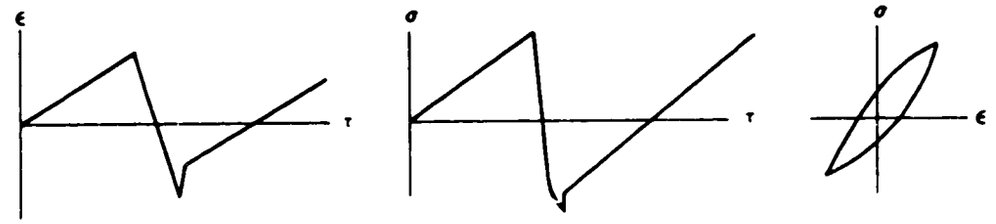

Figure 47 Waveforms and Hysteresis Loops of Verification Tests

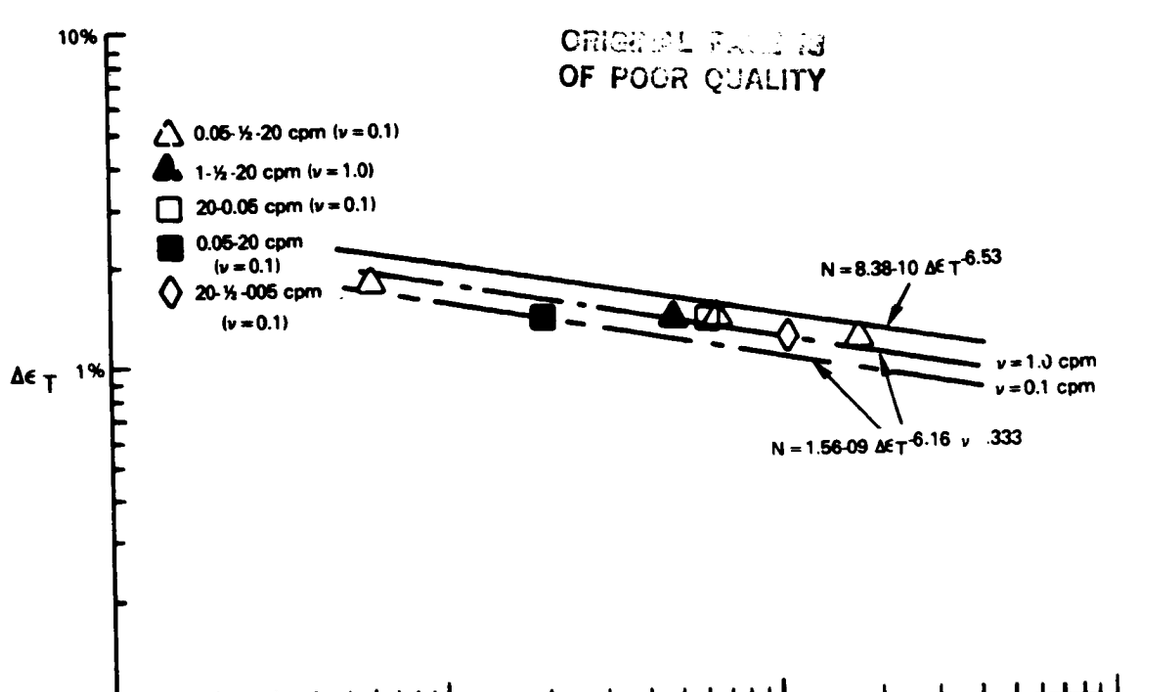

Figure 48 Prediction of Verification Tests with Two Models

C. Fundamental Basis for the Model. One of the major objectives of this program is the identification of a life prediction approach applicable to the high temperature creep-fatigue mechanism. The adaptability of the approach and the resulting model to alternate materials and loading cycles is also a primary benefit of this work. Currently, the most obvious means of developing a basic understanding of the fatigue process, with the highest probability of "transporting" this knowledge to other materials, is to consider life prediction approaches that have a micromechanical basis. Thus, models that attempt to predict the damage associated with specific processes (cavity growth, triple point cracking, etc.) will be given high scores. Models that claim to account for specific damage processes but are based on macroscopic parameters (strain range, etc.) will be scored moderate to high. Models with a purely macroscopic approach will be given low to moderate scores. It is further recognized that a macroscopically based model may ultimately be the best model based on all other criteria and that the requirement of a micromechanical basis may be too restrictive; thus, this criteria is weighted as only 20% of the total score.

D. Amount of Judgment Required to Apply the Model to An Actual Component Loading Cycle. Use of this criterion during the initial model ranking is somewhat premature since the more "component like" loading conditions (thermomechanical, multiaxial, cumulative loading, etc.) will be studied later in the option program. However, an estimate of the amount of judgment and assumptions required is necessary to avoid selecting a model which does an excellent job of correlating the isothermal simple cycle data, but is difficult or cumbersome to apply to the more realistic loading cycles. The method of determining a score for this criterion will initially consider the information required by a life prediction approach. The quantities that can be directly obtained from the loading cycle, e.g., total cycle time, maximum temperature, etc., or that can be directly calculated, e.g., maximum principle stress, strain range, etc., will not be assigned a penalty. Quantities that require a "first level of judgment" will be assigned one penalty point. Examples of these quantities are effective frequency or effective temperature. Quantities that require a "second level of judgment" will be assigned 2 penalty points. Examples of these quantities are physical sizes associated with a material, e.g., critical cavity or crack sizes. As the screening process continues, and additional models are considered, expansion and modification of this criterion will continue. The score for this criterion will then be calculated as:

$$D = 10 - \sum_{i=1}^{n} Pi \qquad (6)$$

where Pi = penalty points associated with each quantity

n = number of quantities required

Life prediction models that have high scores in both the judgment (D) and data requirement/prediction/basis (A,B,C) criteria will be considered for further development in the option program. Models that have high scores in the A,B,C criteria but lower scores in the D criterion may still be considered due to the actual level of uncertainty associated with the quantities during the screening process. A summary of the key equations comprising the screening criteria is presented in Table VII.

Table VII

Key Equations of Life Prediction Ranking System

$$P_1 = Y - 1 \tag{2}$$

$$P_2 = \frac{z - 12}{12} \tag{3}$$

$$A = 10 - (P_1 + P_2) \tag{4}$$

$$B = 10 - \left(\frac{R^2_B - R^2_V}{R^2_B}\right)\left(\frac{SEE_V - SEE_B}{SEE_B}\right) \qquad (B \geq 0) \tag{5}$$

$C = 10$ Microscopic Basis

1 Macroscopic Basis

$$Score_{ABC} = 0.4A + 0.4B + 0.2C \tag{1}$$

$$Score_D = 10 - \sum_{i=1}^{n} Pi \tag{6}$$

3.3 TASK III CRACK INITIATION MODEL EVALUATIONS

The initial examination of various approaches for the prediction of elevated temperature crack initiation considered two well known life prediction models. The Coffin-Manson Model (Ref. 13) was selected as a starting point for microscopic or phenomenological life prediction approaches, while the Damage Rate Model, developed by Majumdar, was considered representative of a more mechanistic approach. The model ranking criteria, discussed in Section 3.3, was used as a "framework" for this initial evaluation. The available fatigue data, presented in Tables V and VI, were grouped into three sets designated A, B, and C.

A; 871°C(1600°F), $\dot{\epsilon} = 1.67\text{-}03\ sec^{-1}$, $R\epsilon = -1$
B; 871°C(1600°F), $\dot{\epsilon} = 1.67\text{-}04\ sec^{-1}$, $R\epsilon = -1$
C; 538°C(1000°F), $\dot{\epsilon} = 1.67\text{-}03\ sec^{-1}$, $R\epsilon = -1$

Set A was considered baseline data and used for regression of model constants. Set B did not show a significant strain rate effect on fatigue life and was considered in the initial model regressions. Set C was used as verification data to evaluate the predictive capability of each model.

The crack initiation life for each specimen test was defined as the number of cycles required to produce a 0.76(0.030 in.) surface crack. Based on the replica data presented in Figure 49, this is equivalent to 15 percent of the total specimen life for tests conducted at 871°C(1600°F) and 50 percent of the total life at 538°C(1000°F). Previous metallurgical examination had indicated that this portion of the life represented a crack depth of approximately two grain diameters and that the crack progressed transgranually from the initiation site. This observation appears to be valid for all three data sets. For the model evaluations, it was assumed that the crack initiation process was represented by the cycle response parameters (inelastic strain and rate, etc.) as measured at the crack initiation life.

3.3.1 Coffin-Manson Model

This model assumes a power law relationship between inelastic strain range and fatigue life. Regression and prediction of the three data sets with this model is presented in Figures 49 to 51 and summarized in Table VIII.

TABLE VIII
REGRESSION AND PREDICTION WITH COFFIN-MANSON MODEL

Data Set	Model Form	R^2	See
A	$N = 0.045\,\Delta\epsilon\ in^{-1.052}$	88.9	15.5
A+B	$N = 0.0375\,\Delta\epsilon\ in^{-1.078}$	90.5	16.2
C	$N = 0.0375\,\Delta\epsilon\ in^{-1.078}$	76.0	32.6

As shown, combining data set B with set A (Figure 50) did not significantly change the model regression. This is due principally to the lack of a strain rate effect on fatigue life for the conditions tested. Using this model as a prediction of data set C (Figure 51) results in a conservative prediction of the crack initiation life at 538°C(1000°F). Despite the apparent temperature effect, these results were used as verification predictions for the model ranking criteria. Application of the ranking procedure results in the following values:

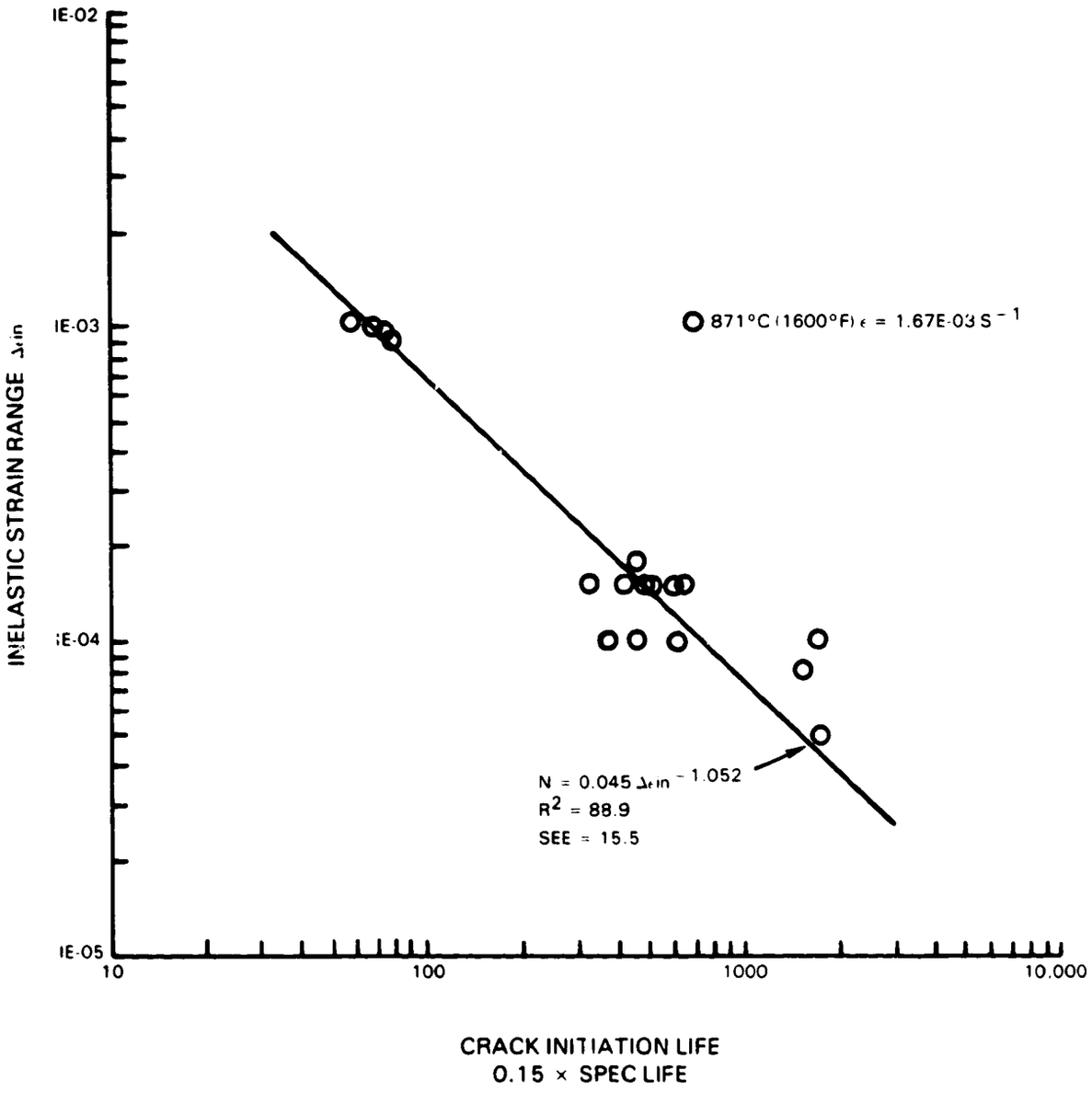

Figure 49 Regression of Coffin-Manson Model to Baseline Data (A)

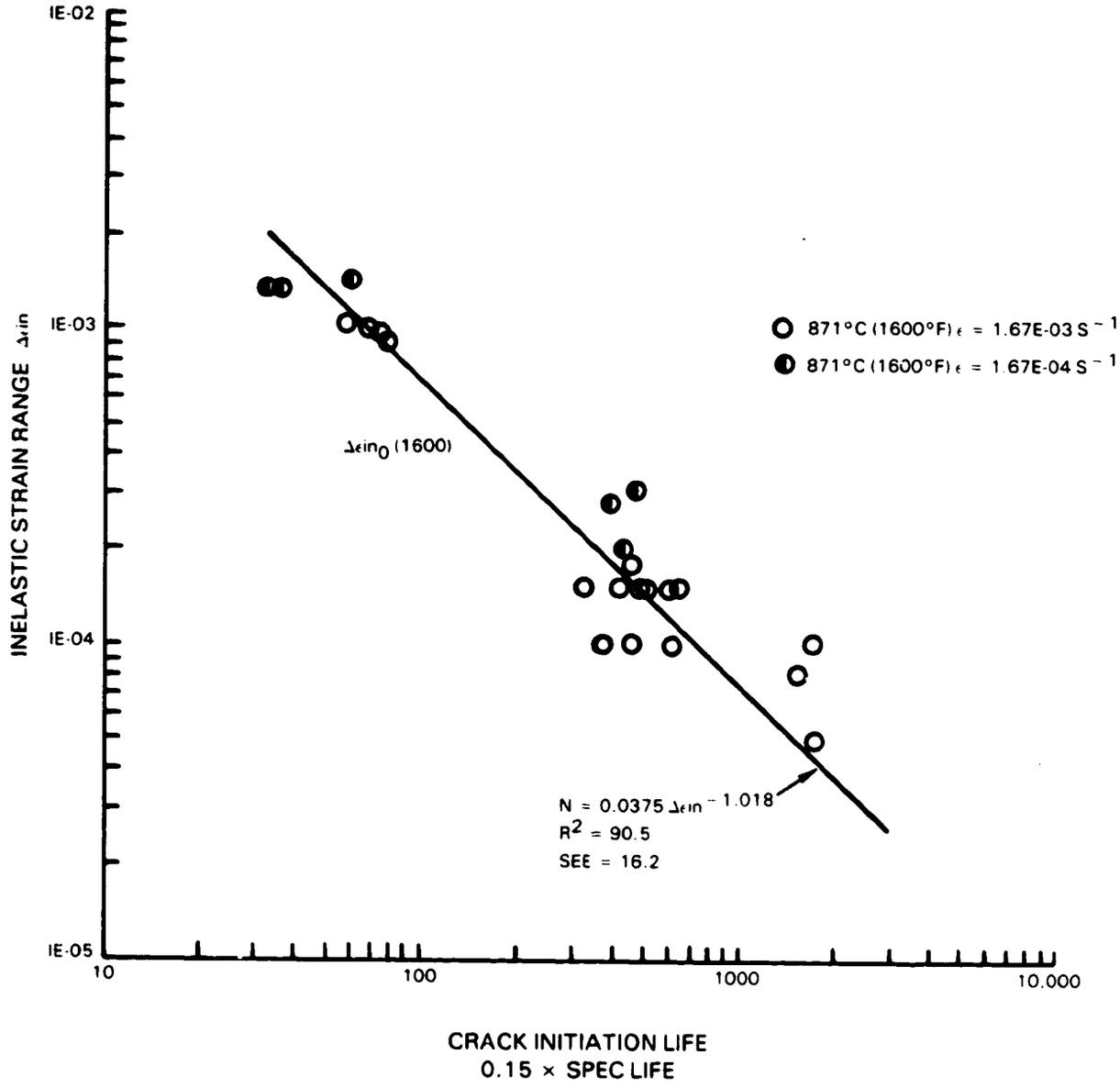

Figure 50 Regression of Coffin-Manson Model to Combined Baseline Data (A+B)

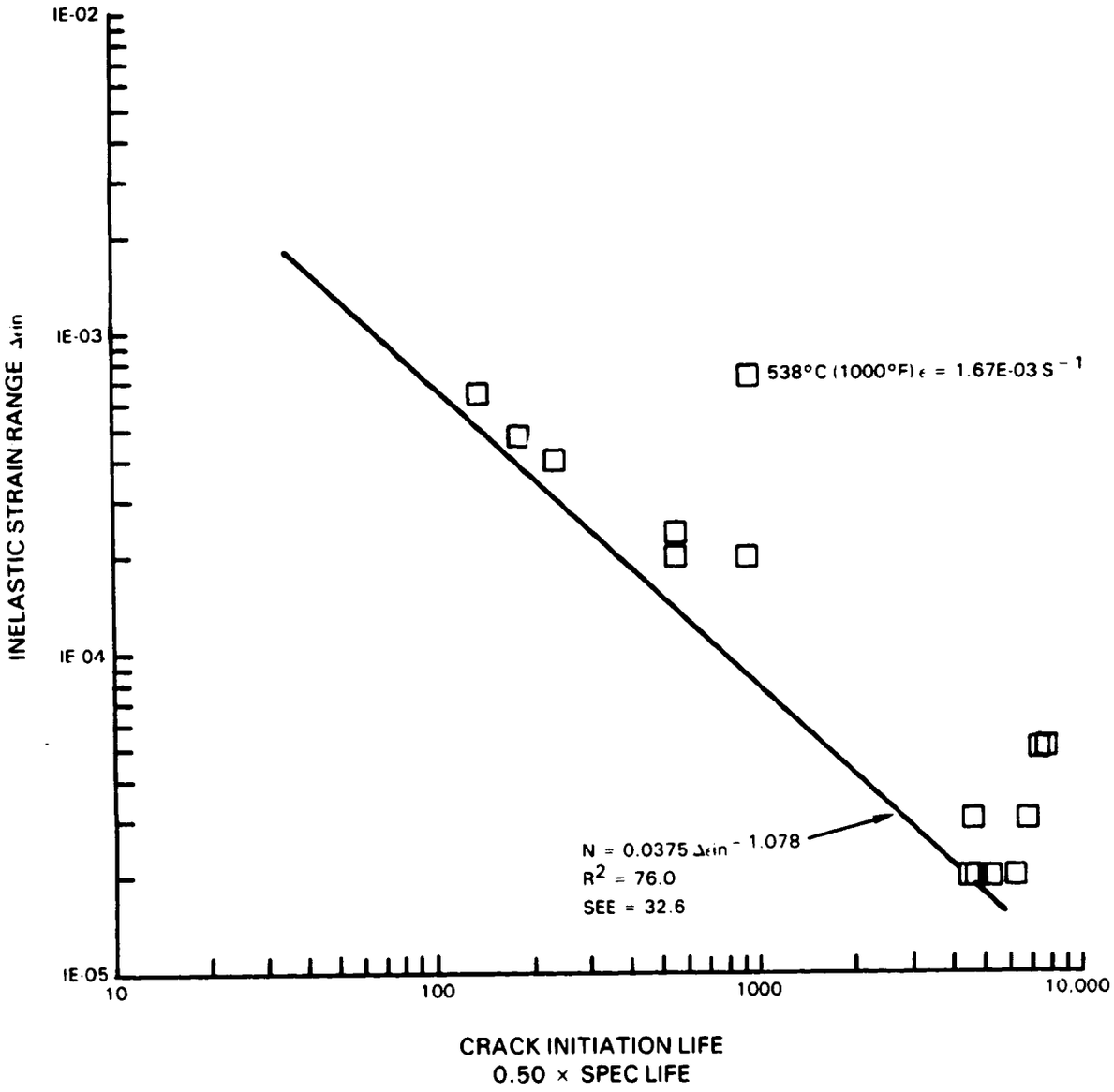

Figure 51 Coffin-Manson Prediction of Verification Data (C)

A. Amount and Types of Test Data Required

1. Independent variables:

$Y = 1$ (one independent variable - $\Delta\epsilon$ in)

$\therefore P_1 = 1 - 1 = 0$

2. Number of data points required:

$Z = 9$ (Regression of model at 871°C (1600°F) with only data points at each strain range results in similar regression constants.)

$$\therefore P_2 = \frac{9-9}{9} = 0$$

3. $A = 10 - (P_1 + P_2) = 10$

B. Regression of Baseline and Prediction of Verification Data

1. $R^2_B = 90.5$ $SEE_B = 16.2$ (data sets A & B)

2. $R^2_V = 76.0$ $SEE_V = 32.6$ (data set C)

3. $$B = 10 - \left(\frac{90.5 - 76}{90.5}\right)\left(\frac{33.6 - 16.2}{16.2}\right) = 9.84$$

C. Fundamental Basis

1. $C = 2$ (Considered a representative score for a macroscopically based model).

D. Amount of Judgment for Application to Component Loading Cycles

1. By the guidelines provided in Section 3.3, no penalty points should be assigned to this approach since the inelastic strain range should be "readily" available from some form of structural analysis. However, investigations by numerous investigators concerning the prediction of fatigue life under thermomechanical, multiaxial or cumulative damage effects indicate that a single parameter approach, e.g., inelastic strain range, is probably not sufficient to accurately capture these effects. For purposes of this preliminary ranking, two penalty points are assigned to this approach.

$\therefore D = 10 - 2 = 8$

The final score for the model would be:

Score ABC = 0.4A + 0.4B + 0.2C = 0.4(10) + 0.4(9.84) + 0.2(2) = 8.34
Score D = 8

3.3.2 Damage Rate Model

The Damage Rate Model assumes that low cycle fatigue is primarily a process of crack propagation and cavity growth. Micro-cracks and cavities are assumed to be present in the virgin material and the majority of the low cycle fatigue life is spent growing these micro-cracks and cavities to a critical crack size at which time they combine to form macro-cracks.

Following the development presented in Reference 1, the model assumes the growth law for the micro cracks and cavities as:

$$\frac{da}{dt} = \begin{cases} aT|\epsilon_{in}|^{m}|\dot{\epsilon}_{in}|^{K} & \text{(For tensile stresses)} \\ aC|\epsilon_{in}|^{m}|\dot{\epsilon}_{in}|^{K} & \text{(For compressive stresses)} \end{cases} \qquad 1)$$

$$\frac{dc}{dt} = \begin{cases} cG|\epsilon_{in}|^{m}|\dot{\epsilon}_{in}|^{Kc} & \text{(For tensile stresses)} \\ C(-G)|\epsilon_{in}|^{m}|\dot{\epsilon}_{in}|^{Kc} & \text{(For compressive stresses)} \end{cases} \qquad 2)$$

where: a = crack length
c = cavity length
t = time
ϵ_{in} = inelastic strain
$\dot{\epsilon}_{in}$ = inelastic strain rate
T, C, G, m, K, Kc = constants

For the current evaluation, a predictive form of the model appropriate to continuous cycling at a constant strain rate is used:

$$Nf = B\left(\frac{\Delta\epsilon_{in}}{2}\right)^{-(m+1)} (\dot{\epsilon}_{in})^{(1-k)} \qquad 3)$$

This form is determined by integrating equations 1 and 2 over an ideal cycle which contains equal tensile and compressive peak stresses and inelastic strains, and constant inelastic strain rate. In addition, it is assumed that the primary cavity growth mechanism is associated with tensile or compressive hold times. Thus, the continuous cycling form of the model does not include cavity growth.

Regression of the model (Equation 3) to data set A produced the values below:

Data Set	Model Form	R^2	SEE
A	$N = 12050\left(\frac{\Delta\epsilon in}{2}\right)^{-4.80} (\dot{\epsilon} in)^{4.92}$	96.6	8.8

As expected, this two-parameter model is able to better fit the baseline data than the Coffin-Manson Model discussed above. A comparison of the baseline data and the prediction for various inelastic strain rates is shown in Figure 52.

Application of this model to data set B results in predicted lives that are significantly smaller than the experimental data. This is due to an apparent lack of a strain rate on crack initiation life for the conditions tested (see Figure 53). A similar situation exists in the prediction of the 538°C(1000°F) tests in data set C (see Figure 54). Here the values of the prediction parameters, R^2 and SEE, are:

$$R^2_V \cong 0.0$$
$$SEE_V = 118.2$$

Application of the ranking procedure results in the following values.

A. Amount and Type of Test Data Required

1. Independent variables

$$Y = 2$$

$$\therefore P_1 = 2 - 1 = 1$$

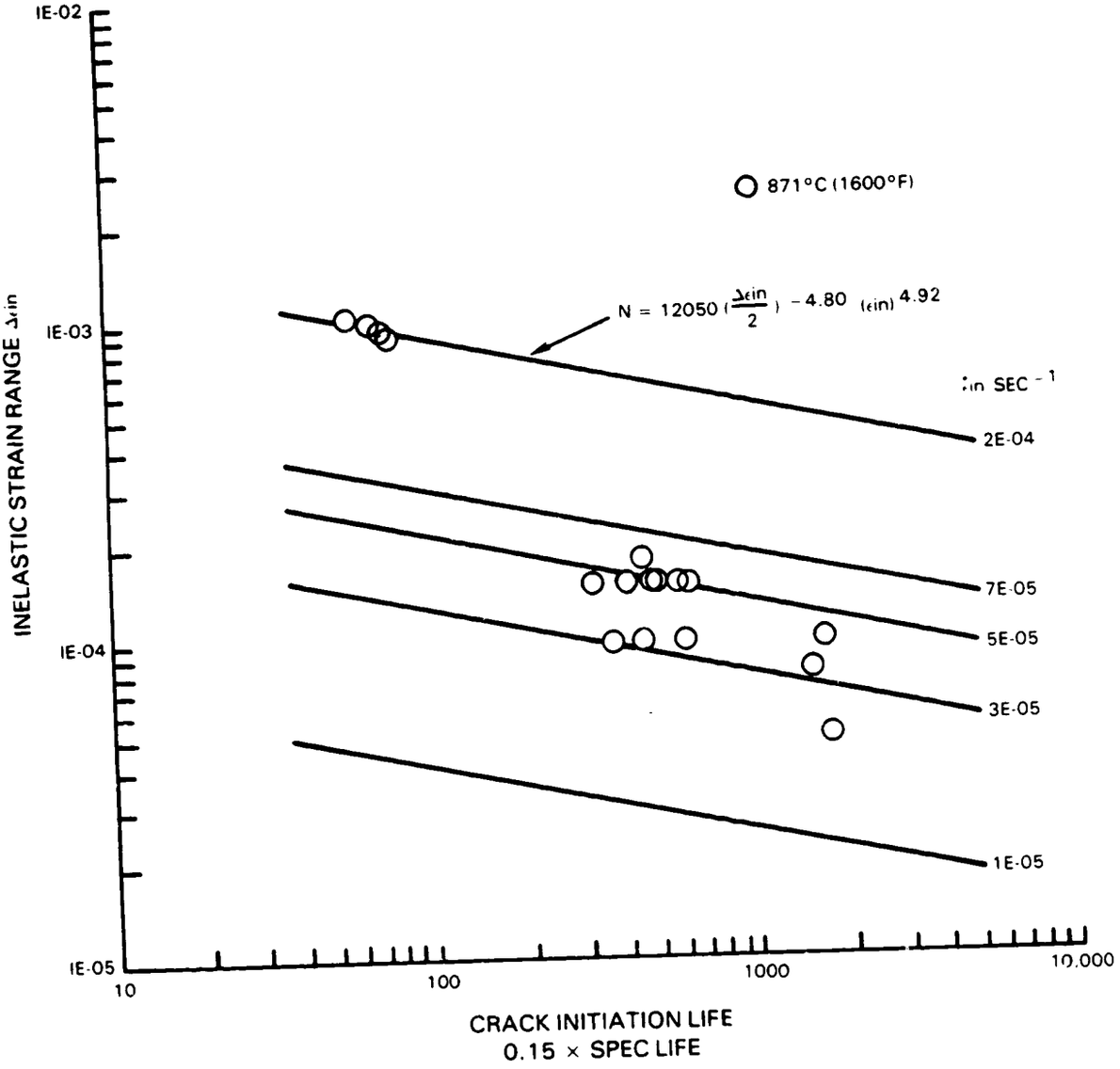

Figure 52 Prediction of Baseline Data With Damage Rate Model

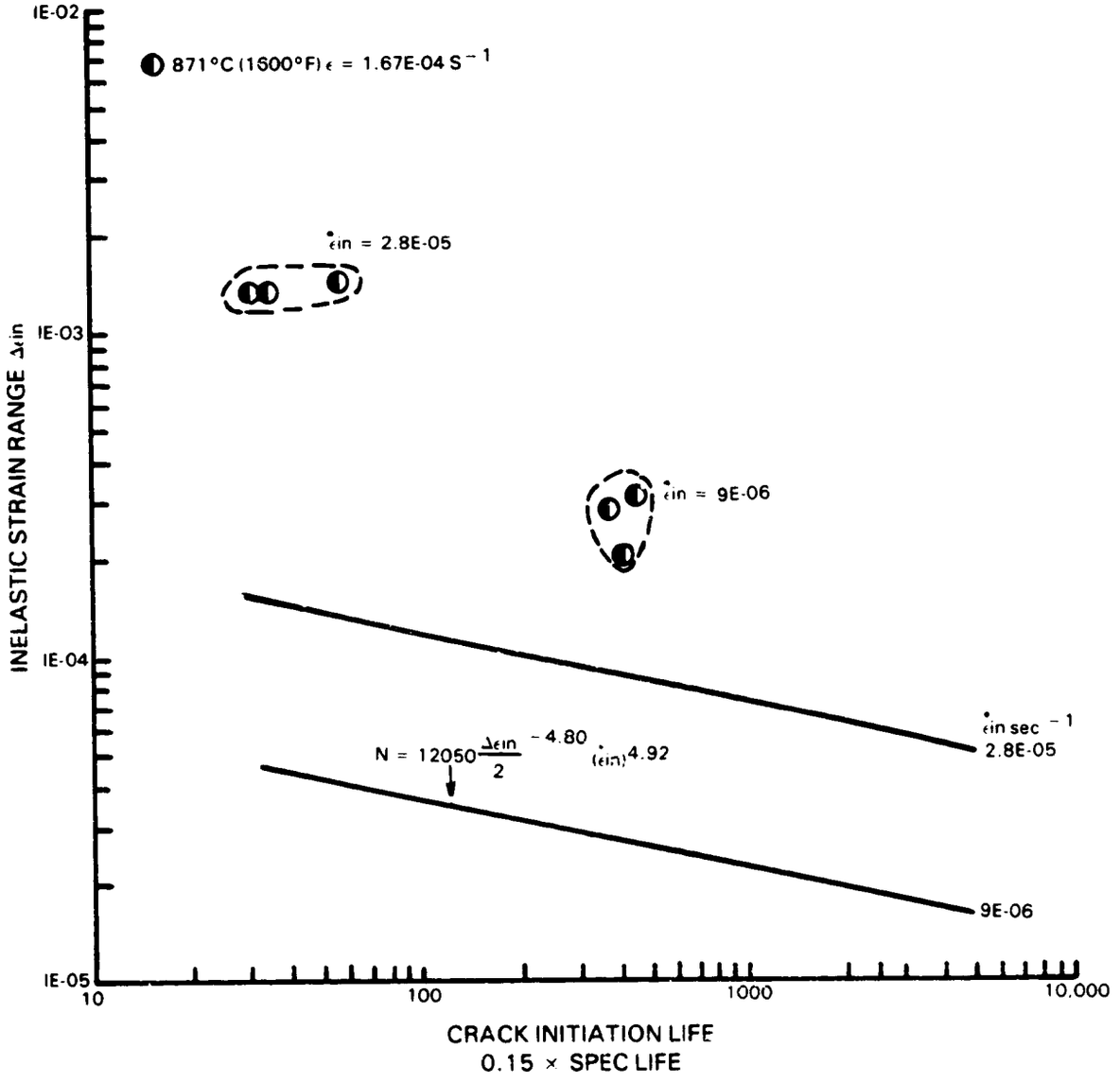

Figure 53 Prediction of Data Set B by Damage Rate Model

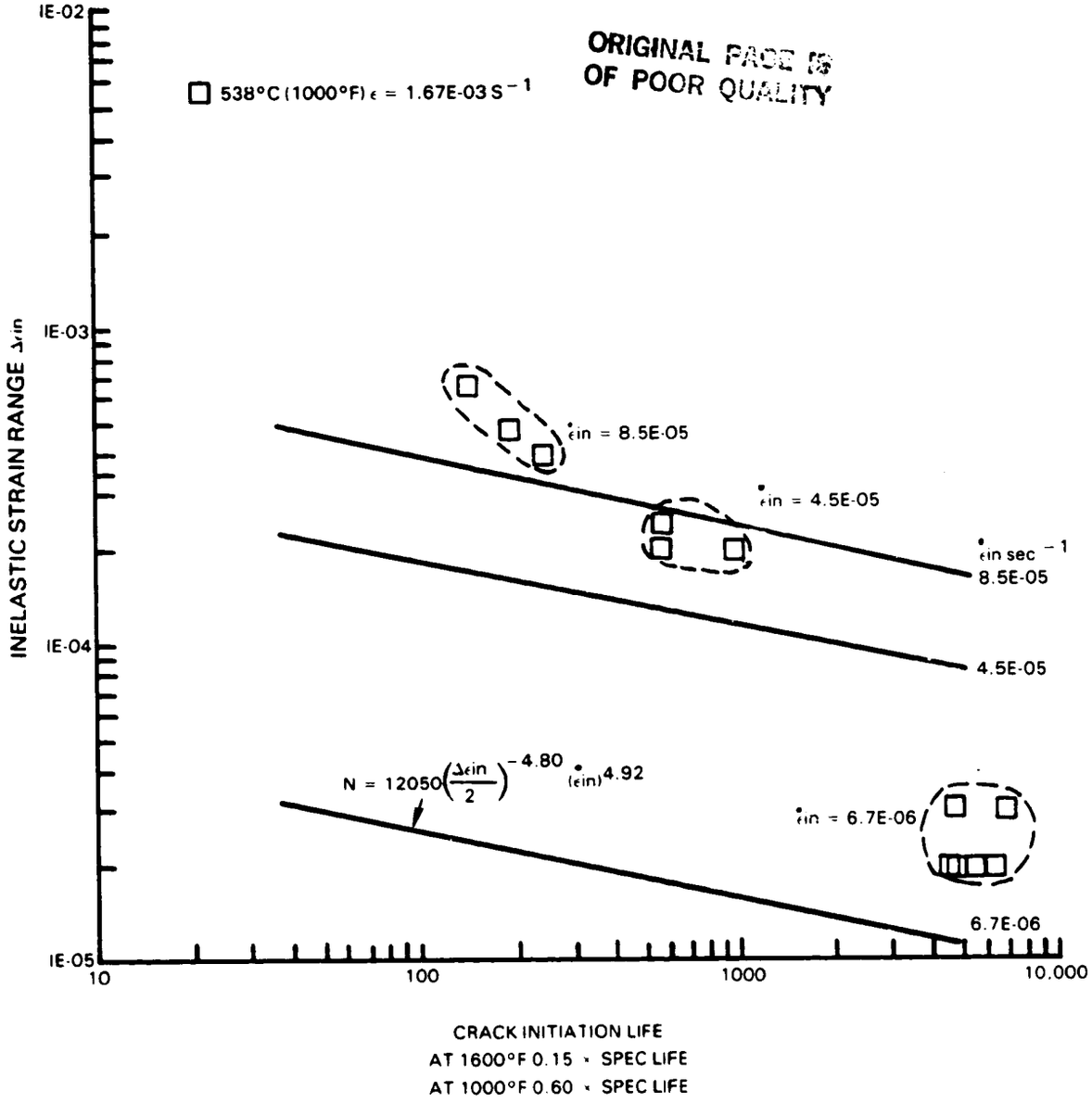

Figure 54 Prediction of Data Set C by Damage Rate Model

2. Number of data points required

$Z = 27$ (Assumes three data points for three strain ranges and three strain rates)

$$\therefore P_2 = \frac{27 - 9}{9} = 2$$

3. $A = 10 - (1 + 2) = 7$

B. Regression of Baseline and Prediction of Verification Data

1. $R^2_B = 96.6$ $SEE_B = 8.8$ (data set A)

2. $R^2_V = 0.0$ $SEE_V = 118.2$ (data sets B or C)

3. $$B = 10 - \left(\frac{96.6 - 0}{96.6}\right)\left(\frac{118.2 - 8.8}{8.8}\right) = -2.43$$

Use $B = 0$

C. Fundamental Basis

1. $C = 7$ (Scored higher than Coffin-Manson for potential of including effects of two damage mechanisms)

D. Amount of Judgment for Application to Component Loading Cycle

1. In the form of the approach used here, two parameters are required (inelastic strain range and rate). By the guidelines presented in Section 3.3, a penalty point would not be assigned to the inelastic strain range, but a single point would be assigned to the inelastic strain rate since an effective value is required. In the originally proposed form, the history of both parameters is required to permit integration throughout a loading cycle.

$\therefore D = 10 - 1 = 9$

The final score for the model would be:

Score ABC = $0.4A + 0.4B + 0.2C = 0.4(7) + 0.4(0) + 0.2(7) = 4.20$

Score D = 9

Based on the preliminary analyses presented above and summarized in Figure 55, the single parameter macroscopic approach would appear to have the greater potential for development of accurate life prediction models for engine relevant conditions. This excercise was intended to demonstrate the application of the ranking procedure and may not reflect a realistic approach until additional test data is available in the second year of the program. Furthermore, the score currently assigned to each approach reflecting the amount of judgement required for application to more complex loading cycles (D) is very qualitative. As additional approaches are included, a more quantitative ranking for this criteria should evolve.

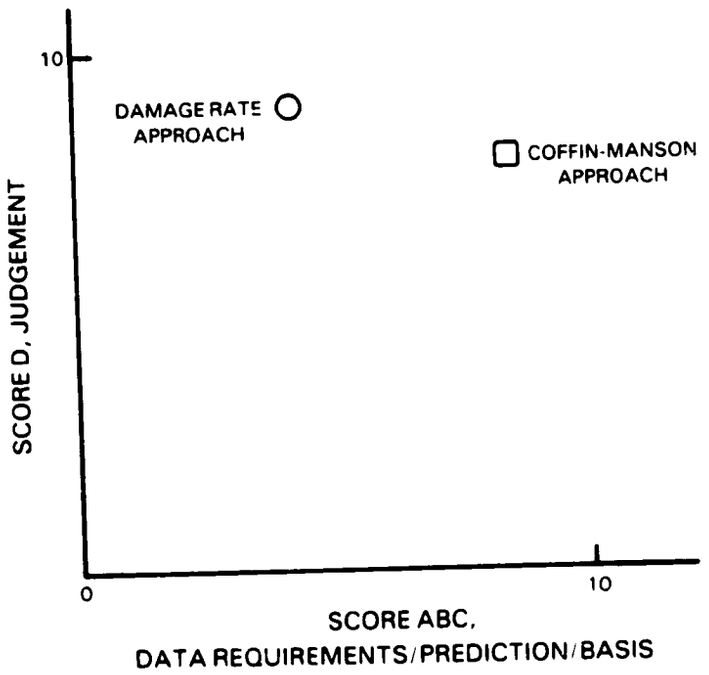

Figure 55 Preliminary Assessment of Two Life Prediction Approaches using Ranking Procedure

SECTION 4.0

FUTURE WORK

In the second year of the base program, fatigue testing will continue following the basic test matrix outlined in Section 3.0. This data will be used to determine model constants and to eliminate the predictive capability of each model considered. A significant effort will be directed toward the identification of the most appropriate approach for high temperature crack initiation life prediction. Models, representative of both macroscopic and microscopic approaches, will be considered. Metallurgical examination will continue in support of this effort to define deformation and failure modes.

REFERENCES

1. Coffin, L.F., "A Review of Fatigue Prediction Methods in the Regime Where Inelastic Strains Dominate", ASME Winter Annv. Meeting, N.Y., N.Y., Dec. 2-7, 1979, pp 1-24.

2. Coffin, L.F., "The Concept of Frequency Separation in Life Prediction for Time-Dependent Fatigue", Symposium on Creep Fatigue Interaction, 1976, pp 349-363.

3. Manson, S.S., Halford G.R., AND Hirschberg, M.H., "Creep Fatigue Analysis by Strain Range Partitioning. Symposium on Design for Elevated Temperature Environment, ASME, 1971, pp 12-28. (NASA TM X-67838, 1971).

4. Manson, S.S., "The Challenge to Unify Treatment of High Temperature Fatigue - A Partisan Proposal Based on Strainrange Partitioning. STP 520, ASTM, 1973, pp 744-782.

5. Halford, G.R., Saltsman, J.F., and Hirschberg, M.H., "Ductility Normalized Strainrange Partitioning Life Relations for Creep-Fatigue Life Prediction. Proceedings of Conf. on Environmental Degradation of Engineering Materials. Virginia Tech. Printing Dept., V.P.I. and State University, Blacksburg, VA, 1977, pp599-612.

6. Chaboche, J.L., "Thermodynamic and Phenomenological Description of Cyclic Visco-Plasticity with Damage", European Space Agency Technical Translation, May 1979.

7. Chaboche, J.L., Policella, H., Kaczmarek, H, "Applicability of the SRP Method and Creep Fatigue Damage Approach to the LCHTF Life Prediction of In-100 Alloy", AGARD-CP-243, Technical Editing and Reproduction Limited, London, 19789, pp 4-1 to 4-20.

8. Lemaitre, J., and Chaboche, J.L., "A Nonlinear Model of Creep Fatigue Damage and Accumulation and Interaction". Presented at the Symposium at IUTAM, Sur La Mechnique Des Milieux et Des Cor Viscoelatiques, Gothenburg, Sweden, September 2-6th, 1974.

9. Maiya, P.S., and Majumdar, S., "Elevated-Temperature Low Cycle Fatigue Behavior of Different Heats of Three Type 304 Stainless Steel", Metallurgical Transactions A, Volume 8a, November 1977, pp. 1651-1660.

10. Majumdar, S., and Miaya, P.S., "Wave Shaped Effects in Elevated Temperature Low Cycle Fatigue on Type 304 Stainless Steel", Change, T.Y., and Krempl, E. (eds.), Inelastic Behavior of Pressure Vessel and Piping Components, PVP-PD-028, ASME, New York, pp. 43-54.

11. Majumdar, S., and Maiya, P.S., "An Interactive Damage Equation for Creep-Fatigue Interaction", Volume 2, ICM3, Cambridge, England, August 1979, pp. 101-109.

12. Bernstein, H.L., "An Evaluation of Four Current Models to Predict the Creep-Fatigue Interaction in Rene' 95", AFML-TR-79-4075, June 1979.

13. Manson, S.S., "Behavior of Materials Under Conditions of Thermal Stress. NACA TN-2933, 1953.